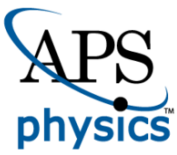

Interplay between optical vortices and condensed matter

Guillermo F. Quinteiro Rosen, Pablo I. Tamborenea, and Tilmann Kuhn

Rev. Mod. Phys. **94**, 035003 — Published 25 August 2022

DOI: 10.1103/RevModPhys.94.035003

Interplay between optical vortices and condensed matter

Guillermo F. Quinteiro Rosen*

IMIT-CONICET and Departamento de Física,
FACENA, Universidad Nacional del Nordeste,
(3400) Ciudad de Corrientes,
Argentina

Pablo I. Tamborenea

Departamento de Física and IFIBA,
FCEN, Universidad de Buenos Aires,
Ciudad Universitaria, Pabellón I,
1428 Ciudad de Buenos Aires,
Argentina

Tilmann Kuhn

Institut für Festkörpertheorie,
Westfälische Wilhelms-Universität Münster,
Wilhelm-Klemm-Str. 10, 48149 Münster,
Germany

(Dated: May 11, 2022)

The interest in the multiple facets of optical vortices has flourished in the last three decades. The article reviews the basic research and applications of the interplay between optical vortices and condensed matter systems. This subfield of optical-vortex physics has rapidly developed in recent years thanks to a vigorous synergy between theory and experiment. After presenting self-contained and focused introductions to optical vortices and condensed-matter optics, the theory and current progress in the research on the interaction of condensed-matter systems and optical vortices are examined. When considering the interaction of optical vortices with condensed matter systems many aspects of the standard theory of the interaction of matter with plane-wave light need to be reformulated. In bulk, the light-matter Hamiltonian matrix elements have to be recalculated and novel selection rules are obtained, reflecting the conservation of total angular momentum. Orbital angular momentum is transferred from the light beam to the photo-excited electrons, generating macroscopic currents. Semiconductor nanostructures add the complexity of their own spatial inhomogeneity, which is handled adequately by the envelope-function approximation. Here again modified matrix elements for the light-matter interaction dictate the allowed and forbidden optical transitions, distinct from the ones obtained in traditional optical excitation with smooth fields. Quantum rings play a central role due to their especially adapted geometry to the cylindrical nature of the twisted light beams. When the electron-electron interaction is taken into account the rich physics of excitons and exciton-polaritons comes into play, modified by the finite orbital angular momentum of the structured light. Furthermore, the new features brought about by optical vortices in plasmonics and in the optical excitation of two-dimensional materials are reviewed. For all these systems theory and recent experiments are discussed. Finally, an overview of current and prospective applications of the interaction of optical vortices with condensed matter systems in the fields of quantum technologies, communications, sensing, and more is presented. Throughout this review an attempt has been made to present not only a survey of the relevant literature but also the authors' perspective on the fascinating and rapidly evolving field of optical vortex - condensed matter interaction.

CONTENTS

* gfquinteiro@exa.unne.edu.ar

I. INTRODUCTION

From early times we seek to understand the interplay between light and matter (Cajori, 1899; Weiner and Nunes, 2017). Clear evidence points to serious attempts to learn about reflection, refraction, and vision before the scientific revolution (16th-17th century), a notable example being the work by Ibn al-Haytham, in the early 11th century, by some considered the father of optics. Brilliant discoveries, most of them familiar to us, took place around the 17th century and helped to shape the revolution. The law of refraction was enunciated in 1621 by Snellius. Newton (1672) used refraction by a prism to show the decomposition of white light into colors. Light projecting out of the direct line-of-sight beyond objects, was first described by Grimaldi, who named the phenomenon diffraction. Huygens (1690) contributed the picture of secondary waves in wavefronts, which together with Young's interference investigations around 1800 set the basis for Fresnel's work that explained diffraction and wrapped up optics phenomena under a coherent wave interpretation of light. Among several corroborations of Fresnel's theory, the predictions by Hamilton (1837) of conical refraction in anisotropic biaxial crystals –experimentally verified soon afterwards using aragonite mineral (Lloyd, 1833)– stands as a most notable one. On the one hand, it is an early example of theoretical prediction guiding successful experiments, and on the other hand it is the earliest known report of a phenomenon involving optical vortices, as we will later see in Sect. II.A. In parallel, the study of electricity and magnetism matured to the point in which Maxwell (1865) unified these phenomena with those of light. Progress in pure optics continued, as attested by the –here most relevant– work of Abbe (1874), who established the resolution limit of optical systems (see Sect. VI). Though diffraction, refraction, and reflection are indeed the result of the interaction of light with objects, our modern splitting of physics sets them under the umbrella of optics.

However, only few years later it turned out that the nature of light as an electromagnetic wave was not the whole truth. Phenomena like the black-body radiation or the photo-electric effect could not be explained at this level. To overcome this difficulty, Planck (1900) postulated the quantization of the energy and Einstein (1905) introduced the concept of light quanta, now generally called photons. A quantum theory of electrodynamics was formulated by Dirac (1927) and in the 1950s and early 1960 seminal papers by Mandel (1958), Sudarshan (1963) and Glauber (1963) opened the field of quantum optics. A milestone with enormous impact in the field of optics was the invention of the laser by Maiman (1960) which, besides its many applications in everyday life, is now the light source for the vast majority of optical experiments.

From a current perspective, the study of light-matter interaction relies strongly on the advances in chemistry, quantum mechanics, atomic physics, and solid state physics. Back to our timeline, modern chemistry (as opposed to alchemy) developed in parallel to optics, from work by celebrated people such as Boyle (1661), Lavoisier (De Morveau *et al.*, 1787; Lavoisier, 1793), Dalton (1808), and Mendeleev (1869), who gave modern form to the notions of gases, atoms, and chemical elements.

Milestones in atomic physics that provided greater insight on light-matter interaction are well known to us, and we recall only few that are most connected to the following sections: in 1900, before quantum mechanics, Drude proposed a model of free-electron motion in metals subjected to electric and magnetic fields using the Lorentz force in a Newtonian mechanics framework (Drude, 1900); later on the model was extended to bound electrons by Lorentz himself. The Drude-Lorentz model has been amply used, for instance, to explain plasmon polaritons, the subject of Sect. IV.C. A more sophisticated and modern way to deal with the light-matter interaction in classical terms is by employing Lagrangian mechanics together with Lorentz force. This leads to a generalized potential in the Lagrangian that depends on the scalar and vector potentials (and the velocity of the particle). By shifting to Hamiltonian mechanics, one defines the well-known minimal-coupling Hamiltonian. This can be quantized for charged particles and/or fields. Historically, other crucial developments are the reformulation in

terms of the dipole approximation in the case of atoms by Göppert-Mayer (1931) and the generalization in terms of the multipolar expansion by Power and Zienau (1959) and Woolley (1971) to describe the interaction of light with non-relativistic particles, that describe the workabout of problems related to gauge (see Sect. III.C.1).

Condensed-matter physics is nowadays a collage of a large number of subject matters. Originally, topics in condensed matter came from its predecessor, solid-state physics, which dealt with metals, semiconductors and their applications. As nicely told by Martin (2019): "Even in the early days of solid-state physics, the name was maligned because the field's topics and techniques were often equally relevant to liquids, molecules, plasmas, and other nonsolids. [...] Critical phenomena such as phase transitions, nonlinear dynamics of fluid systems, and liquid helium research that had little or nothing to do with solids took center stage." Condensed matter physics now encompasses the study of a variety of quantum states such as exciton-polaritons, two-dimensional electron gas, spin lattices, superconductors, Bose-Einstein condensates etc., most of them supported in solid-state media, some of them also in other condensed phases.

The seminal paper by Bloch (1928) constitutes an early milestone in the formulation of a quantum theory of crystalline solids. According to what is now called *Bloch's theorem*, the wave function of an electron in a crystal satisfying the time-independent Schrödinger equation can be written as a plane wave with a lattice-periodic modulation. The corresponding energies $\varepsilon_{n\mathbf{k}}$ can be classified by the wave vector $\mathbf{k}$ restricted to the first Brillouin zone and an additional integer number n, forming the band structure in $\mathbf{k}$-space with n labeling the bands. Combining this band structure with the Fermi statistics of electrons, one could distinguish between metals on the one hand and semiconductors and insulators on the other hand. The wave vector of the electron provides a natural interface for the coupling to light, which is typically also expressed in terms of plane waves. In semiconductors and insulators the coupling to light leads to the excitation of electrons from an occupied band to an empty one or, in the often convenient electron-hole picture, to the creation of electron-hole pairs. However, people soon realized that the Coulomb interaction between the electrons may change qualitatively this picture. Instead of a continuous absorption spectrum in the region close to the band gap discrete absorption lines appeared. The electron and hole form a new quasi-particle, the *exciton*, as introduced by Frenkel (1931) in the limit of strongly bound electron-hole pairs and by Wannier (1937) for weakly bound pairs, the latter ones being realized in typical semiconductor materials. Also in metals the Coulomb interaction leads to new quasi-particles, called *plasmons*, introduced by Bohm and Pines (1953). In the following years many other types of quasi-particles have been introduced like *polarons*, *polaritons*, *magnons*, *Cooper pairs*, and many more (Haken, 1976; Kittel, 1987).

We have built up much of our theoretical knowledge in optics from the concept of plane waves. Plane waves are a perfect building block to represent more complex light beams through Fourier analysis; however, they are often not well suited to describe strongly inhomogeneous waves, which in terms of plane waves correspond to a superposition involving an extremely large number of wave vectors. Optical vortices (OVs) are an example of such strongly space-varying light fields (Allen *et al.*, 2003, 1999; Andrews and Babiker, 2012; Padgett *et al.*, 2004; Torres and Torner, 2011), as we will see in Sect. II.

Since the 1990s a variety of experimental techniques have revealed new effects caused by OVs acting on matter —atoms, molecules, and nanoparticles—, which go beyond our expectations based on the interaction with plane waves. The most prominent ones come from the fact that OVs may carry orbital angular momentum (OAM) (Allen *et al.*, 1992). More recently, researchers have started to predict and measure effects coming from the interaction of OVs with condensed-matter systems, and possible applications to quantum technology and materials science have been proposed.

This article overviews the physics of the interaction of OVs and condensed-matter systems providing both a cohesive formulation of the theoretical basis and a comprehensive review of the current progress in the field. We start with a description of fundamental elements of the theory of OVs (Sect. II) and the theory of condensed matter systems (Sect. III) that are necessary to the development, in Sect. IV, of the theory of the interaction of condensed matter and OVs. Section IV also reviews the progress achieved in several subfields, namely, in semiconductor/conductor bulk and nanostructure physics, exciton-polariton physics, plasmonics, and in the physics of two-dimensional materials. Progress towards applications has also been significant, and it is discussed in Sect. V. Finally, after concluding remarks we present our view on possible future directions for the research of OV-condensed matter interaction in Sect. VI.

II. OPTICAL VORTICES

Vortices are part of our daily lives. Some are evident like whirlpools, tornadoes and hurricanes (typhoones, cyclones), with the astonishingly quiet eye of the storm, see Fig. 1. Other vortices pass unnoticed, for example, amphidromic points of tidal waves in the ocean, where the height of the water remains the same while it changes in their surroundings (Whewell, 1836), or sound waves scattered out of rough surfaces, whose wavefronts exhibit "dislocations" similar to those found in crystals, in which the intensity becomes zero (Nye and Berry, 1974). What do all these phenomena have in common? A vector field, e. g. the wind velocity, has null intensity at the vortex

center and revolves around it.

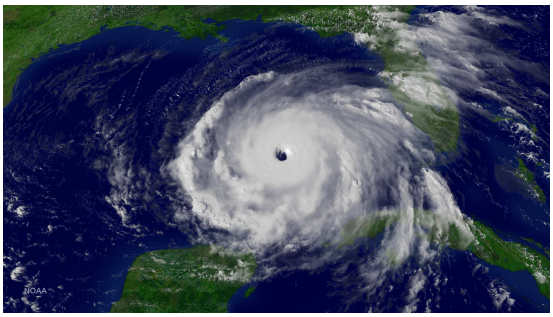

FIG. 1 (color online) Satellite photograph of Hurricane Katrina on August 28 (2005), with a clear view of its eye. With permission of NOAA National Environmental Satellite, Data, and Information Service (NESDIS).

When it comes to optics, however, many of us may be reluctant to accept that vortices happen naturally. After all, as young students we were first taught that light is a bundle of rays following broken paths of straight trajectories, only later to be told that light is an undulatory phenomenon representable by plane waves. After such insistent teachings, it is no surprise that many of us extrapolated ideas and ended up believing that light around us are waves with little spatial structure, although we know about the principle of superposition. But as it happens with whirls in wind and water, optical vortices are indeed ubiquitous phenomena in nature. They appear as a result of light scattering on rough surfaces (speckles) (Baranova *et al.*, 1981) and even from the simple superposition of a few plane waves (Masajada and Dubik, 2001; O'Holleran *et al.*, 2006). Optical vortices are worth studying to free ourselves from previous prejudices, expand our understanding of electrodynamics, and for the sake of the possible advances they can introduce in current technologies.

A. History

A light phenomenon with vortex character was first considered by Hamilton in his work on conical refraction (Hamilton, 1837) and soon afterwards experimentally verified by Lloyd (Lloyd, 1833). In conical refraction a (Gaussian) light beam entering a biaxial crystal along the optical axis is refracted inside it into a cone, emerging as a cylinder (Berry, 2004; Born and Wolf, 2013; Turpin *et al.*, 2016). The outgoing cylindrical beam is a superposition of simpler fields some of which have vortex features. In fact, conical refraction is nowadays used for the generation of OVs from Gaussian beams (Berry *et al.*, 2005; Phelan *et al.*, 2009). Hamilton's prediction and its experimental corroboration by Lloyd were at the time a major achievement; however, it is curious that it was only much later that conical refraction was recognized as a manifestation of vortical optics.

In modern research, examples of OVs appeared in a handful of publications around 1950 (Dennis *et al.*, 2009). Nevertheless, the first systematic study was carried out by Nye and Berry (1974) on what they called dislocations in sound (and applicable to general) waves scattered from rough surfaces. For the scattered wave, they found that screw dislocations can be expressed as an extra complex phase in the field; as we will see in Sect. II.B this is the signature of an optical vortex. The concept of OV was formulated by Coullet *et al.* (1989) [see also Shen *et al.* (2019)].

A few years later Allen *et al.* (1992) published what is, without doubt, the most influential article in the field. They showed that a Laguerre-Gaussian (LG) beam of light –a particular OV– carries a well-defined amount of OAM –as opposed to the spin or intrinsic angular momentum (SAM) associated with the polarization. Research in OVs boomed and in a few years many physics branches and other sciences picked up the idea and applied it to their respective fields.

The concept of quantized vortices in condensed phases has a long history. They have been studied in different systems, such as superfluids (Feynman, 1955), type-II superconductors (Abrikosov, 1957) and Bose-Einstein condensates (Matthews *et al.*, 1999). The spontaneous formation of optical vortices has been observed in semiconductor microcavities forming a surface-emitting vertical cavity laser (Scheuer and Orenstein, 1999) or hosting an exciton-polariton condensate (Lagoudakis *et al.*, 2008). The investigation of phenomena associated with the excitation of a semiconductor by an OV started about a decade ago. Two independent works provided theoretical predictions (Quinteiro and Tamborenea, 2009c) and experimental results (Ueno *et al.*, 2009).

Optical vortices are famous for their OAM, at first sight a startling feature. However, Beth (1936) demonstrated that circularly polarized light carries angular momentum (AM) in units of $\hbar$, which can be transferred to matter. In a quantum theory of light this AM corresponds to the spin of the photon. Moreover, nuclear physics tells about multipole transitions in spontaneous emission: One starts from the classical electrodynamics theory in terms of a single-frequency electric-current source and derives the average energy flux (Poynting vector) of the radiation. Next, one quantizes the electric current to a linear-momentum operator (gradient) and restates the classical single-frequency oscillating state to a transition between initial and final quantum states. All along the calculation there is a phase factor $\exp(i\mathbf{k}\cdot\mathbf{r})$ that, upon expansion and truncation ($kr \ll 1$), yields the well-known electric dipole radiation $\exp(i\mathbf{k}\cdot\mathbf{r}) \simeq 1$, electric quadrupole radiation $i\mathbf{k}\cdot\mathbf{r}$ and so forth, as well as the magnetic 2^n-poles (Basdevant and Rich, 2005; Fermi, 1950; Schiff, 1955). Photons from the 2^n-pole radiation carry angular momentum equal to $n\hbar$ or are superpositions of states with this angular momentum. Finally,

quoting Fermi (1950) "[...] it may frequently be necessary to go several terms down the expansion before finding a non-zero term. The reason is that more than half of all conceivable radiation processes are forbidden because of conservation of angular momentum or because of parity considerations.".

B. Basic Theory

Light fields can be represented using different basis functions. Simplicity usually dictates the choice of one or another. Thus, for light coming from a distant source, e.g., a star, the most appropriate representation is by plane waves. If instead we analyze the field close to a point source, we would likely decide in favor of spherical waves. In the case of a cylindrical geometry Bessel beams provide a basis exhibiting a complete factorization in cylindrical coordinates which, however, decay rather slowly in radial direction. Collimated laser beams are often better described by Gaussian beam profiles. To obtain a basis the Gaussian profile has to be supplemented by a set of transverse mode functions. Depending on the geometry, suitable bases are Hermite-Gaussian functions (in Cartesian coordinates) or Laguerre-Gaussian functions (in cylindrical coordinates).

Optical vortices, also referred to as "twisted light" and "light carrying OAM", are electromagnetic fields[1] with single or multiple points/lines in which the phase[2] cannot be defined and therefore the amplitude vanishes. Figure 2 shows exemplary electric-field profiles in planes perpendicular to the propagation direction (z-direction) at different z-positions at a fixed time or at different times at a given z-position. The Poynting vector swirls around these so-called singularitites[3], much like the wind does around the eye of a tropical hurricane (see Fig. 1) – the electric and magnetic fields may also circulate the singularity[4] but then in general they alternate in time the sense of rotation, as seen in Fig. 2. The singularity may exist in one or several components of the field and is mathematically represented by a phase $\exp(i\ell\varphi)$ in cylindrical coordinates $\{r, \varphi, z\}$, with $r = 0$ denoting the position of the singularity and the integer ℓ being the so-called topological charge. If not stated otherwise, in the following we will always consider beams propagating in the z-direction.

An OV is a curious object with features quite unlike plane waves, as seen in Fig. 2. Let us first concentrate on the transverse components of the field, i.e., the components of $\mathbf{E}$ and $\mathbf{B}$ lying in the xy-plane. Beams with a phase dependence $\sim \exp(i\ell\varphi)$ in these components carry well-defined OAM in the propagation direction related to the spatial (orbital) structure of the beam through the topological charge ℓ. Furthermore, they may carry intrinsic AM related to the handedness of circular polarization characterized by the parameter $\sigma = \pm 1$ referring to the polarization vector $\mathbf{e}_\sigma = (\hat{\mathbf{x}} + i\sigma\hat{\mathbf{y}})/\sqrt{2}$ with $\hat{\mathbf{x}}$ and $\hat{\mathbf{y}}$ denoting Cartesian unit vectors.

OVs are in fact a large family of fields all exhibiting singularities, that can be classified according to different criteria. They naturally split into two topologically distinct classes, according to whether the orbital and intrinsic AM are parallel or antiparallel to each other, i.e., when $\mathrm{sign}(\sigma) = \mathrm{sign}(\ell)$ or $\mathrm{sign}(\sigma) \neq \mathrm{sign}(\ell)$, respectively. In terms of critical points, the electric/magnetic vector field of antiparallel beams at fixed z cycles in time (or along z for fixed time) through sink, source, and center with winding number 1, while the vector field of parallel beams remains a saddle point with winding number -1 as can be seen in Fig. 2 panels b and c, respectively. Out of these two classes, OVs of the antiparallel set differ the most from plane waves, for they may exhibit a magnetic field that dominates over the electric field and strong longitudinal fields' components (Sect. II.C.2).

Another surprising feature is that an OV has a field component along the propagation direction z. Truth is that all real propagating beams (with finite lateral size) possess such a component, otherwise Maxwell's equation $\nabla \cdot \mathbf{E} = 0$ could not be satisfied [Chap. 3 of Novotny (2006)]. But in OVs the longitudinal component can be significant with an intensity overcoming that of the transverse component. Moreover, an $E_z(\mathbf{r})/B_z(\mathbf{r})$ component is required if the light beam has OAM in z, as can easily be deduced from the double vector product in the formula for the angular momentum $\mathbf{L}$ of electromagnetic fields (Cohen-Tannoudji *et al.*, 1989; Jackson, 1999),

$$\mathbf{L} = \frac{1}{\mu_0 c^2} \int \mathbf{r} \times [\mathbf{E}(\mathbf{r}, t) \times \mathbf{B}(\mathbf{r}, t)] d\mathbf{r}, \qquad (1)$$

using SI units with μ_0 denoting the vacuum permeability and c the vacuum speed of light. After Allen *et al.* (1992) OVs received another colorful name: Twisted light, which makes reference to the skrewlike form of the OV wavefront. Note that this surface of constant phase helps us to visualize the unusual space-dependence of the Poynting vector $\mathbf{S} = \mathbf{E} \times \mathbf{H}$, which seems to twist around the propagation axis. However, the reader should be warned not to relate the circulation of the transverse components of the anti-parallel field with the OAM associated to the beam, since this circulation reverses sense for evolving time or z progression, as seen in Fig. 2b. An alternative formulation for the angular momenta of fields

[1] The phenomenon happens in the whole spectrum, thus a more appropriate name would possibly be "electromagnetic vortex" or "twisted electromagnetic field".
[2] Singularities can also exist in the polarization.
[3] Note that the term "singularity" does not refer here to mathematical infinities.
[4] If not otherwise stated, singularity will refer hereafter to a phase singularity.

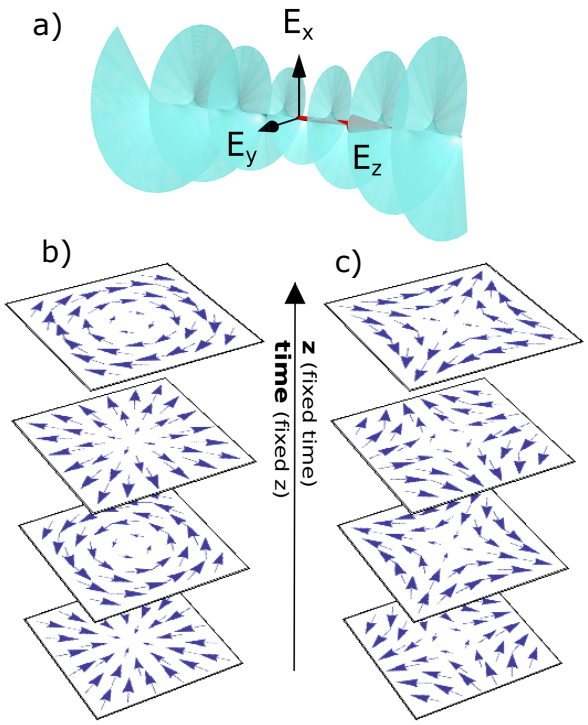

FIG. 2 (color online) Optical vortex, a highly inhomogeneous light field: a) Helical or skrewed wavefront for a circularly-polarized OV with topological charge $\ell = 1$ propagating along z: electric field components are shown, and the atypically strong longitudinal component is stressed in red. Lower panel: Snapshot succession in time/z-coordinate of electric field maps (E_x, E_y) normal to the propagation direction for (b) antiparallel-AM and (c) parallel-AM beams. Antiparallel-AM fields cycle in time/z through sink-center-source to finally reverse sense; what flows in a definite direction around the vortex is in fact the energy (Poynting vector) (Dennis *et al.*, 2009). On the other hand, parallel-AM fields remain saddle critical points.

is possible if the Poynting vector in Eq. (1) is replaced by the canonical momentum; this change unveils interesting phenomena related to the transverse component of the OAM and SAM as described by Bliokh and Nori (2015).

To formalize the ideas above and arrive at full expressions for OV fields we consider, in cylindrical (Sect. II.C) or other non-Cartesian coordinate systems (Sect. II.D), Maxwell's equations, their potentials or the corresponding wave equations in free space.

For electromagnetic fields in vacuum the wave equation is easily derived from Maxwell's equations: Take the curl of Faraday's law ($\nabla \times \mathbf{E} = -\partial_t \mathbf{B}$), use Ampère's law ($\nabla \times \mathbf{B} = \mu_0 \epsilon_0 \partial_t \mathbf{E}$) to eliminate the magnetic field $\mathbf{B}$ and simplify the expression using the absence of sources ($\nabla \cdot \mathbf{E} = 0$ and $\nabla \cdot \mathbf{B} = 0$) together with the identity $\nabla \times (\nabla \times \mathbf{E}) = \nabla(\nabla \cdot \mathbf{E}) - \nabla^2 \mathbf{E}$, leads to

$$\nabla^2 \mathbf{E}(\mathbf{r}, t) - \frac{1}{c^2} \frac{\partial^2}{\partial t^2} \mathbf{E}(\mathbf{r}, t) = 0 \,, \tag{2}$$

with $c^2 = (\mu_0 \epsilon_0)^{-1}$, ϵ_0 being the vacuum permittivity, and the same equation for the magnetic field $\mathbf{B}$. Because the equations are linear (and thus the superposition of fields is possible), one can look for harmonic solutions proportional to $\exp(-i\omega t)$; alternatively, one can assume separability of the space and time dependence of the electric field and split Eq. (2). Then we arrive at the Helmholtz equation

$$\nabla^2 \mathbf{E}(\mathbf{r}, t) + k^2 \mathbf{E}(\mathbf{r}, t) = 0 \,, \tag{3}$$

with $k = \omega/c$ being the absolute value of the wave vector. Like all partial differential equations the Helmholtz equation has a variety of different solutions, reflecting different geometries and boundary conditions.

Let us first concentrate on exact solutions of the Helmholtz equation. We are interested in light fields propagating in z-direction. Propagation-invariant fields –also called non-diffracting beams– are then characterized by an electric field of the form

$$\mathbf{E}(\mathbf{r}, t) = \tilde{\mathbf{E}}(\mathbf{r}_\perp) e^{i(q_z z - \omega t)} + \text{c.c.} \,, \tag{4}$$

with $\mathbf{r}_\perp$ a position vector orthogonal to the propagation direction, c.c. denoting the complex conjugate and $\tilde{\mathbf{E}}(\mathbf{r}_\perp)$ satisfying a two-dimensional Helmholtz equation

$$\nabla_\perp^2 \tilde{\mathbf{E}}(\mathbf{r}_\perp) + \left(k^2 - q_z^2\right) \tilde{\mathbf{E}}(\mathbf{r}_\perp) = 0 \,, \tag{5}$$

where $\nabla_\perp^2$ is the transverse Laplacian operator. It is known that this equation can be further separated in four different types of coordinates: Cartesian, polar, parabolic and elliptic coordinates, leading to plane waves, Bessel beams, Weber beams and Mathieu beams, respectively. We will discuss in particular polar coordinates (Bessel and LG beams) in more detail below and also briefly comment on elliptical coordinates (Mathieu beams) in Sect. II.D.

In addition to the Helmholtz equation the electric field has to satisfy the Maxwell equation $\nabla \cdot \mathbf{E} = 0$. As a consequence, the transverse components $\tilde{\mathbf{E}}_\perp(\mathbf{r}_\perp)$ can be independently chosen among the solutions of the Helmholtz equation, the longitudinal component is then determined as

$$\tilde{E}_z(\mathbf{r}_\perp) = \frac{i}{q_z} \nabla_\perp \cdot \tilde{\mathbf{E}}_\perp(\mathbf{r}_\perp) \,, \tag{6}$$

which again shows that a space dependence of the transverse components in general is associated with a longitudinal component.

Propagation-invariant beams have the advantage of being exact solutions of the Helmholtz equation. However, they have the practical drawback of exhibiting only a weak (e.g., in the case of Bessel beams) or even no (in the case of plane waves) lateral decay. Therefore they are not normalized and carry infinite energy. Consequently, they can only be approximations to real light beams. Any

light beam created in an experiment has a finite lateral extent. Most prominent examples are Gaussian beams which, however, are not propagation invariant but experience diffraction. From Fraunhofer diffraction theory for a slit with width w_0 it is known that the width w of the central maximum (i.e., the distance between the first diffraction minima) in the far field grows with distance z according to $w/w_0 = 2\lambda z/w_0^2 = 4\pi z/(kw_0^2)$, with $\lambda = 2\pi/k$ being the wavelength. Thus, there is a characteristic length, the diffraction length $l = kw_0^2$ (Lax *et al.*, 1975) or the Rayleigh range $z_R = \frac{1}{2}l$ (Loudon, 2003), which describes the length scale on which a Gaussian beam with minimal radius w_0, called the beam waist, widens. The beam is therefore characterized by three different length scales, the wavelength λ, the beam waist w_0 and the diffraction length l. If a beam satisfies the condition $w_0 \ll l$, it is weakly divergent or, in other words, it only consists of plane wave components with wave vectors close to the beam axis. Such beams are called *paraxial beams*. Note that according to the definition of the diffraction length the condition $w_0 \ll l$ also implies $\lambda \ll w_0$. To quantify the divergence of the beam a paraxial parameter f can be defined according to

$$f = \frac{w_0}{l} = \frac{1}{w_0 k}\,. \tag{7}$$

Following Lax *et al.* (1975), this parameter can be used as an expansion parameter for beams not deviating too much from the paraxial limit. The electric field is then written as

$$\mathbf{E}(\mathbf{r},t) = \tilde{\mathbf{E}}(\mathbf{r})e^{i(kz-\omega t)} + \text{c.c.}. \tag{8}$$

Note the difference compared to the ansatz in Eq. (4) referring to non-diffracting beams: Here, $\tilde{\mathbf{E}}(\mathbf{r})$ depends on all three coordinates and the propagation term has the full wave vector $k = \omega/c$. Using the fact that in the transverse directions $\tilde{\mathbf{E}}(\mathbf{r})$ varies on a length scale w_0, while in the longitudinal direction the respective length scale is l, the field can be expanded in a power series in f. Separating the field envelope into transverse ($\tilde{\mathbf{E}}_\perp$) and longitudinal ($\tilde{E}_z\hat{\mathbf{z}}$) parts, it can be shown that the transverse (longitudinal) components of the field come only in even (odd) powers of f (Lax *et al.*, 1975). The zeroth order term then corresponds to the extreme paraxial approximation of a completely transverse beam, satisfying the paraxial wave equation

$$\nabla_\perp^2 \tilde{\mathbf{E}}_\perp(\mathbf{r}) + 2i\,k\,\partial_z \tilde{\mathbf{E}}_\perp(\mathbf{r}) = 0. \tag{9}$$

Typical solutions of the paraxial wave equation are Hermite-Gaussian beams, which factorize in Cartesian coordinates (x, y), and Laguerre-Gaussian beams, which factorize in cylindrical coordinates (r, φ). We will come back in particular to Laguerre-Gaussian modes below.

The longitudinal component in first order of the paraxial parameter is again obtained from the divergence equation for the electric field leading to

$$\tilde{E}_z(\mathbf{r}) = if w_0 \nabla_\perp \cdot \tilde{\mathbf{E}}_\perp(\mathbf{r}). \tag{10}$$

For the construction of higher order terms we refer to Lax *et al.* (1975).

In electrodynamics and optics it is often convenient to introduce potentials, because in this way the homogeneous Maxwell equations are automatically fulfilled. Electromagnetic potentials are per se ambiguous due to gauge invariance (Jackson, 1999): a particular pair of electric $\mathbf{E}$ and magnetic $\mathbf{B}$ fields relates to a family of pairs of vector $\mathbf{A}$ and scalar Φ potentials through

$$\mathbf{E}(\mathbf{r},t) = -\partial_t \mathbf{A}(\mathbf{r},t) - \nabla\Phi(\mathbf{r},t)\,, \tag{11a}$$
$$\mathbf{B}(\mathbf{r},t) = \nabla \times \mathbf{A}(\mathbf{r},t)\,. \tag{11b}$$

Besides the standard scalar and vector potentials also Hertz vector potentials can be used (Wang *et al.*, 2016), but they are less common and we will not discuss them further. Members of the family of potentials differ from each other by scalar functions χ and, starting from an initial pair $(\mathbf{A}^{(1)}, \Phi^{(1)})$, another pair $(\mathbf{A}^{(2)}, \Phi^{(2)})$ within the family is obtained by the gauge transformation

$$\mathbf{A}^{(2)}(\mathbf{r},t) = \mathbf{A}^{(1)}(\mathbf{r},t) + \nabla\chi(\mathbf{r},t)\,, \tag{12a}$$
$$\Phi^{(2)}(\mathbf{r},t) = \Phi^{(1)}(\mathbf{r},t) - \partial_t\chi(\mathbf{r},t)\,, \tag{12b}$$

(the superscripts will be omitted when the gauge is understood). To work with potentials one chooses a particular gauge that suits the needs. The two most used ones, both fixing the divergence of the vector potential[5], are the Coulomb gauge

$$\nabla \cdot \mathbf{A}(\mathbf{r},t) = 0\,, \tag{13}$$

and the Lorenz gauge

$$\nabla \cdot \mathbf{A}(\mathbf{r},t) + \frac{1}{c^2}\frac{\partial\Phi(\mathbf{r},t)}{\partial t} = 0\,. \tag{14}$$

Far away from sources, i.e., in the regime mostly studied here, in the Coulomb gauge the scalar potential vanishes, the gauge is then also called radiation gauge. This is usually the starting point for the quantization of electromagnetic fields in quantum optics. In both gauges the potentials are still not completely determined by the gauge conditions [see Chap. 6 of Jackson (1999)]. In the Coulomb gauge any time-independent gauge field $\chi(\mathbf{r})$ satisfying the Laplace equation $\nabla^2\chi(\mathbf{r}) = 0$ leads again to potentials satisfying the Coulomb gauge. In the Lorenz gauge any gauge function $\chi(\mathbf{r},t)$ satisfying the homogeneous wave equation $(\nabla^2 - c^{-2}\partial_{tt})\chi(\mathbf{r},t) = 0$ leads again to potentials satisfying the Lorenz gauge.

[5] The curl of the vector potential is already fixed by definition (11b).

In particular, choosing a gauge function according to $\partial_t\chi(\mathbf{r},t) = \Phi^{(1)}(\mathbf{r},t)$ leads also in the Lorenz gauge to potentials satisfying $\Phi^{(2)} = 0$ and $\nabla\cdot\mathbf{A}^{(2)} = 0$, which agrees with the Coulomb gauge condition. On the other hand, choosing a gauge function with $\partial_z\chi(\mathbf{r},t) = -A_z^{(1)}(\mathbf{r},t)$ results in potentials with a vanishing longitudinal component of the vector potential, i.e., $\mathbf{A}_z^{(2)} = 0$.

The vector potential in Coulomb and Lorenz gauges and the scalar potential in Lorenz gauge satisfy in free space the same homogeneous wave equation (2) as the electric and magnetic fields. Therefore, everything that has been stated above for the electric field concerning exact and propagation-invariant solutions as well as regarding the paraxial approximation remains valid also for the potentials. In particular, for monochromatic potentials with time dependence $\sim \exp(-i\omega t)$ in the zeroth order of the paraxial approximation the transverse components of the vector potential, both in Coulomb and Lorenz gauges, satisfy the paraxial wave equation

$$\nabla_\perp^2\tilde{\mathbf{A}}_\perp(\mathbf{r}) + 2ik\,\partial_z\tilde{\mathbf{A}}_\perp(\mathbf{r}) = 0. \tag{15}$$

The longitudinal component A_z (in the case of $\Phi = 0$) and the scalar potential Φ (in the case of $A_z = 0$) are of first order in the paraxial parameter and satisfy

$$\tilde{A}_z(\mathbf{r}) = if w_0\nabla_\perp\cdot\tilde{\mathbf{A}}_\perp(\mathbf{r}) \quad \text{if} \quad \Phi = 0, \tag{16a}$$
$$\tilde{\Phi}(\mathbf{r}) = -if c w_0\nabla_\perp\cdot\tilde{\mathbf{A}}_\perp(\mathbf{r}) \quad \text{if} \quad A_z = 0. \tag{16b}$$

Due to the gauge invariance there is no unique way to derive OVs through vector potentials. When looking into the literature, in paraxial optics it is more likely to find derivations in terms of the Lorenz gauge with vanishing A_z (Allen *et al.*, 1992; Dávila Romero *et al.*, 2002; Loudon, 2003), while in non-paraxial optics it is more common to find work using the Coulomb gauge with $\Phi = 0$ (Jáuregui, 2004; Matula *et al.*, 2013; Volke-Sepulveda *et al.*, 2002).

Typically, the derivation starts from a guess on the form of the transverse component $\mathbf{A}_\perp$ of the vector potential. The remaining components (Φ in the case of $A_z = 0$ and A_z in the case of $\Phi = 0$) are then fixed either by the exact gauge condition (in non-paraxial optics) or by Eq. (16) when working in the paraxial approximation. A generalization scheme inspired by the two aforementioned procedures was developed in Quinteiro *et al.* (2019b), and we will further discuss it in Sect. II.C.2 to derive general Bessel beams; a discussion on Laguerre-Gaussian beams is given in Quinteiro *et al.* (2019b). Once scalar and vector potentials are obtained, electric and magnetic fields result from Eqs. (11).

Thus far we have treated the electromagnetic field as a classical quantity. A quantum point of view is indeed necessary in specific problems of OV-condensed matter interaction, e.g., in polariton physics (Sect. IV.B) or if the photon statistics comes into play. Quantization of the fields is usually performed in the Coulomb gauge. Without going into the details at this point of our discussion, it is worth reminding some correspondences between the viewpoint of light waves and photons that help navigate through the literature. A circularly polarized field with handedness $\sigma = \pm1$ is formed out of photons with definite helicity $\sigma = \pm1$ and SAM $\hbar\sigma$ –sometimes called intrinsic AM. And a paraxial classical OV with topological charge ℓ is formed out of photons with OAM $\hbar\ell$, a fact that was verified in a number of experiments (Arnaut and Barbosa, 2000; Courtial *et al.*, 1997; Mair *et al.*, 2001) and is of most relevance for studies on single-photon OV-matter interaction (Sect. IV).

Finally, OVs are not restricted to the visible region of the electromagnetic spectrum and interesting research and applications have been done in other spectral regions, see Sects. II.H and V.C.

C. Single-singularity fields

The family of OVs embraces all sorts of fields with single and multiple phase singularities. Single-singularity fields have been by far the most studied ones, and they also are the easiest to analyze. In the following we describe the two most important cases in cylindrical coordinates: (*i*) Laguerre-Gaussian beams as solutions of the paraxial wave equation, and (*ii*) Bessel beams as solutions of the full wave equation, but also solutions of the paraxial wave equation. Because of its relevance in past and current research in general and singular optics we start from case (*i*), despite it describing an approximate situation.

1. Laguerre-Gaussian beams

Beams with finite lateral extension are obtained as solutions of the paraxial wave equation. In the lowest, i.e., zeroth order of the paraxial parameter f electric and magnetic fields as well as the vector potential are purely transverse and they are described by the paraxial wave equation (9) or (15). Introducing a scalar mode function $u(\mathbf{r})$ we can write

$$\mathbf{A}(\mathbf{r},t) = \mathbf{A}_0 u(\mathbf{r}) e^{i(kz-\omega t)} + \text{c.c.} \tag{17}$$

with a two-dimensional constant vector $\mathbf{A}_0$. The important case of a well-defined intrinsic (or spin) AM is realized for circularly polarized beams with $\mathbf{A}_0 = A_0\mathbf{e}_\sigma$. The electric and magnetic fields have the same structure, only with $\mathbf{A}_0$ replaced by $\mathbf{E}_0 = i\omega\mathbf{A}_0$ and $\mathbf{B}_0 = ik\hat{\mathbf{z}}\times\mathbf{A}_0$ (note that the terms resulting from $\partial_z u(\mathbf{r})$ are of higher order in the paraxial parameter). The mode function satisfies the paraxial wave equation. A factorization in Cartesian coordinates (x, y) leads to the Hermite-Gaussian modes, while the –for our purposes more relevant– factorization

in polar coordinates (r, φ) leads to the Laguerre-Gaussian modes (Barnett *et al.*, 2017)

$$u(\mathbf{r}) = \sqrt{\frac{2p!}{\pi(p+|\ell|)!}} \frac{1}{w(z)} \left(\frac{r\sqrt{2}}{w(z)}\right)^{|\ell|} e^{i\ell\varphi} e^{i\psi(z)} \times L_p^{|\ell|}\left(\frac{2r^2}{w^2(z)}\right) \exp\left[-\frac{r^2}{w^2(z)}\right] \exp\left[-ik\frac{r^2}{2R(z)}\right], \quad (18)$$

where $w(z) = w_0\sqrt{1+(z/z_R)^2}$ is the beam radius, $R(z) = z[1+(z_R/z)^2]$ is the radius of curvature of the wavefront, $\psi(z) = -(|\ell|+2p+1)\arctan(z/z_R)$ is the Gouy phase and $L_p^{|\ell|}$ is a generalized Laguerre polynomial. The parameters w_0 and $z_R = \frac{1}{2}kw_0^2$ are the already mentioned beam waist and the Rayleigh range, respectively. This expression for the mode function shows that LG beams are fields with a single singularity located at $r = 0$ and with topological charge ℓ.

In the lowest order of the paraxial approximation the fields are completely transverse. This is nevertheless inconsistent with real beams with finite width, whose rays travel –at least slightly– at an angle. When a beam diverges/converges a longitudinal component of the field necessarily exists. This component is restored in the first order correction to the paraxial beam according to Eqs. (16). Using the Lorenz gauge with $A_z = 0$ (Loudon, 2003), a scalar potential is obtained according to

$$\Phi(\mathbf{r}, t) = -ifcw_0 e^{i(kz-\omega t)} \mathbf{A}_0 \cdot \nabla_\perp u(\mathbf{r}), \quad (19)$$

leading to a longitudinal component of the electric field

$$\begin{aligned} E_z(\mathbf{r}, t) &= -\partial_z \Phi(\mathbf{r}, t) \\ &= -ce^{i(kz-\omega t)} \mathbf{A}_0 \cdot \nabla_\perp u(\mathbf{r}), \end{aligned} \quad (20)$$

where we have used $f = (w_0 k)^{-1}$ [see Eq. (7)].

A calculation based on the angular momentum density (Cohen-Tannoudji *et al.*, 1989; Jackson, 1999) of the field $u_0(r, z)e^{i\ell\varphi}$ reveals that the ratio of AM in the z-direction to energy is $J_z/W = \ell/\omega + \sigma/\omega$. The separation between spin and orbital AM and what it suggests about the quantization of the OAM (take the energy W being that of a photon $\hbar\omega$) is a delicate matter, and the reader is referred to Sect. 2 of Allen *et al.* (1999).

2. Bessel beams

The Helmholtz Eq. (3) written in cylindrical coordinates is separable. The equations in the angle φ and longitudinal z coordinates are simply solvable by complex exponential functions; the equation for the radial r coordinate is Bessel's differential equation (Arfken and Weber, 1999), for which the solutions and their properties have been extensively studied (Korenev, 2002). Bessel beams (Durnin *et al.*, 1987) have their own benefits, they: (*i*) retain their spatial profile on propagation and are therefore also called non-diffracting beams, (*ii*) describe non-paraxial fields and are therefore valid for any values of the beam parameters, (*iii*) are mathematically simpler than LG beams, (*iv*) have the simplest modal decomposition (Sect. II.F). However, and as it happens with plane waves, they are not realizable in the real world, since they decay very slowly in the radial direction and therefore carry infinite energy.

We now derive Bessel beams by a scheme mentioned in Sect. II.B that uses potentials (Quinteiro *et al.*, 2019b). Let us look for the solution of the Helmholtz equation for the transverse component of the vector potential. Assuming a monochromatic field and circular polarization of the transverse part the solution reads

$$\mathbf{A}_\perp(\mathbf{r}, t) = A_0 J_\ell(q_r r) e^{i\ell\varphi} e^{i(q_z z-\omega t)} \mathbf{e}_\sigma + \text{c.c.}, \quad (21)$$

in which $J_\ell(q_r r)$ is a Bessel functions of the first kind of order ℓ, the latter denoting the topological charge, $q_r = \sqrt{k^2 - q_z^2}$ with the inverse q_r^{-1} being related to the beam waist, and $\mathbf{e}_\sigma$ is the circular polarization vector. As discussed above, this transverse part has to be complemented by a longitudinal component and/or a scalar potential to satisfy the gauge condition. Using the Lorenz condition we get

$$\nabla_\perp \cdot \mathbf{A}_\perp(\mathbf{r}, t) + \partial_z A_z(\mathbf{r}, t) + \frac{1}{c^2}\partial_t \Phi(\mathbf{r}, t) = 0. \quad (22)$$

While in the previous discussions we have always taken either A_z or Φ to be zero, a more general choice is

$$\partial_z A_z^{(\gamma)}(\mathbf{r}, t) = -\gamma \nabla_\perp \cdot \mathbf{A}_\perp(\mathbf{r}, t), \quad (23a)$$

$$\Phi^{(\gamma)}(\mathbf{r}, t) = -i(1-\gamma)\frac{c^2}{\omega} \nabla_\perp \cdot \mathbf{A}_\perp(\mathbf{r}, t) \quad (23b)$$

with a real parameter $0 \leq \gamma \leq 1$. Obviously, $\gamma = 1$ and $\gamma = 0$ restore the abovementioned limiting cases of only A_z or only Φ. From Eq. (21) $\nabla_\perp \cdot \mathbf{A}_\perp$ is determined. Finally, using Eqs. (11) as well as the separation of the propagating part according to Eq.(4), the electromagnetic fields are obtained as

$$\tilde{\mathbf{E}}^{(\gamma)}(\mathbf{r}) = iE_0\Bigg\{ J_\ell(q_r r)e^{i\ell\varphi}\mathbf{e}_\sigma - \frac{1-\gamma}{2}\left(\frac{q_r}{k}\right)^2\left[J_\ell(q_r r)e^{i\ell\varphi}\mathbf{e}_\sigma - J_{\ell+2\sigma}(q_r r)e^{i(\ell+2\sigma)\varphi}\mathbf{e}_{-\sigma}\right] - i\sigma\frac{q_r(q_z^2+\gamma\, q_r^2)}{\sqrt{2}q_z k^2}J_{\ell+\sigma}(q_r r)e^{i(\ell+\sigma)\varphi}\hat{\mathbf{z}}\Bigg\}, \tag{24a}$$

$$\tilde{\mathbf{B}}^{(\gamma)}(\mathbf{r}) = \sigma B_0\Bigg\{ J_\ell(q_r r)e^{i\ell\varphi}\mathbf{e}_\sigma + \frac{\gamma}{2}\left(\frac{q_r}{q_z}\right)^2\left[J_\ell(q_r r)e^{i\ell\varphi}\mathbf{e}_\sigma + J_{\ell+2\sigma}(q_r r)e^{i(\ell+2\sigma)\varphi}\mathbf{e}_{-\sigma}\right] - i\sigma\frac{q_r}{\sqrt{2}q_z}J_{\ell+\sigma}(q_r r)e^{i(\ell+\sigma)\varphi}\hat{\mathbf{z}}\Bigg\}, \tag{24b}$$

with $E_0 = \omega A_0$ and $B_0 = q_z A_0$. This is actually a family of beams. Some interesting choices are: (i) $\gamma = 1$: Close to $r = 0$ for $q_r/q_z \simeq 1$ (i.e., in the strongly non-paraxial regime) the magnetic field may surpass the electric field (Sect. IV.A) while the transverse part of the electric field has a well-defined circular polarization; (ii) $\gamma = 0$: Now the electric field dominates close to the beam center while the transverse part of the magnetic field has a well-defined circular polarization; (iii) $\gamma = \gamma_s = (1+k/q_z)^{-1}$: The ratio between the magnitudes of electric and magnetic fields resembles that of plane waves (Bliokh *et al.*, 2010; Li, 2009). Another family of beams related to Eqs. (24) can be easily obtained from duality, i. e., the replacement of $E \to -cB$ and $B \to E/c$ (Anderson and Arthurs, 1990; Mignaco, 2001).

It should be noted that the potentials of Eq. (23) for different values of γ are not related by a gauge transformation, as is obvious from the fact that the electric and magnetic fields depend on γ. For each value of γ gauge functions χ can be found that either remove Φ or A_z. These gauge transformation will then modify the transverse components $\mathbf{A}_\perp$ of the vector potential [Eq. (21)] in such a way that they also contain counter-circular contributions $\sim \mathbf{e}_{-\sigma}$ with different topological charges.

The fields of Eqs. (24) are characterized by a single singularity at $r = 0$ but with varying topological charges for different parts and components. Several interesting features of such fields, like the mixing of orbital and spin AM or the appearance of longitudinal components, will be discussed in Sect. IV when needed; for more details the reader is also referred to Quinteiro *et al.* (2015, 2017b, 2019b), and references therein.

D. Multiple-singularity fields

Simple solutions to the paraxial or full wave equation are LG and Bessel beams, that present a single singularity at the beam axis located at $r = 0$. More complex fields can of course be built by using the superposition principle; for example, adding two LG beams whose optical axes are parallel but displaced by a distance such that there is essentially no overlap would result in a two-singularity field. However, a different approach based on the fact that, as already mentioned, the wave equation is separable also in other coordinates than in Cartesian and cylindrical coordinates, can be applied. In particular, the solution of the wave equation –both of the exact and the paraxial one– in elliptical coordinates (ξ, η, z) leads to yet another class of elementary beams, among which there are beams that exhibit multiple phase singularities (Alpmann *et al.*, 2010; Gutiérrez-Vega *et al.*, 2000; Gutierrez-Vega *et al.*, 2001; Hernández-Hernández *et al.*, 2010; Mathieu, 1868; Pabon *et al.*, 2017; Shen *et al.*, 2019).

Elliptical and Cartesian coordinates are related by the transformation $x = h\cosh(\xi)\cos(\eta)$, $y = h\sinh(\xi)\sin(\eta)$ with $0 \le \xi < \infty$ and $0 \le \eta < 2\pi$ with curves of constant ξ being ellipses. Due to the separability of the Helmholtz equation (5) solutions are given in the form of products of radial and angular parts, i.e., $\tilde{\mathbf{E}}(\xi,\eta) = \mathbf{E}_0 R(\xi)\Theta(\eta)$ with R and Θ satisfying Mathieu differential equations

$$\frac{d^2R(\xi)}{d\xi^2} - [a - 2b\cosh(2\xi)]R(\xi) = 0, \tag{25a}$$

$$\frac{d^2\Theta(\eta)}{d\eta^2} + [a - 2b\cos(2\eta)]\Theta(\eta) = 0. \tag{25b}$$

Here, a is the separation constant and b is proportional to the ellipticity. These solutions are called Mathieu beams. They present a greater variety of situations, from solutions with single singularities to solutions with multiple singularities. Figure 3 compares a LG beam (single singularity) with a particular Mathieu beam with two singularities on the horizontal axis.

E. Paraxial versus non-paraxial beams

Propagation invariant beams like plane waves, Bessel or Mathieu beams are solutions to both the exact and the paraxial wave equation. In contrast, LG beams as an example of beams with a finite width have only been obtained from the paraxial wave equation. In this section we will take a closer look at the relation between

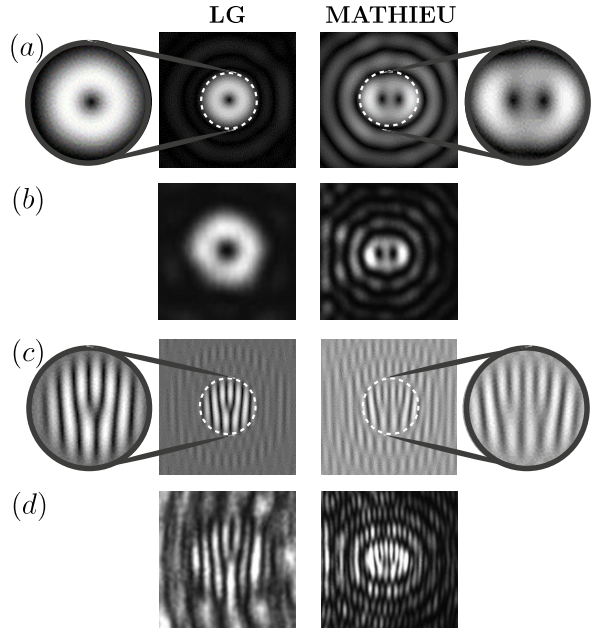

FIG. 3 LG and Mathieu beams. (a) and (c) show numerical simulations of LG (left) and Mathieu (right) beams: (a) single beam intensity and (c) interference pattern with a reference Gaussian beam. (b) and (d) experimental results corresponding to single beam intensity and interference with a Gaussian beam, respectively. The single beam images show a single (LG) or double (Mathieu) zero-intensity point, while the interference images present the characteristic single (LG) or double (Mathieu) fork-like pattern. First and fourth columns are zoom-in's of (a) and (c). Adapted from Pabon *et al.* (2017).

beams described by the full Helmholtz equation and by the paraxial wave equation. We will consider a generic transverse component of the electromagnetic field or the vector potential with a harmonic time dependence according to $\psi(\mathbf{r})\exp(-i\omega t)$, where $\psi(\mathbf{r})$ describes the spatial profile of the wave.

Normalized transverse eigenmodes $v_n(\mathbf{r}_\perp)$ of both the Helmholtz and the paraxial wave equation are given by solutions of the eigenvalue equation

$$-\nabla_\perp^2 v_n(\mathbf{r}_\perp) = q_n^2 v_n(\mathbf{r}_\perp) \tag{26}$$

with eigenvalues q_n^2, where q_n corresponds to a characteristic transverse wave vector of the mode n. Depending on the symmetry, the eigenfunctions can be plane waves in the transverse directions, Bessel functions times $\exp(i\ell\varphi)$, products of Mathieu functions or also other functions that do not factorize in the two transverse coordinates. Propagation-invariant beams are characterized by a single transverse eigenmode (or a superposition of degenerate eigenmodes), which explains that they are solutions to both the Helmholtz and the paraxial wave equation. The Bessel beam of Eq. (21), for example, is a solution with $q_n = q_r$.

The transverse modes have to be complemented by longitudinal modes. Here, the difference between the two types of wave equations comes into play. Since the paraxial wave equation is of first order in z there is one longitudinal mode $\sim \exp(iq_z z)$ for a given transverse mode. In contrast, the Helmholtz equation is of second order in z leading to two modes $\sim \exp(\pm iq_z z)$.

Due to the orthogonality and completeness of the mode functions any solution can be expanded into a sum of these modes. For waves satisfying the paraxial wave equation this leads to

$$\psi(\mathbf{r}_\perp, z) = \sum_n C_n v_n(\mathbf{r}_\perp) e^{i\left(k - \frac{q_n^2}{2k}\right)z}. \tag{27}$$

(Note that when inserting Eq. (27) into the paraxial wave equation the factor $\exp(ikz)$ has to be omitted.) The expansion coefficients C_n are obtained in the standard way from the profile at a given z, e.g., $z = 0$, according to

$$C_n = \int v_m^*(\mathbf{r}_\perp)\psi(\mathbf{r}_\perp, 0) d\mathbf{r}_\perp \,. \tag{28}$$

This demonstrates that if the transverse profile at $z = 0$ is given by a transverse eigenmode, the shape remains fixed and the beam is non-diffracting. On the other hand, we can introduce a propagator $G(\mathbf{r}_\perp, z; \mathbf{r}'_\perp, z')$ according to

$$\psi(\mathbf{r}_\perp, z) = \int G(\mathbf{r}_\perp, z; \mathbf{r}'_\perp, z')\psi(\mathbf{r}'_\perp, z') d\mathbf{r}'_\perp \tag{29}$$

with

$$\begin{aligned} G(\mathbf{r}_\perp, z; \mathbf{r}'_\perp, z') &= \sum_n v_n^*(\mathbf{r}'_\perp) v_n(\mathbf{r}_\perp) e^{i\left(k - \frac{q_n^2}{2k}\right)(z - z')} \\ &= \frac{k}{2\pi i\,(z - z')} e^{ik\left[(z-z') + \frac{|\mathbf{r}_\perp - \mathbf{r}'_\perp|^2}{2(z-z')}\right]}, \end{aligned} \tag{30}$$

where the second form is most easily obtained by using plane waves as transverse eigenmodes. Replacing the longitudinal coordinate z by time, this is exactly the propagator for the time-dependent Schrödinger equation for a free particle, which reflects the equivalence of the paraxial wave equation with the time-dependent Schrödinger equation. The widening of a Gaussian beam along z is thus completely equivalent to the broadening of a Gaussian wave packet with increasing time in quantum mechanics.

Let us now turn to the full Helmholtz equation. Here the expansion of a wave in the eigenmodes reads

$$\psi(\mathbf{r}_\perp, z) = \sum_n v_n(\mathbf{r}_\perp)\left[A_n e^{i\sqrt{k^2 - q_n^2}z} + B_n e^{-i\sqrt{k^2 - q_n^2}z}\right].$$

Obviously, now it is not anymore sufficient to know the wave at a given longitudinal position z; instead, also its

derivative with respect to z is needed. The expansion coefficients are obtained from

$$A_n = \frac{1}{2}\int v_n^*(\mathbf{r}_\perp)\left[\psi(\mathbf{r}_\perp,0) + \frac{\partial_z\psi(\mathbf{r}_\perp,0)}{i\sqrt{k^2-q_n^2}}\right]d\mathbf{r}_\perp, \quad (31a)$$

$$B_n = \frac{1}{2}\int v_n^*(\mathbf{r}_\perp)\left[\psi(\mathbf{r}_\perp,0) - \frac{\partial_z\psi(\mathbf{r}_\perp,0)}{i\sqrt{k^2-q_n^2}}\right]d\mathbf{r}_\perp. \quad (31b)$$

The decomposition with these coefficients is valid for arbitrary beam profiles $\psi(\mathbf{r}_\perp,0)$ and $\partial_z\psi(\mathbf{r}_\perp,0)$ at a fixed longitudinal position, here taken to be $z=0$. In particular we find that as soon as there is more than one transverse mode contributing, the beam has necessarily also a counterpropagating ($\sim B_n$) part. We can now ask: When does this profile correspond to a paraxial beam? First, the z-dependence of a paraxial beam is dominated by e^{ikz}, leading to $\partial_z\psi(\mathbf{r}_\perp,0) \approx ik\psi(\mathbf{r}_\perp,0)$. Second, the transverse wave vector is much smaller than the longitudinal one, i.e., $q_n \ll k$ for all modes appearing in the expansion. Under these conditions $B_n \ll A_n$ and $A_n \approx C_n$, i.e., the counterpropagating part becomes negligible and the coefficient of the term propagating in positive z-direction is essentially the same as in the case of the paraxial wave equation. If we furthermore expand in the exponent $\sqrt{k^2-q_n^2} \approx k - q_n^2/2k$ we recover the solution and thus also the propagator of the paraxial wave equation.

We briefly summarize our understanding on paraxial and non-paraxial solutions. A simplified picture relying solely on the paraxial wave equation leads us to interpret paraxiality as a binary property: either a field satisfies the equation or not; in addition, the paraxial solution is disconnected from the exact solution to the Helmholtz equation. Already Lax *et al.* (1975) showed that instead paraxiality is a feature that comes in degrees. In this section, we further demonstrated that simple approximations on a non-paraxial solution reduce it smoothly to a paraxial solution, thus completing the link between both fields.

F. Representing optical vortices by plane waves

Bessel and Laguerre-Gaussian functions each form sets of solutions that can be used to define more complicated fields through superpositions. This is of course also the case for plane waves, that are routinely used as a basis set to build up other functions using Fourier analysis. For problems involving simple OVs with (approximately) cylindrical symmetry, such as single-singularity beams generated in the lab, a mathematical representation is easiest in terms of Bessel, LG, or other cylindrical basis functions. However, there are important situations in which a decomposition of the OV into a plane wave basis becomes necessary, for instance, in the study of reflection and refraction. The celebrated Fresnel's coefficients relate the amplitudes of incident, reflected and refracted plane waves, and thus are unsuitable for a direct use with OVs. Furthermore, this decomposition provides additional insight in the properties of OVs. The representation in terms of plane waves is referred to as a modal decomposition or an angular spectrum representation (Kaiser *et al.*, 2009; Novotny, 2006; Schmidt *et al.*, 2011; Siegman, 1990). Such a decomposition is possible for all relevant fields, $\mathbf{E}$, $\mathbf{B}$, $\mathbf{A}$ and Φ; here we will concentrate on the decomposition of the $\mathbf{E}$-field.

Starting point is the general representation of the spatial part of a vector field by its plane wave (or spatial Fourier) components

$$\mathbf{E}(\mathbf{r}) = \int \mathcal{E}(\mathbf{q})\mathbf{e}_{\mathbf{q}\sigma}e^{i\mathbf{q}\cdot\mathbf{r}}d\mathbf{q}, \quad (32)$$

where $\mathcal{E}(\mathbf{q})$ denotes the Fourier component of the field and $\mathbf{e}_{\mathbf{q}\sigma}$ its polarization vector. Since we only consider monochromatic waves, all plane waves must have the same frequency. Therefore, the absolute value of $\mathbf{q}$ is fixed to $q = k = \omega/c$. Using spherical coordinates (q,θ_q,φ_q), only integrals over the angles θ_q and φ_q remain.

To be specific, let us concentrate in the following on propagation-invariant beams traveling in z-direction. These beams have a well-defined longitudinal wave vector q_z and thus, since $\cos\theta_q = q_z/k$, a well-define θ_q, such that only the integral over φ_q remains. Fixing θ_q fixes also the perpendicular wave vector $q_r = k\sin\theta_q$. Using cylindrical coordinates (q_r,φ_q,q_z) and (r,φ,z), we have

$$\begin{aligned}\mathbf{q}\cdot\mathbf{r} &= q_r r\left(\cos\varphi_q\cos\varphi + \sin\varphi_q\sin\varphi\right) + q_z z \\ &= q_r r\cos(\varphi_q-\varphi) + q_z z\,, \end{aligned} \quad (33)$$

leading to the decomposition of a propagation-invariant beam according to

$$\mathbf{E}(\mathbf{r}) = e^{iq_z z}\int_0^{2\pi}\tilde{\mathcal{E}}(\varphi_q)\mathbf{e}_{\mathbf{q}\sigma}e^{iq_r r\cos(\varphi_q-\varphi)}d\varphi_q. \quad (34)$$

The beam therefore represents a superposition of plane waves with wave vectors $\mathbf{q}$ lying on the surface of a cone around the propagation direction $\hat{\mathbf{z}}$. To specify the beam, we have to fix the angle dependence $\tilde{\mathcal{E}}(\varphi_q)$ and the polarization vectors $\mathbf{e}_{\mathbf{q}\sigma}$ of the plane wave components.

As an example, let us decompose the electric field of Eq. (24a) into plane waves. The electric field has the general form

$$\begin{aligned}\mathbf{E}^{(\gamma)}(\mathbf{r}) = iE_0e^{iq_z z}\Big[&c_\sigma^{(\gamma)}J_\ell(q_r r)e^{i\ell\varphi}\mathbf{e}_\sigma \\ &+c_{-\sigma}^{(\gamma)}J_{\ell+2\sigma}(q_r r)e^{i(\ell+2\sigma)\varphi}\mathbf{e}_{-\sigma} \\ &-i\sigma c_z^{(\gamma)}J_{\ell+\sigma}(q_r r)e^{i(\ell+\sigma)\varphi}\hat{\mathbf{z}}\Big] \end{aligned} \quad (35)$$

with coefficients $c_\sigma^{(\gamma)}$, $c_{-\sigma}^{(\gamma)}$ and $c_z^{(\gamma)}$ as can be deduced from Eq. (24a). Using the Jacobi-Anger identity or the corresponding integral representations of the Bessel functions

[see also their multiple uses in Sect. IV],

$$J_m(q_r r) = \frac{1}{2\pi i^m}\int_0^{2\pi} e^{iq_r r\cos\eta} e^{-im\eta} d\eta\,, \qquad (36)$$

with $\eta = \varphi_q - \varphi$, we can identify the integrand in Eq. (34) as

$$\tilde{\mathcal{E}}(\varphi_q)\mathbf{e}_{\mathbf{q}\sigma} = \frac{iE_0}{2\pi i^\ell} e^{i(\ell+\sigma)\varphi_q}\Big[c_\sigma^{(\gamma)} e^{-i\sigma\varphi_q}\mathbf{e}_\sigma + i^{-2\sigma} c_{-\sigma}^{(\gamma)} e^{i\sigma\varphi_q}\mathbf{e}_{-\sigma} - i\sigma i^{-\sigma} c_z^{(\gamma)}\hat{\mathbf{z}}\Big]. \qquad (37)$$

Using the identities $i^{-2\sigma} = -1$ and $i^{-\sigma} = -i\sigma$, we thus obtain the angle-dependent weight

$$\tilde{\mathcal{E}}(\varphi_q) = (-1)^\ell i^{\ell+1}\frac{\sqrt{N}E_0}{2\pi} e^{i(\ell+\sigma)\varphi_q} \qquad (38)$$

and the polarization vector

$$\begin{aligned}\mathbf{e}_{\mathbf{q}\sigma} &= \frac{1}{\sqrt{N}}\Big[c_\sigma^{(\gamma)} e^{-i\sigma\varphi_q}\mathbf{e}_\sigma - c_{-\sigma}^{(\gamma)} e^{i\sigma\varphi_q}\mathbf{e}_{-\sigma} - c_z^{(\gamma)}\hat{\mathbf{z}}\Big] \\ &= \frac{1}{\sqrt{N}}\Bigg\{\Big[1 - \frac{1-\gamma}{2}\Big(\frac{q_r}{k}\Big)^2\Big] e^{-i\sigma\varphi_q}\mathbf{e}_\sigma \\ &\quad - \frac{1-\gamma}{2}\Big(\frac{q_r}{k}\Big)^2 e^{i\sigma\varphi_q}\mathbf{e}_{-\sigma} - \frac{q_r(q_z^2+\gamma\, q_r^2)}{\sqrt{2}q_z k^2}\hat{\mathbf{z}}\Bigg\}, \end{aligned} \qquad (39)$$

with N being a normalization constant for the polarization vector. In the latter form the explicit expressions for the coefficients from Eq. (24a) have been inserted. According to Eq. (38) plane waves with different angles in the xy-plane indeed contribute with a weight given by a phase factor $\exp(im\varphi_q)$, as might be expected for an OV. The polarization vector $\mathbf{e}_{\mathbf{q}\sigma}$ of Eq. (39) of the plane-wave component traveling in direction $\mathbf{q}$ becomes more transparent when expressed in terms of unit vectors in spherical coordinates (q, θ_q, φ_q), given by

$$\begin{aligned}\mathbf{e}_q &= \hat{\mathbf{x}}\sin\theta_q\cos\varphi_q + \hat{\mathbf{y}}\sin\theta_q\sin\varphi_q + \hat{\mathbf{z}}\cos\theta_q, \\ \mathbf{e}_{\theta_q} &= \hat{\mathbf{x}}\cos\theta_q\cos\varphi_q + \hat{\mathbf{y}}\cos\theta_q\sin\varphi_q - \hat{\mathbf{z}}\sin\theta_q, \\ \mathbf{e}_{\varphi_q} &= -\hat{\mathbf{x}}\sin\varphi_q + \hat{\mathbf{y}}\cos\varphi_q.\end{aligned}$$

Using $\cos\theta_q = q_z/k$, $\sin\theta_q = q_r/k$ and $\mathbf{e}_\sigma = (\hat{\mathbf{x}} + i\sigma\hat{\mathbf{y}})/\sqrt{2}$, the polarization vector (39) can be rewritten as

$$\mathbf{e}_{\mathbf{q}\sigma} = \frac{1}{\sqrt{2N}}\Bigg\{\frac{\cos^2\theta_q + \gamma\sin^2\theta_q}{\cos\theta_q}\mathbf{e}_{\theta_q} + i\sigma\mathbf{e}_{\varphi_q}\Bigg\}. \qquad (40)$$

We notice that, as it should be, all plane wave components are indeed transverse, i.e., they have no component along $\mathbf{e}_q$. Furthermore, all components are in general elliptically polarized. When looking at different values of γ we find: (i) $\gamma = 1$: The major axis of the ellipse is along $\mathbf{e}_{\theta_q}$; (ii) $\gamma = 0$: The major axis of the ellipse is along $\mathbf{e}_{\varphi_q}$; (iii) $\gamma = \gamma_s = \cos\theta_q/(1+\cos\theta_q)$: The beam is a superposition of circularly polarized plane waves as discussed, e.g., by Jentschura and Serbo (2011) and Matula *et al.* (2013). Figure 4 shows the modal recomposition in action producing an OV that captures the qualitative features seen in Fig. 2, interestingly with a superposition of only four plane waves (Dennis *et al.*, 2009).

Laguerre-Gauss modes are not propagation-invariant and thus not characterized by a well-defined q_z. Therefore, their decomposition requires the inclusion of varying q_z (and also q_r), which corresponds to an angular weight function $\mathcal{E}(\theta_q, \varphi_q)$ depending on both the polar and the azimuthal angle (Barnett and Allen, 1994).

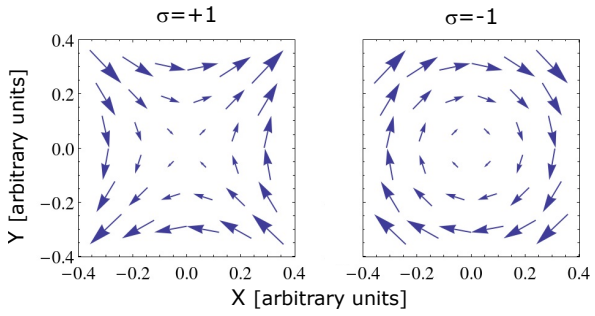

FIG. 4 (color online) Vector fields resulting from the sum of four plane waves, each traveling in a direction $\mathbf{k}$ lying on the surface of the same cone but differing in their relative phase. All four plane waves share the same phase $\ell = 1$, but the polarization is $\sigma = +1$ on the left and $\sigma = -1$ on the right. The composite fields are in perfect qualitative agreement with those calculated as for example, from Eq. (21) and shown in Fig. 2.

The modal decomposition offers an alternative way to study the OV-matter interaction, based on the action of a multitude of plane wave. An example is the treatment of the reflection and refraction of a LG beam impinging at an angle on a dielectric interface to understand the Goos-Hänchen and Imbert-Fedorov effects of OVs (Lusk *et al.*, 2018). Here a LG beam is numerically decomposed into plane waves. The Fresnel coefficients then determine the reflection and transmission of each plane wave, that are finally summed up to yield the complete fields. Another interesting example is that of the electronic excitation in bulk semiconductors in which one may choose to decompose the OV into plane waves to match Bloch electron states, or conversely retain the simplest representation of an OV in terms of Bessel functions and transform the electronic states to cylindrical coordinates (Sect. IV.A.2).

G. Generation and measurement

Optical vortices are by now routinely created in many labs. Various techniques to produce such beams are available. They mostly work by converting a laser output beam into an OV, but there are also ways to directly generate a coherent OV beam (Forbes, 2017; Pan *et al.*, 2020; Seghilani *et al.*, 2016; Yin *et al.*, 2003).

A spiral phase plate is the most intuitive converter (Kotlyar *et al.*, 2005). It is a transparent cylinder with

one of its bases carved into a spiral. A conventional (Gaussian or the like) light beam incident on a base emerges as an OV: geometrically, a ray impinging at a particular position along the surface arc traverses a different optical path than other rays and thus picks a relative phase.

The use of diffraction gratings with dislocations, typically having the shape of a fork, is widely spread (Carpentier *et al.*, 2008). In simple terms, the fringes' design is the pattern resulting from the interference between a plane wave and an OV and printed on a transparent glass; upon illumination by a plane wave (Gaussian beam) different OV beams (orders) are transmitted, with varying topological charge. Fork gratings can also be made to work in reflection. Moreover, a Spatial Light Modulator (SLM) based on high-resolution liquid crystal displays can be used to modulate the beam in real time.

Other alternative techniques are available. A Q-plate is a birefringent liquid crystal, that converts SAM into OAM. Some of its advantages are the high conversion efficiency, easy alignment, and its possible use in a wide range of frequencies (Rubano *et al.*, 2019). As anticipated in Sect. II.A conical diffraction can be used to generate OV beams (Berry *et al.*, 2005; Phelan *et al.*, 2009; Turpin *et al.*, 2016); here the cylindrical beam coming out of the biaxial crystal is a superposition of fields with and without OAM, that can be separated. Another way is to convert Hermite-Gaussian into LG beams with cylindrical lenses (Padgett and Allen, 2002). Metamaterials are also employed to shape beams (Chen *et al.*, 2019; Zhang *et al.*, 2020a). Well suited for photonic applications are microring resonators (Cai *et al.*, 2012; Zhu *et al.*, 2013) and micrometer size lasers that can emit OVs with controllable topological charge and polarization (Miao *et al.*, 2016; Zhang *et al.*, 2020b).

Lastly, we mention that the aforementioned methods focus on creating phase singularities on input beams. The radial profile (LG, Bessel, Mathieu, etc.) has to be further considered and introduced. For example, Bessel beams can be generated using axicons, a conical optical element that transforms the beam into a ring by mapping each source point into the optical axis (Arlt and Dholakia, 2000; Bock *et al.*, 2012; Jaroszewicz *et al.*, 2005; Kazak *et al.*, 1999).

The same ideas and methods just described can be used to measure the topological charge of an unknown field (Chen *et al.*, 2019). The most basic fact one wishes to learn is whether the unknown beam is an OV or not. This one decides by making the beam interfere with another one, either a plane wave (Gaussian) or a spherical wave. With the former (latter) the interference pattern of an OV is that of a fork (spiral) (Carpentier *et al.*, 2008). If the beam is indeed an OV, one can infer the topological charge from the number of bifurcations (arms). As expected, this rudimentary method has been by now much improved by more delicate techniques using: a single cylindrical lens to measure fractional (Alperin *et al.*, 2016) and spectra of (Volyar *et al.*, 2019) OAM, sets of spatial light modulators for real-time measurements (Berkhout *et al.*, 2010), and more.

H. Optical vortices in physics, chemistry and biology

After the work by Allen *et al.* (1992) the subject of OVs blossomed, specially in optics with research on basic theory, generation, and measurement (Allen *et al.*, 2003; Andrews, 2008); and in only few years it was expanding to other areas of physics.

The interaction of OVs with atoms started with theoretical studies on their motion under the torque exerted by LG beams and the transfer of OAM (Allen *et al.*, 1996; Andrews, 2008; Van Enk, 1994), and experimental work on the interaction of an OV with an ensemble of cold cesium atoms (Tabosa and Petrov, 1999). Several other studies followed, deepening the understanding on the basics of absorption of OVs and exploring other properties, such as the exchange of OAM in the interaction with molecules and the role of the dipole-moment approximation (Babiker *et al.*, 2002) the generation of currents (Köksal and Berakdar, 2012), interaction in an atomic Bose-Einstein condensate (Bhowmik *et al.*, 2016; Mondal *et al.*, 2014), the photoexcitation of many-electron atoms (Scholz-Marggraf *et al.*, 2014; Surzhykov *et al.*, 2015), and the photoionization of H_2^+ (Peshkov *et al.*, 2015). These and other works pointed to the expected transfer of OAM to atoms (internal and center-of-mass degrees of freedom) and to the existence of higher than dipolar electronic transitions (Sect. II.A). Schmiegelow *et al.* (2016) provided a direct experimental demonstration of the transfer of OAM to a single trapped ion, with implications on the importance of the longitudinal component of the field (Quinteiro *et al.*, 2017c) (Sect. II.C), the alignment of the beam axis with the atom (Afanasev *et al.*, 2018; Peshkov *et al.*, 2017; Quinteiro *et al.*, 2010) (Sect. IV.A.3.b), and the characteristic length scale associated with the singularity (Sect. VI.B.1). Theoretical work continues describing subwavelength trapping (Schulze *et al.*, 2017), interaction with Rydberg atoms (Mukherjee *et al.*, 2017), the scattering by hydrogenic ions (Peshkov *et al.*, 2018), resonant scattering by fast ions (Serbo *et al.*, 2021), multipolar transitions (Solyanik-Gorgone *et al.*, 2019), Bose-Einstein condensates (Das *et al.*, 2020; Ghosh Dastidar *et al.*, 2022), trapping by counter-propagating beams (Koksal *et al.*, 2020, 2019), and more (Babiker *et al.*, 2018; Franke-Arnold, 2017).

Naturally, the studies in atom-OV interaction have been accompanied by studies in molecules. A primary concern has been to establish whether the OAM of light plays a role in chiral molecule-light interaction, as it is well known with spin AM. Studies pointing in the pos-

itive –OAM does affect chiral matter– (Brullot *et al.*, 2016; Forbes and Andrews, 2018b; Rosales Guzmán, 2015; Woźniak *et al.*, 2019; Ye *et al.*, 2019) and negative (Andrews *et al.*, 2004; Araoka *et al.*, 2005; Babiker *et al.*, 2002; Giammanco *et al.*, 2017; Löffler *et al.*, 2011; Mathevet *et al.*, 2013) direction exist, and the accumulated evidence so far indicates that the effect does take place at the quadrupole electronic transition level (Sect. III.C.1), and can be induced using Bessel beams or tight focusing mixing orbital and spin AM (Monteiro *et al.*, 2009; Zhao *et al.*, 2007) (Sect. II.C.2). Other research into more general properties of OV-molecule interaction were conducted on, for example, the photo-induced currents and magnetic fields in ring-shape molecules (Köksal and Koç, 2017a) and nanocages (Köksal and Koç, 2017b), and twisted excitons in molecules (Zang and Lusk, 2017).

Other fields also profit from OVs. The propagation properties of OVs in a plasma was investigated by Nobahar *et al.* (2019), and Zhang *et al.* (2021) proposed the generation of high-order OV harmonics by irradiating a plasma with a circularly polarized Gaussian beam. Optical vortices out of the visible spectrum have also been investigated. In the ultraviolet regime, they can improve lithography and ablation techniques (Hernández-García *et al.*, 2017; Pabon *et al.*, 2017). Metalenses can generate OVs in microwaves (Zhang *et al.*, 2018) and V-shaped antennas can generate OVs in the terahertz range (He *et al.*, 2013). In the radio frequency regime corresponding studies were conducted (Mohammadi *et al.*, 2010; Thidé *et al.*, 2014, 2007). In astronomy, a so-called vortex coronograph technique can be used to improve imaging of exoplanets (Foo *et al.*, 2005; Serabyn *et al.*, 2010), and there are methods to determine the OAM of light (Berkhout and Beijersbergen, 2008) or the rotation (Lavery *et al.*, 2013; Tamburini *et al.*, 2011) of astronomical sources. In biology, Shi *et al.* (2017) studied the transmission of LG beams through mouse brain tissue to explore possible uses of OVs for imaging purposes. Optical tweezers with OVs can help manipulate biological molecules and structures (Grier, 2003; Otte and Denz, 2020). Also single-cell nanosurgery using OVs are reported to produce in organelles less damage than conventional optical tweezers (Jeffries *et al.*, 2007). Finally, OVs can much improve microscopy, e.g., in biology and nanotechnology, by Stimulated Emission Depletion (STED) (Keller *et al.*, 2007) and other techniques (Ritsch-Marte, 2017).

III. CONDENSED MATTER BASICS

Condensed-matter physics encompasses a vast collection of phenomena in different materials, from liquids to crystalline solids. This review focuses on the interaction of OVs with bulk solids and structured systems like quantum rings, a two-dimensional electron gas either in a quantum well or in modern 2D materials, quantum dots, semiconductor microcavities, dielectric-metal interfaces, and topological insulators. In this section, we discuss the basic physics behind crystals in the bulk and nanostructure forms, their excitations –such as single-particle excitations, excitons, exciton-polaritons, plasmon-polaritons–, and condensed-matter optics including the topics of gauge invariance, the vertical-transition approximation, and dynamics of material excitations.

A. Crystalline solids

A crystal is a solid with well-ordered elementary units, either atoms or collections of atoms, forming a lattice. This periodicity determines much of the electronic structure and single-particle excitations, as well as the dynamics of their collective excitations –excitons, plasmons, phonons, and magnons (Ashcroft and Mermin, 1976; Ibach and Lüth, 2013; Kittel, 1987).

A classification criterion advantageous to discuss optical processes is to separate the set of crystalline solids into insulators, semiconductors and metals, i.e., by their electrical conductivity. The description of electron dynamics in solids was continuously improved in successive steps. Drude (1900) postulated his celebrated model for conduction in metals, in which electrons move according to Newton's laws including the Lorentz force, bounce on fixed and randomly located ions, and thermalize to a classical Maxwell-Boltzmann velocity distribution. The Drude model explained the Hall effect, and combined with experiments it predicted electron relaxation times and mean free paths in metals. Nowadays, it is still an ubiquitous tool in research, and plays, for example, an important role in the theory of surface plasmon polaritons (Sect. IV.C). Sommerfeld (1928) introduced the Fermi-Dirac distribution and the wave nature of electrons through the free electron wave functions $\exp(i\mathbf{k}\cdot\mathbf{r})$, with quasi-momentum $\mathbf{k}$. A significant improvement comes from incorporating the periodicity of the ionic arrangement (Bragg and Bragg, 1913). The general form of the electron wave function in a periodic potential is given by the Bloch theorem (Bloch, 1928), which states that the single-particle wave function $\psi_{b\mathbf{k}}(\mathbf{r})$ can be written as

$$\psi_{b\mathbf{k}}(\mathbf{r}) = \frac{1}{\sqrt{V}} e^{i\mathbf{k}\cdot\mathbf{r}} u_{b\mathbf{k}}(\mathbf{r})\,, \tag{41}$$

with the quasi-momentum $\mathbf{k}$,[6] the band index b and a normalization volume V. The microscopic function $u_{b\mathbf{k}}(\mathbf{r})$ has the periodicity of the lattice and satisfies the orthogonality relation

$$\frac{1}{v}\int_v d\mathbf{r}\, u^*_{b'\mathbf{k}}(\mathbf{r}) u_{b\mathbf{k}}(\mathbf{r}) = \delta_{bb'}\,, \tag{42}$$

[6] Rigorously speaking, the quasi-momentum of the electron is $\hbar\mathbf{k}$.

where the integral runs over a single unit cell with volume v. The electron states are grouped in energy bands with energy $\varepsilon_{b\mathbf{k}}$ (Ashcroft and Mermin, 1976). The Bloch

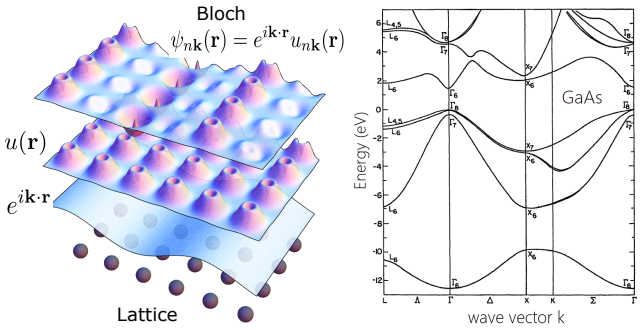

FIG. 5 (color online) In the independent-electron approximation, the single electron states are grouped into energy bands due to their interaction with the lattice. Left: Schematic plot of the Bloch wave functions. Right: Band structure of GaAs, adapted from Cohen and Chelikowsky (2012).

description together with the Fermi-Dirac statistics of the electrons finally achieves a microscopic description of metals, semiconductors and insulators. In conductors, the electronic ground state is characterized by partially-filled energy bands. In contrast, semiconductors and insulators have at zero temperature fully-occupied energy bands separated by a band-gap from empty energy bands, see Fig. 5.

In contrast to the fairly simple solution for energy bands and wave function found in the Bloch model, the many-body problem of electron-electron interactions is of such a complexity that no single solution is known. Instead, approximations to specific situations are applied. Ab-initio calculations of the electronic structure of solids are most often based on the density-functional theory and its variants (Hohenberg and Kohn, 1964; Kohn and Sham, 1965). In the optical excitation of a direct band-gap semiconductor (e.g., GaAs, see Fig. 5), the absorption of light induces the transition of electrons between valence and conduction bands. The mutual interaction between electrons and holes gives rise to quasi-particles called excitons (Frenkel, 1931; Wannier, 1937). Here the essential physics is captured by the dynamical Hartree-Fock approximation –a mean-field approach leading to the semiconductor Bloch equations (Haug and Koch, 2009; Lindberg and Koch, 1988; Rossi and Kuhn, 2002). An alternative approach is based on the Bethe-Salpeter equation for the two-particle correlation function (Albrecht *et al.*, 1998; Drueppel *et al.*, 2018; Onida *et al.*, 2002; Rohlfing and Louie, 1998; Strinati, 1988).

A lattice made out of static ions is clearly unrealistic; not only temperature but also quantum fluctuations cause the ions to move. At low temperatures, every ion undergoes small oscillations around its equilibrium position (lattice site) that lead to the normal modes of vibrations, with dispersion relation $\omega_s(\mathbf{k})$ for branch s and wave vector $\mathbf{k}$. A quantum description yields the picture of phonons as the quanta of crystal vibrations, analogous to photons in quantum electrodynamics (Ashcroft and Mermin, 1976; Ibach and Lüth, 2013).

The spin degree of freedom of electrons and ions plays an important role in optical selection rules and a variety of magnetic phenomena. We will discuss its relevance to OV-crystal interaction in Sect. IV.A.3.a.

The evolution in our understanding of electronic excitations is a neat example of how particles are to be thought of in solid-state physics. In Drude's and Sommerfeld's model electrons are individual particles randomly scattering from individual ions. Incorporating the effect of the whole lattice potential leads to "dressed" states and the corresponding quasi-particles, the Bloch electrons. Incorporating the electron-electron interaction leads to Landau's quasi-particles (Abrikosov *et al.*, 2012) in metals and excitons in semiconductors (Dexter and Knox, 1965).

This process of hybridization of correlated excitations yielding new quasi-particles goes on: including light as a degree of freedom one finds exciton-(Sect. IV.B) and plasmon-(Sect. IV.C) polaritons or, including phonons, one finds polarons. A description based on collective excitations is a clever way to deal with the complexity found in condensed matter, and also hints to the interconnectedness of idealized individual physical units (such as the Sommerfeld electron).

B. Structured systems

Modern technology and condensed matter physics are inextricably intertwined. And the electronic industry based on the solid state has constantly sought device miniaturization, since the invention of the transistor in the late 1940s or even earlier (Mills, 2011), and it has driven intense basic research on small semiconductor, metal, and hybrid structures (see Fig. 6).

The theory of nanoscale ($10^{-9} - 10^{-8}$m) systems is built upon that of the bulk crystal and will be discussed in Sects. III.C.3 and IV.A.1. However, nanostructures exhibit new effects due to their reduced dimensionality, the number of excitations involved, the existence of interfaces, the combination of different materials, etc. that require the reexamination of bulk models. Are the classical and semiclassical (e.g., Drude) models applicable? Can one use thermodynamics for a system with few particles? What assumptions are not valid for optics at the nanoscale? The result of almost half a century of research is a well-developed understanding of nanostructures that deserves dedicated attention (Bastard, 1988; Ihn, 2010). Section IV discusses in depth the interaction of OVs with structured systems.

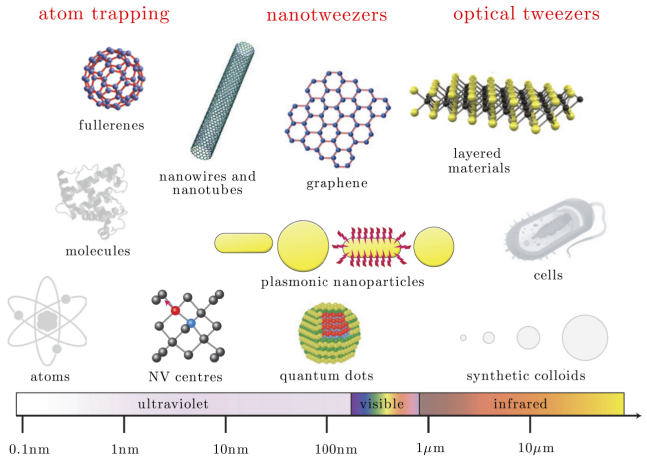

FIG. 6 (color online) Comparison of structures of different types and sizes. From Maragò *et al.* (2013).

C. Condensed-matter optics

Among crystals, semiconductors exhibit the richest response to light in the visible range of the electromagnetic spectrum. Halfway between metals and insulators, the electronic ground state has a completely filled valence (highest occupied energy) band separated from a completely empty conduction (lowest unoccupied energy) band by a few electronVolts. Light in the visible range therefore carries the necessary amount of energy to induce electronic interband transitions between valence and conduction bands. Metals with the Fermi energy lying inside the conduction band and metallic-dielectric hybrid systems present also interesting features. Their interaction with light is to a large extent understandable in terms of the Drude model for electrons in a single band (Sect. IV.C).

The general formulation of light-matter interaction is based on the minimal coupling Hamiltonian, in which the electromagnetic field is described in terms of potentials instead of fields. As discussed in Sect. II.B, potentials are not uniquely defined by the fields, instead different gauges can be chosen. In the analysis of the light-matter interaction the consideration of the problem of gauge invariance is therefore important, in particular in the case of extended systems (solid state bulk or nanostructures) and/or strongly varying electromagnetic fields (Sect. III.C.1). Due to the phase singularities OVs are indeed strongly varying fields; moreover, under certain experimental conditions, the spatial variation can be further enhanced by tight focusing of a free propagating beam or by near-field techniques (Sect. IV.C).

A prevailing model of the interband optical excitation is that of vertical transitions, in which the photon's linear momentum is neglected. However, the vertical transition approximation is incompatible with strongly inhomogeneous light beams such as OVs, and must be thus revisited (Sect. III.C.2).

Finally, the modeling of the dynamics of the optical excitation and the subsequent relaxation and dephasing processes of the generated electronic excitations are discussed in Sect. III.C.3.

1. Gauge invariance

As a starting point for a theoretical description of the light-matter interaction (Cohen-Tannoudji *et al.*, 1989) it is convenient to take the Lagrangian L for a particle of charge q and mass m_0 in the presence of electromagnetic fields represented by scalar (Φ) and vector ($\mathbf{A}$) potentials [see Chap. 1 of Goldstein (1980)]

$$L = \frac{1}{2} m_0 \dot{\mathbf{r}}^2 - V(\mathbf{r}) + q\dot{\mathbf{r}} \cdot \mathbf{A}(\mathbf{r},t) - q\Phi(\mathbf{r},t)\,, \qquad (43)$$

with the electrostatic potential energy V due to the lattice and possibly other static sources and the canonical momentum

$$\mathbf{p} = \frac{\partial L}{\partial \dot{\mathbf{r}}} = m_0 \dot{\mathbf{r}} + q\mathbf{A}(\mathbf{r},t)\,. \qquad (44)$$

By a Legendre transformation $h = \mathbf{p}\cdot\dot{\mathbf{r}} - L$ the so-called minimal coupling Hamiltonian is obtained as

$$h = \frac{1}{2m_0}[\mathbf{p} - q\mathbf{A}(\mathbf{r},t)]^2 + V(\mathbf{r}) + q\Phi(\mathbf{r},t), \qquad (45)$$

which is the key quantity for the transition to a quantum mechanical description. The Hamiltonian is likewise expressed in terms of the electromagnetic potentials instead of fields. This can be a source of troubles in calculations and the interpretation of results, in particular if approximations like the truncation of a basis are performed.

Electromagnetic potentials are auxiliary functions that assist us in the calculations involving the physically real and measurable electric and magnetic fields. Gauge transformations do not change the fields (Sect. II.B): The values of measurable electromagnetic quantities and their dynamics –governed by Maxwell's equations– are unaffected.

When charges enter the picture, one expects to have corresponding invariant equations of motion (EoM) and quantities. The Schrödinger equation for the minimal coupling Hamiltonian is preserved under a gauge transformation if the wave function undergoes a local phase transformation $\psi^{(2)} = T_\chi \psi^{(1)} = \exp(iq\chi/\hbar)\psi^{(1)}$.[7] The Hamiltonian transforms concomitantly by[8] $h^{(2)} = T_\chi h^{(1)} T_\chi^\dagger - q\partial_t \chi$. All other operators

[7] This is also the case in relativistic quantum mechanics with the Dirac equation.

[8] The transformed Hamiltonian can also be written by replacing old by new potentials.

transform according to $O^{(2)} = T_\chi O^{(1)} T_\chi^\dagger$, which ensures that matrix elements and mean values of operators are invariant: $\langle\psi^{(1)}|\, O^{(1)}\, |\varphi^{(1)}\rangle = \langle\psi^{(2)}|\, O^{(2)}\, |\varphi^{(2)}\rangle$. Note the special transformation rules that obeys h –the operator driving the system's dynamics– and the scalar and vector potentials [Eqs. (12)]. A physically meaningful quantity $\mathcal{O}$ should have gauge-invariant eigenvalues of its operator O and it should retain its functional form upon transformation: $O^{(2)} = O^{(1)}(\mathbf{A}^{(2)}, \Phi^{(2)})$ (Scully and Zubairy, 1997). Examples of physical and non-physical quantites are the mechanical ($\boldsymbol{\pi} = \mathbf{p} - q\mathbf{A}$) and canonical ($\mathbf{p} = -i\hbar\nabla$) momenta, respectively. Evidently, the Hamiltonian Eq. (45) is not a physical operator, but by excluding the scalar potential one gets a physical operator called the instantaneous energy (Yang, 1976). Nor is $h_0 = \mathbf{p}^2/(2m_0) + V$ a physical operator if $\mathbf{A} \neq 0$.

In addition to eigenvalues and expectation values of operators, one is concerned with transition probabilities (Ballentine, 2014; Yang, 1976) induced by the optical field. These transition rates are usually calculated in the framework of time-dependent perturbation theory. For this purpose the minimal coupling Hamiltonian is split into an unperturbed part

$$h_0 = \frac{\mathbf{p}^2}{2m_0} + V(\mathbf{r})$$

in the absence of electromagnetic fields and a perturbation that depends on scalar and/or vector potentials, for instance,

$$h_I = -\frac{q}{2m_0}[\mathbf{p}\cdot\mathbf{A}(\mathbf{r},t) + \mathbf{A}(\mathbf{r},t)\cdot\mathbf{p}] + q\Phi(\mathbf{r},t), \quad (46)$$

in which the quadratic term in $\mathbf{A}$ has been neglected. Perturbation theory then predicts transition rates between eigenvectors $|\eta_i\rangle$ of h_0, satisfying the eigenvalue equation $h_0\,|\eta_i\rangle = \varepsilon_i\,|\eta_i\rangle$. In most cases one is interested in the transition rates for monochromatic fields with frequency ω, for which the interaction Hamiltonian –like the potentials and fields– can be split into a positive and a negative frequency part according to

$$h_I = h_I^{(+)} e^{-i\omega t} + h_I^{(-)} e^{i\omega t}. \quad (47)$$

Transition rates in first-order perturbation theory –describing single photon absorption or emission processes– are then given by Fermi's golden rule

$$\Gamma_{fi} = \frac{2\pi}{\hbar}\left[\left|\langle\eta_f|h_I^{(+)}|\eta_i\rangle\right|^2 \delta\left(\varepsilon_f - \varepsilon_i - \hbar\omega\right) + \left|\langle\eta_f|h_I^{(-)}|\eta_i\rangle\right|^2 \delta\left(\varepsilon_f - \varepsilon_i + \hbar\omega\right)\right]. \quad (48)$$

Using higher-order perturbation theory transition rates for multi-photon absorption and emission processes can be obtained.

Obviously, these transition rates involve gauge-dependent quantities. Therefore the question arises: Do the transition rates change if the potentials are transformed by a gauge function χ according to Eq. (12) leading to a modified interaction Hamiltonian $h_I^{(2)} = h_I^{(1)} + \Delta h_{I\chi}$, where $h_I^{(1)}$ refers to the interaction Hamiltonian in the original gauge. Using the fact that also χ has a harmonic time dependence and can be separated in positive and negative frequency components, the correction terms are given by

$$\Delta h_{I\chi}^{(\pm)} = -\frac{q}{2m_0}\left[\mathbf{p}\cdot\nabla\chi^{(\pm)}(\mathbf{r}) + \nabla\chi^{(\pm)}(\mathbf{r})\cdot\mathbf{p}\right] \pm i\omega q\chi^{(\pm)}(\mathbf{r}). \quad (49)$$

As can be easily checked, the gauge field satisfies the commutation relation

$$\left[h_0, \chi^{(\pm)}(\mathbf{r})\right] = \frac{\hbar}{2m_0 i}\left[\mathbf{p}\cdot\nabla\chi^{(\pm)}(\mathbf{r}) + \nabla\chi^{(\pm)}(\mathbf{r})\cdot\mathbf{p}\right]. \quad (50)$$

Using this relation, the matrix elements of the correction terms to the interaction Hamiltonian are given by

$$\langle\eta_f|\Delta h_{I\chi}^{(\pm)}|\eta_i\rangle = -\frac{iq}{\hbar}\left(\varepsilon_f - \varepsilon_i \mp \hbar\omega\right)\langle\eta_f|\chi^{(\pm)}(\mathbf{r})|\eta_i\rangle\,. \quad (51)$$

These matrix elements therefore vanish when the energies satisfy the energy selection rules in Eq. (48). From this result we can draw several conclusions: (*i*) transition rates for resonant transitions, as described by Fermi's golden rule, are unchanged and are therefore gauge invariant; (*ii*) this does not hold anymore, if approximate eigenfunctions of h_0, obtained, e.g., from a variational calculation, are used for the calculation of the rate (Dalgarno and Lewis, 1956); (*iii*) transitions in the case of a decaying states may also depend on the gauge (Fried, 1973; Lamb Jr *et al.*, 1987). This is again related to the fact that h_0 does not completely describe the unperturbed system, but there are other parts, e.g., electron-phonon interaction or radiative decay due to the coupling to the photon vacuum, which lead to dephasing and a finite lifetime of the excited state.

For two-photon transitions, where the rate involves the summation of intermediate states, it has been shown that the exact result from second-order perturbation theory is independent of the gauge, while a truncation of the basis of the intermediate states can lead to strongly gauge-dependent results and the convergence behavior with increasing number of basis functions may strongly depend on the gauge (Bassani *et al.*, 1977). Furthermore, non-resonant two-photon transitions in the case of a broadened line may also depend on the gauge (Kobe, 1978). However, for not too large broadenings this gauge dependence will be very weak because the deviations of the energy from the resonance condition are very small.

To avoid such possible gauge dependencies one may try to find a formulation of the coupling only in terms of measurable fields. The dipole-moment approximation

for the coupling of light to atoms (or other sufficiently localized structures) accomplishes this. Let us assume that a smooth external electromagnetic field with wavelength much larger than the spatial extent of the electron wave function is impinging on an atom centered at $\mathbf{r} = 0$. If the sources of the field are far away $\Phi^{(1)} \simeq 0$ can be assumed and $\mathbf{A}^{(1)}(\mathbf{r}, t)$ can be approximated by $\mathbf{A}^{(1)}(0, t)$. Then, the Hamiltonian in the Coulomb gauge reads $h^{(1)} = [\mathbf{p} - q\mathbf{A}^{(1)}(0, t)]^2/(2m_0) + V(\mathbf{r})$. The Göppert-Mayer (1931) gauge transformation $\chi = -\mathbf{r} \cdot \mathbf{A}^{(1)}(0, t)$ produces new potentials $\mathbf{A}^{(2)} = 0$ and $\Phi^{(2)} = -\mathbf{r} \cdot \mathbf{E}(0, t)$, and consequently $h^{(2)} = \mathbf{p}^2/(2m_0) + V(\mathbf{r}) - q\mathbf{r} \cdot \mathbf{E}(0, t)$, i.e., a Hamiltonian completely described in terms of the electric field.

We note, however, that the Hamiltonian with the electric dipole coupling is only an approximation. The exact gauge transformation results in a vector potential $\mathbf{A}^{(2)}(\mathbf{r}, t) = \mathbf{A}^{(1)}(\mathbf{r}, t) - \mathbf{A}^{(1)}(0, t)$, which only vanishes in the case of a homogeneous electromagnetic field, i.e., in the limit of an infinite wavelength. Moreover, even in the case of a system much smaller than the wavelength one can find a gauge transformation to a null vector potential only in the cases when the coupling to the magnetic field is negligible. If there is a non-negligible magnetic coupling $\mathbf{A} \neq 0$ in all gauges.

In general, the dipole-moment approximation fails to describe extended matter states and/or highly inhomogeneous light fields. In the case of the coupling to a crystalline solid, however, a formulation in terms of dipole moments remains possible due to the Bloch theorem and the smallness of the length of the unit cell compared to the wavelength. The dipole moment then refers to a single unit cell. In other cases it can be improved by other gauge transformations (Cohen-Tannoudji *et al.*, 1989; Quinteiro *et al.*, 2015, 2017b) or by formally extending the dipole-moment Hamiltonian to $h_I = -q\mathbf{r} \cdot \mathbf{E}(\mathbf{r}, t)$ (Kira *et al.*, 1999). All these transformations share the fact that they retain some spatial dependence of the potentials and fields, see Sect. IV.A.2.

2. Vertical transition approximation

A widely used approximation in semiconductor optics is that of vertical transitions (Dresselhaus, 2001). The excitation of an electron from valence to conduction band annihilates a photon with energy around that of the semiconductor band-gap. Let us exemplify this for the excitation of a GaAs bulk crystal (band-gap energy $E_g = 1.44$ eV at 300 K). The corresponding photon's linear momentum is $q \simeq 8 \times 10^{-3}$ nm^{-1}.[9] The quasi-momentum k of the electron is restricted to the first Brillouin zone with maximum value $k_{\max} = \pi/a \simeq 6$ nm^{-1}, where a is the linear size of the unit cell. By arguing that $q \ll k_{\max}$, one often neglects q. This is equivalent to neglecting the spatial variation of the light field over a unit cell. Neglecting furthermore the spatial variation of the light field over the whole system leads to the vertical transition approximation. In the electron-hole or exciton picture a vertical transitions corresponds to the generation of an electron-hole pair or an exciton with vanishing center-of-mass momentum.

This vertical transition approximation has proven very useful. However, the conservation of linear momentum in the light-matter interaction must be taken into account in some cases of historical and current interest. In the late 1950s Hopfield (1958) developed the theory of hybrid exciton-photon quasiparticles, known as exciton-polaritons, a topic that has regained interest in recent years in particular in the field of semiconductor nanostructures and is currently extensively explored in theory, experiments and applications (Sect. IV.B). A decade later, and almost simultaneously, Grinberg (1970) and Gibson with coworkers (Cameron *et al.*, 1975; Gibson *et al.*, 1970; Gibson and Walker, 1971) investigated the photon-drag effect; in Grinberg's words "In the absorption of light by free carriers, the momentum of the electromagnetic wave is absorbed together with its energy. Consequently, the electron system can acquire a translational motion that is manifest in the form of a current or a voltage [...]". The effect is nowadays being used in commercial detectors. If the light is circularly polarized carriers may pick both the photon's linear momentum and spin AM resulting in the generation of a spin-dependent electric current (Shalygin *et al.*, 2007).

Taking into account the linear momentum of the photon the transitions are not anymore vertical, nevertheless there is still a well-defined momentum transfer. In the electron-hole picture the generated electron-hole pair has a center-of-mass momentum given by the photon's momentum. In contrast, for strongly inhomogeneous light fields, the photon does not anymore have a well-defined momentum, which leads to a broading of the transitions in k-space and thus to an uncertainty in the center-of-mass momentum of the generated exciton or electron-hole pair (Herbst *et al.*, 2003; Hess and Kuhn, 1996; Rossi and Kuhn, 2002).

In structures with cylindrical symmetry it is often convenient to characterize the electronic state not by the linear momentum $\mathbf{k}$ but by its OAM with respect to the symmetry axis, specified by a quantum number m. Also here, a light field which can be assumed to be spatially homogeneous over the structure leads to "vertical" transitions in the sense that the quantum number m of the initial and final state in an absorption or emission process is the same.

To describe the interaction of OVs with condensed matter, the assumption of a slowly varying field is violated in particular in the region around the phase sin-

[9] Rigorously speaking, the photon's linear momentum is $\hbar\mathbf{q}$.

gularity and has therefore to be abandoned. Here, the transfer of OAM has to be incorporated in the models in a similar way as the linear momentum in the case of polaritons or the photon drag effect. In fact, based on such an approach circular photo-currents in bulk (Quinteiro and Tamborenea, 2009c) and nanostructures (Quinteiro and Berakdar, 2009) have been predicted. Later measurements have recently confirmed this effect (Ge, 2020; Ji *et al.*, 2020).

3. Dynamics under light excitation

In a nutshell, a light beam creates an out-of-equilibrium many-electron state by altering the populations of conduction and valence bands as well as the quantum coherences within and between bands (Rossi and Kuhn, 2002). With no further energy input, the overall state eventually relaxes and loses quantum coherence through different channels, most notably electron-phonon and electron-electron scattering and radiative recombination. Many tools have been developed to measure and model the generation of a non-equilibrium state in matter by means of an optical excitation and the subsequent relaxation and dephasing back to the equilibrium state.

The dynamics of optically excited semiconductors are conveniently described starting from a second quantization picture with creation (annihilation) operators $a^\dagger_{b\alpha}$ ($a_{b\alpha}$) denoting the creation (annihilation) of an electron in the state $\psi_{b\alpha}(\mathbf{r})$ in band b with quantum number α. In bulk material α is the three-dimensional wave vector $\mathbf{k}$ of the Bloch electron and the Bloch function $\psi_{b\mathbf{k}}(\mathbf{r})$ is given by Eq. (41). In a spatially confined system α may be a purely discrete (multi-)index (e.g., in the case of a quantum dot) or a combination of discrete and a continuous index (e.g., a subband index and a two-dimensional wave vector in the case of a quantum well). The states in such systems are often well described in terms of the envelope function approximation (Bastard, 1988; Ihn, 2010) by a wave function

$$\psi_{b\alpha}(\mathbf{r}) = \mathcal{E}_{b\alpha}(\mathbf{r}) u_b(\mathbf{r}), \tag{52}$$

for a state with energy $\varepsilon_{b\alpha}$. Here, $\mathcal{E}_{b\alpha}(\mathbf{r})$ denotes the envelope function and the k-dependence of the lattice periodic Bloch function is neglected, i.e., $u_{b\mathbf{k}}(\mathbf{r})$ is replaced by the function at the band edge $u_{b\mathbf{k}_0}(\mathbf{r}) = u_b(\mathbf{r})$ (Bastard, 1988). The Hamiltonian of the non-interacting electrons then reads

$$H_0 = \sum_{b\alpha} \varepsilon_{b\alpha} a^\dagger_{b\alpha} a_{b\alpha}, \tag{53}$$

while the coupling to a light field in any gauge has the general structure

$$H_I = \sum_{b'\alpha',b\alpha} h^I_{b'\alpha',b\alpha} a^\dagger_{b'\alpha'} a_{b\alpha}, \tag{54}$$

with $h^I_{b'\alpha',b\alpha} = \langle b'\alpha'|h_I|b\alpha\rangle$ and the interaction Hamiltonian h_I, such as Eq. (46).

The expectation value of any single-particle operator of the electrons can be calculated from the single-particle density matrix

$$\rho_{b'\alpha',b\alpha}(t) = \langle a^\dagger_{b'\alpha'}(t) a_{b\alpha}(t)\rangle, \tag{55}$$

which satisfies the equation of motion

$$\begin{aligned} i\hbar\frac{d}{dt}\rho_{b'\alpha',b\alpha} &= \left\langle \left[a^\dagger_{b'\alpha'} a_{b\alpha}, H_0 + H_I\right]\right\rangle \\ &= \left(\varepsilon_{b\alpha} - \varepsilon_{b'\alpha'}\right)\rho_{b'\alpha',b\alpha} \\ &+ \sum_{b''\alpha''} \left(h^I_{b\alpha,b''\alpha''}\rho_{b'\alpha',b''\alpha''} - h^I_{b''\alpha'',b'\alpha'}\rho_{b''\alpha'',b\alpha}\right). \end{aligned} \tag{56}$$

Note that while here we have explicitly used the Heisenberg picture, $\rho_{b'\alpha',b\alpha}(t)$ as an expectation value is independent of the picture and the same equation (56) could be obtained by using the Liouville-von Neumann equation in the Schrödinger picture. Often, when dealing with the dynamics of optically excited semiconductors, it is sufficient to restrict the model to two bands, the valence (v) and the conduction (c) band. Then, the system is described by three single-particle density matrices, the intraband coherences $\rho_{v,\alpha'\alpha} \equiv \rho_{v\alpha',v\alpha}$ and $\rho_{c,\alpha'\alpha} \equiv \rho_{c\alpha',c\alpha}$ (including occupations for $\alpha = \alpha'$), and the interband coherence $\rho_{vc,\alpha'\alpha} \equiv \rho_{v\alpha',c\alpha}$. We will come back to these equations for various types of structures in the following Sections. As a reference for the description of solid-state systems driven by OVs, here we will give a brief overview of the theoretical background for the standard case of a bulk semiconductor excited by a homogeneous light field.

In the case of a homogeneous excitation of a bulk semiconductor the single-particle density matrices are diagonal in the wave vector $\mathbf{k}$ and the dynamical variables reduce to the electron occupations in the valence and conduction bands, $\rho_{v,\mathbf{k}}$ and $\rho_{c,\mathbf{k}}$, as well as the interband coherence (also called interband polarization) $\rho_{vc,\mathbf{k}}$. The coupling to the light field is treated in terms of the vertical transition approximation. The interaction matrix elements in the electric field gauge then reduce to $h^I_{c\mathbf{k},v\mathbf{k}} = -\mathbf{d}_{cv}\cdot\mathbf{E}(t)$ with the interband dipole matrix element

$$\mathbf{d}_{cv} = \frac{q}{v}\int_v u^*_c(\mathbf{r})\,\mathbf{r}\,u_v(\mathbf{r})d\mathbf{r}. \tag{57}$$

A more detailed discussion of the coupling to the light field including intraband and interband processes as well as spatially inhomogeneous light fields will be given in Sect. IV.A.1.

In the simplest case the optical excitation is described in terms of a generation rate $g_{\mathbf{k}}$ according to

$$\frac{d}{dt}\rho_{c,\mathbf{k}} = -\frac{d}{dt}\rho_{v,\mathbf{k}} = g_{\mathbf{k}}, \tag{58}$$

where $g_{\mathbf{k}}$ is obtained from Fermi's golden rule and reads for a spatially homogeneous light field $\mathbf{E}$ with frequency ω

$$g_{\mathbf{k}} = \frac{2\pi}{\hbar^2}|\mathbf{d}_{cv}\cdot\mathbf{E}|^2\left(\rho_{v,\mathbf{k}}-\rho_{c,\mathbf{k}}\right)\delta(\omega_{\mathbf{k}}-\omega)\,, \tag{59}$$

with $\hbar\omega_{\mathbf{k}} = \varepsilon_{c\mathbf{k}} - \varepsilon_{v\mathbf{k}}$. In the case of excitation by a short laser pulse the δ-function is replaced by the spectral shape of the pulse.

The coupling to the light field, however, does not only generate populations of electrons and holes, it also creates an interband coherence $\rho_{vc,\mathbf{k}}$ between the light-coupled states. In the present case of non-interacting electrons a closed set of EoM for the occupations and the interband coherence is obtained,

$$\frac{d}{dt}\rho_{c,\mathbf{k}} = -\frac{d}{dt}\rho_{v,\mathbf{k}} = -\frac{2}{\hbar}\mathrm{Im}\left[\mathbf{d}_{cv}\cdot\mathbf{E}(t)\rho^*_{vc,\mathbf{k}}\right], \tag{60a}$$

$$\frac{d}{dt}\rho_{vc,\mathbf{k}} = -i\omega_{\mathbf{k}}\rho_{vc,\mathbf{k}} + \frac{i}{\hbar}\mathbf{d}_{cv}\cdot\mathbf{E}(t)\left(\rho_{v,\mathbf{k}}-\rho_{c,\mathbf{k}}\right) \tag{60b}$$

with Im[...] denoting the imaginary part. Each optically coupled pair of valence and conduction band states represents a two-level system and Eqs. (60) correspond to a set of optical Bloch equations (OBE) for each of these two-level systems (Haug and Koch, 2009). An extension including intraband terms of the electric field can be found in Rossi and Kuhn (2002). Generalizations of the OBE to the case of excitation of semiconductor bulk and various elementary nanostructures will be discussed in Sects. IV and V.

The EoM (60) have been derived in the electron picture. Alternatively, one may work in the electron-hole picture, in which the annihilation of an electron with wave vector $\mathbf{k}$ in the valence band is replaced by the generation of a hole with wave vector $-\mathbf{k}$. Instead of the occupation of the valence band states one then uses the occupation of hole states given by $\rho_{h,-\mathbf{k}} = 1-\rho_{v,\mathbf{k}}$, the other two variables remain the same. The excitation of an electron from the valence to the conduction band is then interpreted as the generation of an electron-hole pair, where electron and hole have opposite momenta. An advantage of the electron-hole picture is the fact that before the optical excitation the system is in the well-defined vacuum state with all dynamical variables being zero. In this review, however, we will mainly use the equally valid electron picture, because it provides a more compact notation, especially in systems with more than two bands or when including intraband processes.

In a real semiconductor, in particular in the case of excitation close to the band gap, the many-body nature of the electronic system cannot be neglected. The attractive Coulomb interaction between electron and hole leads to the formation of bound exciton states which manifest themselves in discrete absorption lines below the band gap. The general structure of the electron-electron interaction Hamiltonian in a multiband model is given by

$$H_{ee} = \frac{1}{2}\sum_{ijkl}\langle ij|\,h_{ee}\,|kl\rangle a_i^\dagger a_j^\dagger a_l a_k\,, \tag{61}$$

in which latin characters collect band and envelope indices (for example, $i = b_i\alpha_i$) and

$$h_{ee} = \frac{q^2}{4\pi\epsilon_0\epsilon_s|\mathbf{r}-\mathbf{r}'|}$$

with the static dielectric constant ϵ_s. For the two-band bulk system of Bloch states this leads to

$$H_{ee} = \frac{1}{2}\sum_{\mathbf{k}\mathbf{k}'\mathbf{g}\neq 0} V_{\mathbf{g}}\Big(2a^\dagger_{c\mathbf{k}+\mathbf{g}}a^\dagger_{v\mathbf{k}'-\mathbf{g}}a_{v\mathbf{k}'}a_{c\mathbf{k}} + a^\dagger_{v\mathbf{k}+\mathbf{g}}a^\dagger_{v\mathbf{k}'-\mathbf{g}}a_{v\mathbf{k}'}a_{v\mathbf{k}} + a^\dagger_{c\mathbf{k}+\mathbf{g}}a^\dagger_{c\mathbf{k}'-\mathbf{g}}a_{c\mathbf{k}'}a_{c\mathbf{k}}\Big)\,,$$

with $V_{\mathbf{g}} = q^2/(V\epsilon_0\epsilon_s g^2)$ and we have neglected terms that do not conserve the number of particles in each band as well as the interband exchange term (Fetter and Walecka, 2012). Those terms are of short-range nature and are therefore often of minor importance. To obtain the contribution from electron-electron interaction to the EoM of the single-particle density matrices we need the commutators of $a^\dagger_{b'\mathbf{k}'}a_{b\mathbf{k}}$ with H_{ee}. For the interband operator $a^\dagger_{v\mathbf{k}'}a_{c\mathbf{k}}$ this leads to

$$[a^\dagger_{v\mathbf{k}'}a_{c\mathbf{k}}, H_{ee}] = \sum_{\mathbf{k}_1,\mathbf{g}\neq 0} V_{\mathbf{g}}\Big(a^\dagger_{v\mathbf{k}'}a^\dagger_{v\mathbf{k}_1+\mathbf{g}}a_{v\mathbf{k}_1}a_{c\mathbf{k}+\mathbf{g}} - a^\dagger_{v\mathbf{k}'+\mathbf{g}}a^\dagger_{c\mathbf{k}_1-\mathbf{g}}a_{c\mathbf{k}_1}a_{c\mathbf{k}} + a^\dagger_{v\mathbf{k}'}a^\dagger_{c\mathbf{k}_1+\mathbf{g}}a_{c\mathbf{k}_1}a_{c\mathbf{k}+\mathbf{g}} - a^\dagger_{v\mathbf{k}'+\mathbf{g}}a^\dagger_{v\mathbf{k}_1-\mathbf{g}}a_{v\mathbf{k}_1}a_{c\mathbf{k}}\Big)\,. \tag{62}$$

Analogous equations are obtained for the intraband operators.

When taking the expectation value of Eq. (62) we observe that we get expectation values of four operators. Thus, instead of getting a closed set of EoM, this constitutes the starting point of an infinite hierarchy of equations for expectation values of an increasing number of operators, much like the BBGKY hierarchy of statistical thermodynamics (Huang, 1963).

A variety of techniques has been developed to treat such many-body systems. In a correlation expansion approach (Rossi and Kuhn, 2002) [also called cumulant or cluster expansion approach (Fiori *et al.*, 2013; Kira *et al.*, 1999)] one starts again with the single-particle density matrices ρ_c, ρ_v and ρ_{vc}. The expectation values of four operators appearing in their EoM, which represent two-particle density matrices, are then separated into a sum over all possible factorizations into single-particle density matrices and a rest containing two-particle correlations. The same factorization scheme is applied to higher-order density matrices leading to correlations among an increasing number of particles. Setting up EoM for these higher correlations leads to an infinite set of equations of

motion, that needs to be truncated by an approximation in order to become closed.

On the lowest order, all correlations are neglected which leads to the time-dependent Hartree-Fock approximation. Considering again a spatially homogeneous system only single-particle density matrices which are diagonal in $\mathbf{k}$ are non-zero. Reordering the operators in Eq. (62), such that creation and annihilation operators in a factorization are next to each other leads to

$$\left\langle [a^\dagger_{v\mathbf{k}} a_{c\mathbf{k}}, H_{ee}] \right\rangle = -\sum_{\mathbf{g}\neq 0} V_{\mathbf{g}} \left[\rho_{vc,\mathbf{k}+\mathbf{g}} \left(\rho_{v,\mathbf{k}} - \rho_{c,\mathbf{k}} \right) - \rho_{vc,\mathbf{k}} \left(\rho_{v,\mathbf{k}+\mathbf{g}} - \rho_{c,\mathbf{k}+\mathbf{g}} \right) \right] . \quad (63)$$

Note that the restriction of the summation to $\mathbf{g} \neq 0$, which reflects the total charge neutrality, eliminates all Hartree-type factorizations.

Adding the contributions from electron-electron interaction to the OBE (60) leads to the semiconductor Bloch equations (SBE) (Lindberg and Koch, 1988). They have the same structure as the OBE, however with renormalized energies and field couplings:

$$\frac{d}{dt}\rho_{c,\mathbf{k}} = -\frac{d}{dt}\rho_{v,\mathbf{k}} = -2\mathrm{Im}\left[\tilde{\Omega}(t) \rho^*_{vc,\mathbf{k}} \right] , \quad (64a)$$

$$\frac{d}{dt}\rho_{vc,\mathbf{k}} = -i\tilde{\omega}_{\mathbf{k}} \rho_{vc,\mathbf{k}} + i\tilde{\Omega}(t) \left(\rho_{v,\mathbf{k}} - \rho_{c,\mathbf{k}} \right) . \quad (64b)$$

The external light field is complemented by an internal field resulting from the interband term of the Coulomb interaction leading to an effective Rabi frequency $\tilde{\Omega}(t)$ according to

$$\hbar\tilde{\Omega}(t) = \mathbf{d}_{cv} \cdot \mathbf{E}(t) + \sum_{\mathbf{g}\neq 0} V_{\mathbf{g}} \rho_{vc,\mathbf{k}+\mathbf{g}} . \quad (65)$$

The energies of the electrons in the valence and conduction bands are renormalized by the intraband Coulomb terms, respectively, leading to the effective transition frequency $\hbar\tilde{\omega}_{\mathbf{k}} = (\tilde{\varepsilon}_{c\mathbf{k}} - \tilde{\varepsilon}_{v\mathbf{k}})$. For the conduction band states this leads to

$$\tilde{\varepsilon}_{c\mathbf{k}} = \varepsilon_{c\mathbf{k}} - \sum_{\mathbf{g}\neq 0} V_{\mathbf{g}} \rho_{c,\mathbf{k}+\mathbf{g}} . \quad (66)$$

For the valence band states the derivation produces the analogous result. However, the single-particle energy usually is defined in such a way that it already includes the energy renormalization of the completely filled valence band. Therefore, only the missing electrons in the valence band, i.e., the holes, contribute to the renormalization and we have

$$\tilde{\varepsilon}_{v\mathbf{k}} = \varepsilon_{v\mathbf{k}} + \sum_{\mathbf{g}\neq 0} V_{\mathbf{g}} \left(1 - \rho_{v,\mathbf{k}+\mathbf{g}} \right) . \quad (67)$$

This result is indeed directly obtained if the calculations are performed in the electron-hole picture. The internal field gives rise to the appearance of exciton lines in the absorption spectrum while the energy renormalizations lead to a density-dependent reduction of the band gap. In the linear response regime the occupations in the valence and conduction bands are replaced by their equilibirum values and Eq. (64b) can be written in the form of a Wannier equation driven by a homogeneous light field, reflecting the excitation of excitons with vanishing center-of-mass motion. In Sect. IV.A.2 the Wannier equation for the case of excitation of a bulk semiconductor by a Bessel-type OV will be derived and we will see that under these conditions excitons with a non-vanishing center-of-mass momentum are generated.

Going beyond the level of the SBE and including correlation effects, either due to the Coulomb interaction or due to electron-phonon interaction, one obtains scattering and dephasing contributions which lead to a redistribution of the carriers in the bands and to a loss of interband coherence. Keeping only correlations up to a given level, the equations for these correlations can be solved numerically, which corresponds to a quantum kinetic description of scattering and dephasing processes (Schilp *et al.*, 1994). Alternatively, they can be formally solved by performing a Markov approximation, which leads to scattering contributions to the SBE similar to a Boltzmann equation (Rossi and Kuhn, 2002).

For inhomogeneous optical excitation, the vertical transition approximation fails, and electron states with different initial and final quasi-momentum are coupled; here, off-diagonal variables such as $\rho_{c,\mathbf{k}'\mathbf{k}}(t)$, $\rho_{v,\mathbf{k}'\mathbf{k}}(t)$, and $\rho_{vc,\mathbf{k}'\mathbf{k}}(t)$ are relevant. The off-diagonal terms contain the information on the space dependence and the EoM then also describe spatial transport phenomena. The factorization of the Coulomb contributions to the equation of motion [Eq. (62) and the corresponding equations for the intraband variables] now also involves Hartree-like factorizations describing the self-consistent electric field caused by the inhomogeneous charge distribution. While the spatial information is rather hidden in this non-diagonal momentum representation, a more intuitive interpretation is provided by a Wigner function representation in terms of functions $\rho_{c,\mathbf{K}}(\mathbf{r},t)$, $\rho_{v,\mathbf{K}}(\mathbf{r},t)$, and $\rho_{vc,\mathbf{K}}(\mathbf{r},t)$, where $\mathbf{K} = \frac{1}{2}(\mathbf{k}+\mathbf{k}')$ and the $\mathbf{r}$-dependence is obtained from a Fourier transformation with respect to $\mathbf{k}-\mathbf{k}'$ (Rossi and Kuhn, 2002). We will come back to the Wigner and other mixed momentum-position representations when discussing the excitation of a bulk semiconductor by OVs in Sect. IV.A.2. Non-linear scattering and dephasing terms in the EoM of single-particle density matrices for inhomogeneous systems have also been derived by employing Lindblad-type superoperators (Rosati *et al.*, 2014).

Another widely used approach to describe optically induced dynamics in many-body systems is based on nonequilibrium Green's functions (Balzer and Bonitz, 2013; Haug and Jauho, 2008). The main difference compared to density matrix-based approaches is the fact that

the basic variables, the single-particle Green's functions, are two-time functions. The theory has been developed in the 1960s by Kadanoff and Baym (1962) and by Keldysh (1965) as a generalization of the equilibrium Green's function approach. While in the equilibrium case a single type of Green's function contains the full information about the system, out of equilibrium in general four different functions are needed. The information on the dynamics of occupations and coherences is obtained from the "less" and "greater" Green's functions $G^<$ and $G^>$ while spectral information is provided by the retarded and advanced Green's function G^r and G^a, respectively. For electrons in the general multiband system $G^<$ and G^r are defined as

$$G^<_{b\alpha,b'\alpha'}(t_1,t_2) = -i\langle a^\dagger_{b'\alpha'}(t_2)a_{b\alpha}(t_1)\rangle\,,$$
$$G^r_{b\alpha,b'\alpha'}(t_1,t_2) = -i\Theta(t_1-t_2)\langle[a_{b\alpha}(t_1),a^\dagger_{b'\alpha'}(t_2)]_+\rangle,$$

with $\Theta(x)$ denoting the Heaviside step function and $[\ldots,\ldots]_+$ being the anticommutator. $G^>$ and G^a are defined analogously. On the level of time-dependent Hartree-Fock theory this approach leads for the equal time variables again to the SBE. Many-body effects like scattering and dephasing can then be described in terms of a generalized Dyson equation, which can be treated within a diagrammatic expansion using Feynman diagrams. Nonequilibrium Green's functions have been used to study the effects of OV pulses on the disordered surface of a topological insulator, as will be discussed in Sect. IV.A.3.d.

Yet another popular approach is the use of the Liouville-von Neumann equation (Rossi, 2011) for the dynamics of the density operators $\rho(t)$ by the equation $i\hbar d\rho/dt = -[\rho, H]$ –note the difference in sign compared to the Heisenberg equation of motion. Here, expectation values result from $\langle\mathcal{O}\rangle(t) = \mathrm{Tr}[\mathcal{O}\rho(t)]$. This approach is particularly useful in the case of systems with a discrete spectrum, such as atoms or semiconductor nanostructures like quantum dots, interacting with a bath. Relaxation and dephasing processes are often described in terms of a Lindblad superoperator (Lindblad, 1976) acting on ρ, which leads to a non-unitary time-evolution but preserves basic properties of the density operator like Hermiticity and positivity (Breuer and Petruccione, 2002). For important special cases –a prototypical example being the coupling of a semiconductor quantum dot to acoustic phonons– a numerically exact solution of the optically driven many-body problem can be obtained in the framework of a real-time path integral approach (Vagov *et al.*, 2011).

The experimental exploration of the crystal's excited states and their evolution is done with linear and nonlinear optical techniques (Axt and Kuhn, 2004; Kalt and Klingshirn, 2019; Lu and Fu, 2018; Shah, 1999; Shree *et al.*, 2021). In photoluminescence spectroscopy the sample is excited at a fixed high energy and the resulting photons emitted by the electrons undergoing radiative decay are recorded as a function of frequency; in a variant of that, photoluminescence excitation, the system is excited at varying energies, and the resulting emission is measured at a fixed frequency. Non-linear spectroscopic techniques (Boyd, 2020; Cundiff, 2008) rely on the fact that the polarization of the system responds to a strong electric field in non-linear ways $P \propto \chi^{(n)}E^n$, with $\chi^{(n)}$ being an n-th order susceptibility. They are more powerful than linear methods, because they can probe a variety of processes, such as the decay of populations and dephasing of coherences. In a typical experiment a sequence of laser pulses is used to "pump" the crystal creating the out-of-equilibrium state and to "probe" the state of the system after some delay. Specific techniques are pump-probe spectroscopy that measures the dynamics of populations generated by the pump beam, but also time-dependent energy shifts, intraband coherences or a perturbed free-induction decay (Joschko *et al.*, 1997; Koch *et al.*, 1988; Krügel *et al.*, 2007), Faraday/Kerr rotation that measures the spin dynamics and spin decoherence (Kikkawa and Awschalom, 1999; Kugler *et al.*, 2011), and four-wave mixing as well as 2D spectroscopy (Cundiff and Mukamel, 2013) that, depending on the pulse sequence and the extraction of the signal, can measure both interband coherence and population dynamics and allows for the separation of homogeneous and inhomogeneous broadening (Honold *et al.*, 1988; Koch *et al.*, 1993; Lindberg *et al.*, 1992). Pump-probe and four-wave mixing spectroscopy on bulk semiconductors using OV pulses will be discussed in Sect. IV.A.2.

When it comes to measuring nanostructures, bulk techniques can only probe an ensemble of particles, missing important properties of individual particles that are blurred by, e.g., inhomogeneous broadening. Single nanostructure measurements are better suited for this task. One can use emission or extinction (absorption) spectroscopy (Chatterjee *et al.*, 2018). In the latter the extinction of light going through the nanostructure at different frequencies is measured, yielding a spectrum that reveals large portions of the energy level structure. In contrast, typical emission spectroscopy relies on the emission of light from the lowest excited energy states. Also pump-probe (Henzler *et al.*, 2021; Sotier *et al.*, 2009) or four-wave-mixing (Patton *et al.*, 2006; Wigger *et al.*, 2020) techniques are nowadays sensitive enough to be applied to single nanostructures.

In all the cases discussed so far the coupling to the light is used as an excitation and/or measurement tool with the goal to obtain information on the spectral and/or dynamical properties of the material system. In some situations, however, when the coupling is sufficiently strong, the light becomes part of the system and one cannot anymore separate system and light dynamics. Instead, the coupling of electronic excitations and light leads to the emergence of new quasiparticles, such as different types

of polaritons. Prominent examples are exciton polaritons in semiconductor micro-cavities which have been extensively studied in the past years (Deng *et al.*, 2010; Kavokin *et al.*, 2017; Weisbuch *et al.*, 1992). Their generation and dynamics have been modeled based on the Heisenberg equation of motion (Ciuti *et al.*, 2001; Portolan *et al.*, 2008; Quinteiro *et al.*, 2012; Shelykh *et al.*, 2009; Vasilieva *et al.*, 2018), one-particle Green's functions (Citrin, 1994; Quinteiro, 2008; Quinteiro *et al.*, 2006; Savona *et al.*, 1999, 1997), and the Liouville equation (Quinteiro and Piermarocchi, 2005; Shelykh *et al.*, 2005). In addition, the Gross-Pitaevskii equation, the bosonic version of the Hartree-Fock equation, has been used for the quasi-bosonic polaritons to account for their interaction and the excitation by a source field (Gippius *et al.*, 2007; Liew and Shelykh, 2009; Shelykh *et al.*, 2006).

In metallic nanostructures the light couples to the electron plasma. Close to surfaces of the metal or interfaces between the metal and a dielectric environment this gives rise to the formation of surface plasmon polaritons, which are another example of quasi-particles that treat light and matter on equal footing. Simple models of plasmonics combine the Drude model for electrons in metals and Maxwell's equations of electrodynamics (Maier, 2007). Here, the Drude model provides a dielectric function for the response of the electron plasma in the metal to an external perturbation. This and the dielectric constant of the dielectric material are plugged into the Helmholtz equation for the propagation of the electromagnetic field; the solutions are the plasmon polaritons. For plasmon polaritons in the sub-wavelength scale, a quasi-static approximation for the fields can be used, for example, in a tiny metallic sphere surrounded by a dielectric. For larger particles for which the quasi-static approximation fails, one can resort to Mie theory (Mie, 1908). The imaging of plasmon polaritons can be done using different techniques, and near-field microscopy stands among them as a powerful one. In photon scanning tunneling microscopy a metallic tip is brought close to the surface, so that it couples to the evanescent field; this makes possible the collection of photons out of the surface and their measurement (Maier, 2007).

IV. OPTICAL VORTICES MEET CONDENSED MATTER

About a decade ago, two independent works addressed the topic of the excitation of condensed matter systems by OVs. One of them provided theoretical predictions (Quinteiro and Tamborenea, 2009c) and the other experimental results (Ueno *et al.*, 2009). The former predicted the generation of circular electric currents in bulk semiconductors, a new type of "circular photon-drag" effect. The latter demonstrated, using four-wave-mixing techniques, the transfer of OAM to excitons in GaN semiconductors. Since then, many groups have contributed to the advancement of the subject by investigating the interaction of OVs with bulk semiconductors, nanostructures, metals, metal-dielectric interfaces, micro-cavities, and more. In this section we review the basic tools to study the interaction of light beams having phase singularities with condensed-matter systems, and in doing so we report on what has been learned so far about each system from theory and experiments.

A. Semiconductor optics and the silent assumptions

Two pervasive assumptions must be abandoned before theoretical progress and real understanding in OV-semiconductor physics can be made –some of them must also be reexamined in the broader interface between condensed-matter and OVs, see Table I. The first one is the vertical transition approximation (Sect. III.C.2), in which the momentum of the photon is neglected, that eliminates from the start most important effects of OV-semiconductor interaction, such as the generation of electric currents in bulk or the excitation of normally inaccessible states in quantum dots. The second one is the dipole moment approximation (Sect. III.C.1) that assumes a constant electric field at the position of the matter system; if the system is localized at the optical phase singularity (intensity zero point), then the dipole moment approximation fails completely to account for the interaction. We note that these two assumptions are related. They are most detrimental, and their reevaluation, as has been done in previous and will be done in this and the following sections, shows that they can (and indeed must) be safely dropped. The reexamination of other well-entrenched –though not extremely harmful– assumptions widens our understanding of the topic, and provides extra tools to model particular problems.

The dipole-like interaction Hamiltonian $H_I = -\mathbf{d}\cdot\mathbf{E}(\mathbf{r},t)$ with $\mathbf{d} = q\mathbf{r}$ has proven useful in treating the interaction of semiconductors with inhomogeneous fields,e.g., accounting for the transfer of linear momentum in exciton-polariton physics [Khitrova *et al.* (1999), Appendix A.2]. However, Quinteiro *et al.* (2015) recognized that the proper electric interaction Hamiltonian for parallel momenta OVs is different and must be derived by ways of a new *twisted-light* gauge transformation, leading to the interaction Hamiltonian $H_I = -[1/(\ell+1)]\mathbf{d}_\perp\cdot\mathbf{E}(\mathbf{r},t)$ for flat structures, which was further generalized to include the interaction with anti-parallel momenta OVs by using the Poincaré gauge with interaction Hamiltonian $H_I = -\mathbf{d}\cdot\mathbf{E}^{\rm eff}(\mathbf{r},t) - \mathbf{m}_B\cdot\mathbf{B}^{\rm eff}(\mathbf{r},t)$, with $\mathbf{m}_B = -(q/2m)(\mathbf{p}\times\mathbf{r})$ and effective fields of the form $\mathbf{E}^{\rm eff} = f_{E\perp}(\ell)\mathbf{E}_\perp(\mathbf{r},t) + f_{Ez}(\ell)E_z(\mathbf{r},t)$ and correspondingly for $\mathbf{B}^{\rm eff}$ (Quinteiro *et al.*, 2017b).

Bulk is the archetypical system to theoretically study

TABLE I Silent assumptions based on Quasi-Homogeneous (QH) beams –plane waves, Gaussian beams, etc.– mainly used in condensed-matter optics, and their applicability to describe the interaction with OVs.

SILENT ASSUMPTIONS		
Feature	**Beams**	
	Quasi-Homogeneous	**Optical Vortex**
Coupling	dipole moment or dipole-like electric interaction	non-dipole
k-space transition	vertical	tilted
Interaction field	E	E and B
Interaction with field component	transverse	transverse and longitudinal
Convenient representation	plane waves	Bessel, LG, Mathieu and other functions
Archetypical system	bulk	quantum ring
Optical-to-structure axes displacement: effects on	transition amplitudes	transition amplitudes and selection rules

the interaction of condensed matter with spatially uniform light –typified by plane waves–, providing the simplest approach and clearest results and interpretation. This is due, mostly, to the fact that both the envelope part of the Bloch electronic wave function and plane waves are usually treated in Cartesian coordinates. However, for OVs the situation is different: vortices are written most easily in cylindrical coordinates, and the analytical treatment of their interaction with bulk systems is thus cumbersome (Sect. IV.A.2).

Fourier analysis and plane waves are widespread tools to understand wave optics and quantum mechanics, and it is easy to oversee that other bases are good representations as well. In fact, a light field with a single-singularity is much more easily represented by a single Bessel or LG function.

The research on the effects produced by uniform light brings about another prejudice. Light at the optical frequencies predominantly interacts with matter via its electric field. However, some OVs present a specially intense magnetic field that makes the magnetic interaction dominant [consider Eq. (24b) for $\{\sigma = \pm 1, \ell = \mp 2, \gamma = 1\}$; for details see Quinteiro *et al.* (2019b)].

The widespread use of plane waves may lead us to disregard the longitudinal component of the beam in the light-matter interaction; OVs present significant components in the direction of propagation [see Eqs. (24)] –the presence of a field component E_z does not contradict the transversality of the field, for each plane wave composing the beam is transverse to its propagation direction, or in other words $\nabla \cdot \mathbf{E} = 0$ is satisfied (Sect. II.F).

Finally, the relative position of the vortex optical axis and nanostructure symmetry axis has a direct influence on optical selection rules, in stark contrast to the interaction with plane waves that present no optical axis whatsoever and their positioning with respect to the system is irrelevant. The subject of displaced optical axes brings about the topic of intrinsic and extrinsic AM, as discussed, e. g., by Bliokh and Nori (2015).

1. Basics

Among several approaches to model the light-matter interaction –such as the Gross-Pitaevski equation for exciton-polaritons in micro-cavities or non-equilibrium Green's functions–, the method of reduced density matrices has found the most widespread application in the study of the OV-semiconductor interaction. As anticipated in Sect. III.C.3, the basic variables are the intraband ($b = b'$) and interband ($b \neq b'$) single-particle density matrices $\rho_{b'\alpha',b\alpha}(t) = \langle a^\dagger_{b'\alpha'}(t) a_{b\alpha}(t)\rangle$ with the operators $a^\dagger_{b\alpha}$ ($a_{b\alpha}$) denoting the creation (annihilation) of an electron in the state $\psi_{b\alpha}$ [Eq. (52)] in band b with envelope function quantum number α. The equations of motion for $\rho_{b'\alpha',b\alpha}(t)$ are most conveniently obtained by using the Heisenberg EoM for the operators. When many-body interactions, such as the Coulomb interaction or the electron-phonon interaction, are involved, higher-order density matrices involving more than one creation and one annihilation operator appear in the EoM of the single-particle density matrices, and the resulting hierarchy of equations has to be truncated at a certain level.

An essential building block is the matrix element of the light-matter interaction Hamiltonian h_I, that enters the derivation of the EoM through its second quantization form $H_I = \sum_{bb'\alpha\alpha'} \langle b'\alpha'| h_I |b\alpha\rangle a^\dagger_{b'\alpha'} a_{b\alpha}$ –the matrix element also features in other common calculations, such as in Fermi's Golden Rule to calculate transition rates, as shown in Eq. (59) for the homogeneous case. In the following we first present the matrix element for an arbitrary basis, and next the EoM; in doing so we comment on the silent assumptions and their incompatibility with a sound description of OV-matter interaction.

We model a direct band-gap semiconductor with wave functions $\psi_{b\alpha}(\mathbf{r})$ that can represent either a Bloch state for bulk [see Eq. (41)] or the state of a nanostructure in the Envelope Function Approximation [see Eq. (52)] excited by an OV. Following the standard practice, only states close to the band edges (with the approximation for the microscopic wave function $u_{b\mathbf{k}} \to u_{b\mathbf{k}_0} \doteq u_b$, $\mathbf{k}_0$ being the wave vector at the corresponding band edge) are used, so $\psi_{b\alpha}(\mathbf{r}) = \mathcal{E}_{b\alpha}(\mathbf{r}) u_b(\mathbf{r})$ [Eq. (52)]. For bulk, according to Bloch's theorem, the envelope function is given by a plane wave $\mathcal{E}_{\mathbf{k}}(\mathbf{r}) = \exp(i\mathbf{k}\cdot\mathbf{r})/\sqrt{V}$ [Eq. (41)]. We remark that the electron spin –or in the presence of spin-orbit coupling the z-component of the total angular

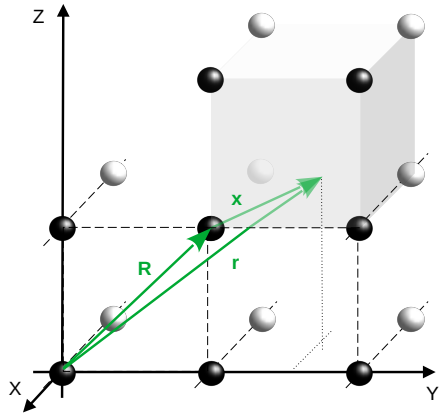

FIG. 7 (color online) Pictorial representation of a crystal with the change of variables to calculate the interaction Hamiltonian matrix element: $\mathbf{r} \to \mathbf{x} + \mathbf{R}$, in which $\mathbf{R}$ points to unit cells, and $\mathbf{x}$ maps points within a unit cell.

momentum– can either be included in the band index b or the state index α. Since the interaction Hamiltonian depends only on spatial coordinates the corresponding matrix elements are diagonal in spin, but not in the total angular momentum. Therefore, the interaction selects the spin and angular momentum projections that are excited –the so-called optical orientation (Meier and Zakharchenya, 2012)– through the polarization of the light and the microscopic wave function u_b (Bastard, 1988). In Sect. IV.A.3 we will come back to the spin-orbit interaction and discuss this point in more detail.

The OV-matter interaction Hamiltonian in its general form reads [see Eq. (46)]

$$\begin{aligned} h_{OV} &= -\frac{q}{2m_0}[\mathbf{p}\cdot\mathbf{A}(\mathbf{r},t) + \mathbf{A}(\mathbf{r},t)\cdot\mathbf{p}] + q\Phi(\mathbf{r},t) \\ &= -\frac{q}{m_0}\mathbf{A}(\mathbf{r},t)\cdot\mathbf{p} + q\Phi'(\mathbf{r},t)\,, \end{aligned} \tag{68}$$

with $\Phi'(\mathbf{r},t) = \Phi(\mathbf{r},t) - (\hbar/2m_0 i)[\nabla\cdot\mathbf{A}(\mathbf{r},t)]$ and the $\mathbf{A}^2$ term being neglected. Different gauges will be considered for special cases, as they may require specific approximations (Sect. IV.A.3).

The matrix element is handled by recognizing that the periodicity in the unit cell $[u_b(\mathbf{r}+\mathbf{R}) = u_b(\mathbf{r})]$ allows one to do an additional simplification (Haug and Koch, 2009): The integral over the whole crystal is separated into integrals over the unit cell and a summation over all the unit cells in the volume $V = Nv$ with v being the volume of the unit cell and N the number of unit cells; thus, with $\mathbf{r} \to \mathbf{x} + \mathbf{R}$ (see Fig. 7)

$$\begin{aligned} \langle b'\alpha'|\, h_{OV}^{(\mathbf{A})}\,|b\alpha\rangle &= \langle b'\alpha'|\, h_{OV}^{(\mathbf{A}1)}\,|b\alpha\rangle + \langle b'\alpha'|\, h_{OV}^{(\mathbf{A}2)}\,|b\alpha\rangle \\ &= -\frac{q}{m_0} v \sum_{\mathbf{R}} \mathcal{E}^*_{b'\alpha'}(\mathbf{R})\mathbf{A}(\mathbf{R},t)\cdot\left[\mathcal{E}_{b\alpha}(\mathbf{R})\frac{1}{v}\int_v d\mathbf{x}\, u^*_{b'}(\mathbf{x})\,\mathbf{p}\,u_b(\mathbf{x}) - i\hbar\nabla\mathcal{E}_{b\alpha}(\mathbf{R})\frac{1}{v}\int_v d\mathbf{x}\, u^*_{b'}(\mathbf{x})\,u_b(\mathbf{x})\right], \end{aligned} \tag{69a}$$

$$\begin{aligned} \langle b'\alpha'|\, h_{OV}^{(\Phi)}\,|b\alpha\rangle &= \langle b'\alpha'|\, h_{OV}^{(\Phi 1)}\,|b\alpha\rangle + \langle b'\alpha'|\, h_{OV}^{(\Phi 2)}\,|b\alpha\rangle \\ &= q\, v \sum_{\mathbf{R}} \mathcal{E}^*_{b'\alpha'}(\mathbf{R})\mathcal{E}_{b\alpha}(\mathbf{R})\left[\nabla\Phi'(\mathbf{R},t)\cdot\frac{1}{v}\int_v d\mathbf{x}\, u^*_{b'}(\mathbf{x})\mathbf{x}\,u_b(\mathbf{x}) + \Phi'(\mathbf{R},t)\,\frac{1}{v}\int_v d\mathbf{x}\, u^*_{b'}(\mathbf{x})\,u_b(\mathbf{x})\right]. \end{aligned} \tag{69b}$$

Here we have assumed that the envelope functions and the potentials vary slowly over a unit cell and kept only the lowest orders. The two terms in Eq. (69a) arise from the action of the momentum operator $\mathbf{p} = -i\hbar\nabla$ on the lattice-periodic part and the envelope part of the wave function, respectively, while the two terms in Eq. (69b) reflect the lowest orders in the expansion of Φ'.

The microscopic wave functions $u_{b\mathbf{k}_0}$ at a fixed $\mathbf{k}_0$ form a complete orthonormal system in a unit cell, thus $v^{-1}\int_v d\mathbf{x}\, u^*_{b'}(\mathbf{x})\, u_b(\mathbf{x}) = \delta_{bb'}$. Therefore, the second terms on the right hand side of Eqs. (69a) and (69b) give rise to intraband processes. Replacing $v\sum_{\mathbf{R}}$ by the integral $\int d\mathbf{R}$ over the whole system, these process are described by the matrix elements

$$\langle b\alpha'|\, h_{OV}^{(2)}\,|b\alpha\rangle = \int d\mathbf{R}\,\mathcal{E}^*_{b\alpha'}(\mathbf{R})\left[\frac{i\hbar q}{m_0}\mathbf{A}(\mathbf{R},t)\cdot\nabla + q\Phi'(\mathbf{R},t)\right]\mathcal{E}_{b\alpha}(\mathbf{R}). \tag{70}$$

If the microscopic wave functions u_b have a well-defined parity, the first terms on the right hand side of Eqs. (69a) and (69b) give rise to purely interband processes, because the operators $\mathbf{p}$ and $\mathbf{x}$ both have odd parity. In many typical semiconductors the parities of u_b are different in the valence (v) and the conduction (c) band; then these terms induce dipolar transitions between valence and conduction band. With $b' = c$ and $b = v$ and introducing the momentum and dipole matrix elements, $\mathbf{p}_{cv} = v^{-1}\int_v d\mathbf{x}\, u^*_c(\mathbf{x})\mathbf{p}u_v(\mathbf{x})$ and $\mathbf{d}_{cv} = qv^{-1}\int_v d\mathbf{x}\, u^*_c(\mathbf{x})\mathbf{x}u_v(\mathbf{x})$ [see Eq. (57)], respectively,

we obtain for the interband-transition matrix element

$$\langle c\alpha'|\, h^{(1)}_{OV}\,|v\alpha\rangle = \int d\mathbf{R}\, \mathcal{E}^*_{c\alpha'}(\mathbf{R})\Big[-\frac{q}{m_0}\mathbf{A}(\mathbf{R},t)\cdot\mathbf{p}_{cv} + \nabla\Phi'(\mathbf{R},t)\cdot\mathbf{d}_{cv}\Big]\mathcal{E}_{v\alpha}(\mathbf{R}). \quad (71)$$

Assuming a bulk semiconductor with plane wave envelope functions and a spatially homogeneous electric field $\mathbf{E}(t)$, we recover the vertical transition approximation, either in the Coulomb gauge with $\mathbf{A}(t) = -\int_{t_0}^{t}\mathbf{E}(t')dt'$ and $\Phi = 0$ or in the dipole (Göppert-Mayer) gauge with $\mathbf{A} = 0$ and $\Phi' = \Phi = -\mathbf{r}\cdot\mathbf{E}(t)$, that leads to $\nabla\Phi'(\mathbf{R},t) = -\mathbf{E}(t)$ (Sect. III.C.3). We want to remark that in some semiconductors, a prototype being cuprous oxide Cu_2O, the parities of valence and conduction band states at the band extrema are the same. In this case one has to take into account the linear order in $\mathbf{k}$ in the expansion of the microscopic wave functions $u_{b\mathbf{k}}$ around the band extrema, which leads to weaker, so called "second class" transitions (Elliott, 1957; Nikitine, 1969).

The Rotating Wave Approximation (RWA) simplifies further the coupling Hamiltonian. Recalling that all fields are real quantities, we separate the potentials into the positive and negative frequency components $\mathbf{A} = \mathbf{A}^{(+)} + \mathbf{A}^{(-)}$, with $\mathbf{A}^{(\pm)} \propto \exp(\mp i\omega t)$ and correspondingly for Φ. The RWA stipulates that in a frame rotating with the light field only slowly varying terms are to be retained. For a light field resonant or near-resonant to an interband transition $\mathbf{A}^{(+)}$ and $\Phi^{(+)}$ ($\mathbf{A}^{(-)}$ and $\Phi^{(-)}$) account for the absorption (emission) of light by the material system. On the other hand, a matrix element $\langle b'\alpha'|\, h_{OV}\,|b\alpha\rangle$ implies the transition $b\alpha \to b'\alpha'$. Therefore, matrix elements compatible with the RWA are: (i) a transition from valence to conduction band induced by $A^{(+)}$, (ii) a transition from conduction to valence induced by $A^{(-)}$ (Cohen-Tannoudji *et al.*, 1998; Scully and Zubairy, 1997). For light fields in the optical frequency range intraband terms are far off-resonant and are therefore neglected in RWA. They are usually important if there is –either only or in addition to the optical field– a static or low-frequency electromagnetic field leading, e.g., to intraband transport terms (Rossi and Kuhn, 2002) or phenomena like the static or dynamical Franz-Keldysh effect (Franz, 1958; Jauho and Johnsen, 1996; Keldysh, 1958). Furthermore, they become important in the case of strongly off-resonant or extremely strong light fields, where the RWA is not applicable, e.g., when dealing with two-photon transitions (Duc *et al.*, 2005) or high harmonic generation (Golde *et al.*, 2008). If not explicitly stated otherwise, in the following we will assume that the RWA is applicable and we will neglect the intraband matrix elements $h^{(2)}_{OV}$.

To describe the interaction with OVs, one has to depart from traditional semiconductor optics by keeping the spatial structure of the beam at the level of the whole system in Eq. (71).[10] From a different standpoint, one is abandoning the vertical-transition and dipole-moment approximations, at least in their most strict sense. A strict dipole-moment approximation requires a spatially uniform vector potential $\mathbf{A}$ and a scalar potential Φ linear in $\mathbf{r}$, that brings the integrals in the case of bulk Bloch functions, where α corresponds to the wave vector $\mathbf{k}$, into a $\delta_{\mathbf{k}\mathbf{k}'}$ or in the case of angular momentum eigenstates, where α comprises an angular momentum quantum number m, into a $\delta_{mm'}$. In contrast to smooth fields, OVs have a spatial structure that strongly varies on the scale of the semiconductor. For example, a monochromatic Bessel beam with angular frequency ω, single topological charge ℓ and polarization σ for general γ [Eq. (23)] reads

$$\tilde{\mathbf{A}}(\mathbf{r},t) = A_0 J_\ell(q_r r)e^{i\ell\varphi}\mathbf{e}_\sigma - i\gamma\sigma\frac{q_r}{q_z}\frac{A_0}{\sqrt{2}}J_{\ell+\sigma}(q_r r)e^{i(\ell+\sigma)\varphi}\mathbf{e}_z \quad (72a)$$

$$\tilde{\Phi}(\mathbf{r},t) = i(1-\gamma)\sigma\frac{c^2}{\omega}\frac{A_0}{\sqrt{2}}q_r J_{\ell+\sigma}(q_r r)e^{i(\ell+\sigma)\varphi}, \quad (72b)$$

with amplitude A_0. The space dependence of the potentials clearly precludes the simplification of Eq. (71) leading to vertical transitions in $\mathbf{k}$ or m or, more general, diagonal transitions in α. Note that the dipole-moment approximation at the level of the microscopic wave function is however retained; therefore, multipolar transitions are only possible between envelope states –for further discussion see Sect. VI.B.3.

By using the interband matrix elements of the interaction Hamiltonian according to Eq. (71) we can now specify the general EoM (56) to the two-band case, leading to

[10] This is not to be confused with a "parametrical" dependence, in which $\mathbf{R}$ is a constant indicating the position of a nanostructure, and no integration is performed on $\mathbf{R}$.

$$i\hbar\frac{d}{dt}\rho_{vc,\alpha\alpha'} = \Delta_{c\alpha',v\alpha}\rho_{vc,\alpha\alpha'} + \sum_\beta \left(\langle c\alpha'| h^{(1)}_{OV} |v\beta\rangle \rho_{v,\alpha\beta} - \langle c\beta| h^{(1)}_{OV} |v\alpha\rangle \rho_{c,\beta\alpha'} \right), \tag{73a}$$

$$i\hbar\frac{d}{dt}\rho_{v,\alpha\alpha'} = \Delta_{v,\alpha'\alpha}\rho_{v,\alpha\alpha'} + \sum_\beta \left(\langle v\alpha'| h^{(1)}_{OV} |c\beta\rangle \rho_{vc,\alpha\beta} - \langle c\beta| h^{(1)}_{OV} |v\alpha\rangle \rho_{cv,\beta\alpha'} \right), \tag{73b}$$

$$i\hbar\frac{d}{dt}\rho_{c,\alpha\alpha'} = \Delta_{c,\alpha'\alpha}\rho_{c,\alpha\alpha'} + \sum_\beta \left(\langle c\alpha'| h^{(1)}_{OV} |v\beta\rangle \rho_{cv,\alpha\beta} - \langle v\beta| h^{(1)}_{OV} |c\alpha\rangle \rho_{vc,\beta\alpha'} \right), \tag{73c}$$

with $\Delta_{c\alpha',v\alpha} = (\varepsilon_{c\alpha'} - \varepsilon_{v\alpha})$, and $\Delta_{b,\alpha'\alpha} = (\varepsilon_{b\alpha'} - \varepsilon_{b\alpha})$ for $b \in \{c, v\}$. The contributions of the Coulomb interaction are not included here. As discussed in Sect. III.C.3 they involve two-particle density matrices (i.e., expectation values of four operators) which after factorization give rise to renormalizations of energies and light field similar to the homogeneous bulk case [Eq. (64)]. In Sect. IV.A.2 the Coulomb term will be considered when discussing excitonic effects associated with the excitation of bulk semiconductors by an OV.

In the case of a homogeneous bulk semiconductor the single particle density matrices are diagonal in $\mathbf{k}$. With the interaction matrix elements for a homogeneous electric field Eqs. (73) immediately reduce to Eqs. (60), implying vertical transitions.

In general, however, due to the non-diagonal character of the interaction matrix elements even a density matrix which is initially diagonal in α will not remain diagonal in the course of time. Assuming, for instance, at a given time the single particle density matrices to be diagonal in α, according to the EoM (73) in the next time step the density matrix elements with all combinations $(\alpha\alpha')$, for which also the interband matrix element $\langle c\alpha'| h^{(1)}_{OV} |v\alpha\rangle$ is nonzero, will be nonzero.

Due to the lack of the diagonal (or vertical) nature of the light-induced transitions, the EoM are considerably more complicated than the Eqs. (60) for the homogenous bulk system, for they couple in principle all possible values of the quantum number α in each band, even without taking into account many-body effects. If one is not only interested in the carrier generation process itself, typically the EoM have to be complemented by some relaxation terms. In the simplest case one can just include phenomenological interband and intraband relaxation times. A more microscopic description of scattering, relaxation and recombination processes can be obtained by adding Boltzmann-like scattering terms, which can be formally derived, e.g., by a correlation expansion of the terms induced by the coupling of the electrons to phonons, to other electrons, or to the photon vacuum (Rossi and Kuhn, 2002).

Besides a full numerical solution of the system of equations involving a suitable restriction of the set of quantum numbers or a suitable discretization in the case of (quasi-)continuous quantum numbers, general approaches to solve this system of equations under specific conditions exist, which provide further insight into the optical properties and dynamics induced by the excitation with OVs. Under low-excitation conditions, a perturbative, iterative approach in terms of the amplitude of the driving field (or its potentials) provides approximate solutions for interband and intraband density matrices for a system initially in its electronic ground state. To lowest order, i.e., without electromagnetic fields, the only non-zero matrix elements are the valence-band populations $\rho^{(0)}_{v,\alpha\alpha'} = \delta_{\alpha\alpha'}$ while $\rho^{(0)}_{c,\alpha\alpha'} = \rho^{(0)}_{vc,\alpha\alpha'} = 0$ (the superscript indicates the order). The only non-zero source term then appears in interband coherences $\rho_{vc,\alpha\alpha'}$; thus, the lowest order interband coherence $\rho^{(1)}_{vc,\alpha\alpha'}$ is linear in the driving, e.g., in the vector potential amplitude A_0 [see Eq. (72)]. This in turn induces a second order term in the intraband coherences and occupations. Following this iterative process, it is clearly seen that interband (intraband) coherences come only in odd (even) powers of the amplitude. Keeping in mind that the interband density matrix elements oscillate with the frequency of the band gap while the intraband coherences oscillate with frequencies corresponding to energy differences in the bands, the transfer of OAM from light to electrons can thus be separated into fast (odd) and slow (even) contributions. However, we want to remark that this separation into fast and slow variables is only possible if the RWA is applicable. Non-RWA contributions in the interband matrix elements of the interaction Hamiltonian lead to additional fast contributions in the intraband density matrices. Including intraband matrix elements according to Eq. (70) interband and intraband coherences as well as occupations appear in all orders of the field.

A different approach based on a quasi-equilibrium approximation relies on the difference in time scales of scattering-induced relaxation and light-induced excitation processes. For sufficiently strong scattering the intraband populations can be approximated by quasi-equilibrium distributions with a given temperature and chemical potential, allowing for a solution of the interband coherence that feeds slowly varying EoM for intraband coherences or populations (Chow and Koch, 1999). In this way, absorption spectra of highly excited semiconductors can be obtained.

2. Bulk

Bloch states are the natural representation of electrons in a bulk crystal; though not specially well-suited to describe the interaction with OVs, they still shed light onto interesting features that complement those learned from a representation of electrons in cylindrical states, and connect well to what we learned about the modal decomposition of OVs in Sect. II.F.

In semiconductor optics, one is mostly concerned with interband processes, in which an electron undergoes transitions between valence and conduction bands, separated from each other by the band gap E_g. The transition is induced by resonant or nearly resonant light $\hbar\omega \simeq E_g$. The simplest theoretical model is that of a two-band semiconductor excited by a monochromatic single-singularity OV. Working in the Coulomb and radiation gauge, the scalar potential vanishes and the relevant light-matter interaction matrix element [Eq. (71)] between Bloch states $\psi_{b\alpha}(\mathbf{r}) = \exp(i\mathbf{k}\cdot\mathbf{r})u_b(\mathbf{r})/\sqrt{V}$ is given by

$$\langle c\mathbf{k}'|\, h_{OV}^{(1)}\,|v\mathbf{k}\rangle = -\frac{q}{m_0}\mathbf{p}_{cv}\cdot\frac{1}{V}\int d\mathbf{R} e^{-i(\mathbf{k}'-\mathbf{k})\cdot\mathbf{R}}\mathbf{A}(\mathbf{R},t)\,,$$

i.e., it involves the Fourier transform of the beam profile. Irrespective of the particular form of the single-singularity OV being considered (see Sect. II.C), the vector potential has in the component j the form

$$A_j(\mathbf{r},t) = A_{0j}(r)e^{in_j\varphi}e^{i(q_z z-\omega t)} + \text{c.c.}\,, \qquad (74)$$

with $n_j = \ell, \ell+\sigma, \ldots$ and $A_{0j}(r)$ the space- and n_j-dependent amplitude. We handle the calculation of the matrix elements in the following way. Because of the symmetry of the light field we use a normalization volume of the Bloch functions in the form of a cylinder with radius R_0 and height L. We split the integral into an in-plane integral and one in z-direction and use the vectors $\boldsymbol{\kappa} = \mathbf{k}' - \mathbf{k}$ and $\mathbf{R}$ in cylindrical coordinates $\{\kappa_r, \varphi_\kappa, \kappa_z\}$ and $\{R, \varphi, Z\}$, respectively, leading to $\boldsymbol{\kappa}\cdot\mathbf{R} = \kappa_r R\cos(\varphi_\kappa - \varphi) + \kappa_z Z$ [see Eq. (33)]. The z-integral simply reduces to $\int dZ\, e^{i(q_z-\kappa_z)z} = L\delta_{q_z,\kappa_z}$. To simplify the in-plane integral we introduce the Jacobi-Anger identity $e^{iu\cos\eta} = \sum_t i^t J_t(u)e^{i\eta t}$ (Korenev, 2002) [compare to Eq. (36)]. The resulting matrix element is

$$\langle c\mathbf{k}'|\, h_{OV}^{(1)}\,|v\mathbf{k}\rangle|_j = -\frac{q}{m_0}p_{cv,j}(-i)^{n_j}\delta_{q_z,\kappa_z}e^{-i\omega t}e^{in_j\varphi_\kappa} \times\frac{2}{R_0^2}\int dR\, R\, J_{n_j}(\kappa_r R)A_{0j}(R)\,,$$

where we have taken into account that due to the RWA only the positive frequency component $\mathbf{A}^{(+)}$ of the potential contributes to the matrix element describing a transition from valence to conduction band.

A simplification of the last integral is possible if we specify the radial profile of the beam. If the beam profile is of Bessel type, $A_{0j}(R) = A_{0j}J_{n_j}(q_r R)$, we use the orthogonality $\int_0^\infty RJ_\alpha(\kappa_r R)J_\alpha(q_r R)dR = \delta(\kappa_r - q_r)/q_r$ and replace the delta function $\delta(q_r-\kappa_r)$ by $(R_0/\pi)\delta_{q_r,\kappa_r}$ appropriate for the cylindrical normalization volume with radius R_0. The contribution of the j-th component of the vector potential to the matrix element then reads

$$\langle c\mathbf{k}'|\, h_{OV}^{(1)}\,|v\mathbf{k}\rangle|_j = -(-i)^{n_j}p_{cv,j}A_{0j}\frac{2q}{\pi m_0 q_r R_0} \times\delta_{q_r,\kappa_r}\delta_{q_z,\kappa_z}e^{in_j\varphi_\kappa}e^{-i\omega t}\,. \qquad (75)$$

The factor δ_{q_z,κ_z} imposes conservation of the linear momentum in the z-direction, the factor δ_{q_r,κ_r} fixes the in-plane distance of the vectors $\mathbf{k}'$ and $\mathbf{k}$. However, there is no explicit expression signaling the conservation of OAM, which is obviously due to the fact that Bloch states are not eigenstates of the angular momentum operator.

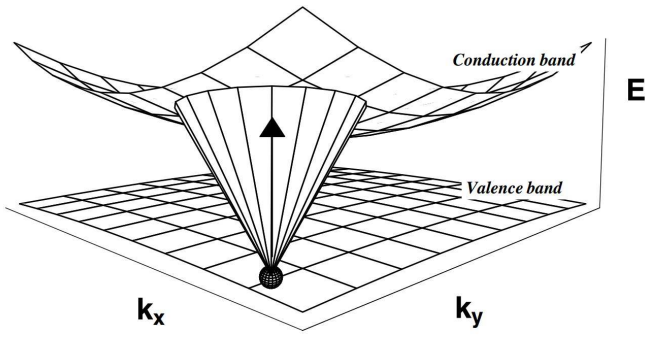

FIG. 8 Pictorial representation of the electronic excitation of a bulk semiconductor in the Bloch electron representation. An electron in the valence band is promoted to a superposition state in the conduction band. From Quinteiro and Tamborenea (2009c).

We can get additional insight by looking at the infinitesimal time evolution of an electron initially in the Bloch state $\psi_{v\mathbf{k}}(\mathbf{r})$. Realizing that the evolution operator for a single particle state in the interaction picture for short times δt is given by $U = 1 - (i\delta t/\hbar)h_{OV}$ leads to $\psi(\mathbf{r},\delta t) = \psi(\mathbf{r},0) - (i\delta t/\hbar)\delta\psi(\mathbf{r})$. Assuming initially an electron in the Bloch state $\psi_{v\mathbf{k}}(\mathbf{r})$, we obtain

$$\begin{aligned}\delta\psi(\mathbf{r}) &= \sum_{\mathbf{k}'}\psi_{c\mathbf{k}'}\langle c\mathbf{k}'|\, h_{OV}^{(1)}\,|v\mathbf{k}\rangle \\ &= -\frac{2q}{\pi m_0 q_r R_0}e^{-i\omega\delta t}\sum_j(-i)^{n_j}p_{cv,j}A_{0j} \\ &\quad\times\int d\varphi_\kappa e^{in_j\varphi_\kappa}\psi_{c\mathbf{k}+\bar{\boldsymbol{\kappa}}}(\mathbf{r}) \\ &= f(\mathbf{r})\psi_{c\mathbf{k}}(\mathbf{r})\,, \end{aligned} \qquad (76)$$

in which the action of δ_{κ,q_r} and δ_{q_z,κ_z} has been incorporated by defining $\bar{\boldsymbol{\kappa}} = (q_r, \varphi_\kappa, q_z)$. The second form stresses the fact that the new wave function is not an eigenstate of the crystal Hamiltonian (Quinteiro and Tamborenea, 2009c). Pictorially, the excitation looks like a cone in momentum space with fixed aperture q_r, see Fig. 8. The final superposition is formed by states lying

on the curve resulting from the intersection of the cone and the conduction band, each state having a particular phase $\exp(in_j\varphi_\kappa)$. The existence of a cone-like excitation is not surprising: According to Sect. II.F the OV can be decomposed into a superposition of plane waves with wave vectors lying on the surface of a cone and varying phases. In the picture of plane waves, each component induces a one k-state-to-one k-state electronic transition, with conservation of its linear momentum; the whole excitation is however one k-state to a superposition of many k-states.

The expectation value of the OAM picked by electrons, and the concomitant electric current density $\mathbf{j} = (q\hbar/m_0)\mathrm{Im}[\psi^*\nabla\psi] - (q^2/m_0)\mathrm{Re}[\psi^*\mathbf{A}\psi]$ can be studied in powers of A_0 (Quinteiro and Tamborenea, 2009a). The first order ($\propto A_0^1$) current is of microscopic origin and analogous to the optical polarization induced by plane waves: The vector potential imprints its spatial and temporal pattern onto the electronic state, see Fig. 9, and a net circulation around $r = 0$ is only observed for $\{\ell = \pm 1, \sigma = \mp 1\}$, but with zero time average. The second order ($\propto A_0^2$) current is macroscopic and produces a net circulation with non-zero average. The circular electric current generated by OVs in semiconductor represent a new example of photon-drag effects which has recently been observed in experiments (Ge, 2020; Ji *et al.*, 2020).

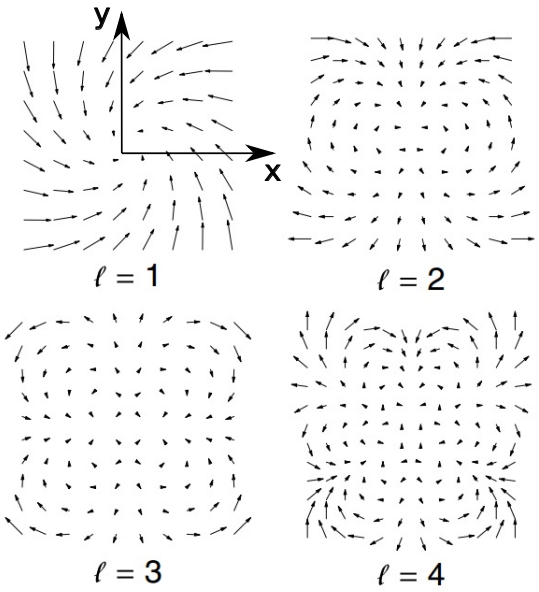

FIG. 9 First order electric current in bulk for $\ell = 1...4$ and fixed polarization $\sigma = -1$. The current cycles in time and z following the electric field as shown in Fig. 2. From Quinteiro and Tamborenea (2009c).

Extensions to the simple model just explained have been done so far in two directions. On the one hand, a model still without electron-electron interaction was used to predict electronic transitions, OAM transfer and electric currents using a more suitable representation of electrons by envelope states factorizing in cylindrical coordinates instead of the plane-wave envelope of Bloch states (Quinteiro and Tamborenea, 2010). On the other hand, using Bloch states and including electron-electron interaction the EoM relevant for excitons and derived quantities were deduced (Quinteiro, 2010).

The symmetry mismatch between OVs and Bloch states led to a complex model of the optical excitation in bulk, that ultimately required the transformation of Bloch states to a cylindrical representation using the Jacobi-Anger identity. One can face the OV-bulk problem instead directly by using cylindrical coordinates. For a large system and in the presence of the envelope function approximation bulk properties are independent of the chosen boundary, being this a cubic box or a cylinder. Since the optical excitation takes place at the band edges the envelope function approximation is applicable and one can describe electron states by [see also Eq. (52)]

$$\psi_{b\mathbf{k}m}(\mathbf{r}) = NJ_m(k_r r)e^{im\varphi}e^{ik_z z}u_b(\mathbf{r})\,,$$

defined inside a large cylinder of height L, radius R_0, quasi-momenta k_z, k_r and OAM $\hbar m$. The electron wave function with the normalization constant N is expressed in cylindrical coordinates $\{r, \varphi, z\}$ (Quinteiro and Tamborenea, 2010). From the strong similarities between the representation of a typical single-singularity OV [Eq. (72)] and electron states in a cylinder we foresee that the light-matter matrix element will be simpler than in the case of Bloch states based on plane waves. The interband matrix element with vector potential according to Eq. (74) having $A_{0j}(r) = A_{0j}J_{n_j}(q_r r)$ reads in the basis of the cylinder functions

$$\begin{aligned}\langle c, k_r', m', k_z'|\, h_{OV}^{(1)}\, |v, k_r, m, k_z\rangle \\ = -\frac{q}{m_0}p_{cv,j}A_{0j}NN'\delta_{k_z',k_z+q_z}\delta_{m',m+n_j} \\ \times \int dR\, RJ_{m'}(k_r'R)J_{n_j}(q_rR)J_m(k_rR)\,. \qquad (77)\end{aligned}$$

In fact, by fixing the final values m' and k_z', the matrix element reflects the conservation of the ~~orbital~~ quantum number m and the linear quasi-momentum k_z, and only the radial quantum numbers k_r' and k_r are coupled by an integral over the Bessel functions of the beam and initial and final electron states. We thus obtain a complementary situation compared to the calculation in the Bloch state basis. While there the transfer in the radial component of the Bloch wave vector κ_r was fixed while the angle was continuous, now the change of the angle dependence, characterized by the quantum numbers m' and m, is fixed and the radial quantum number in the Bessel function changes continuously.

It is instructive to look at the lowest order results of interband and intraband variables obtained for a monochromatic Bessel beam. Assuming a sufficiently small paraxiality parameter q_r/q_z the longitudinal field

component can be neglected and we assume a transverse vector potential amplitude $\mathbf{A}_0$ and a beam with a given topological charge ℓ. The zeroth order is given by a completely filled valence band, i.e., $\rho^{(0)}_{v,\alpha\alpha'} = \delta_{\alpha\alpha'}$ with $\alpha = (k_r, m, k_z)$, and all other density matrices vanish.

In first order we obtain from Eqs. (73) an interband coherence according to

$$\rho^{(1)}_{vc,\alpha\alpha'} = -\langle c\alpha'|\, h^{(1)}_{OV}\, |v\alpha\rangle \frac{1 - e^{-i(\varepsilon_{c\alpha'} - \varepsilon_{v\alpha} - \hbar\omega)t/\hbar}}{\varepsilon_{c\alpha'} - \varepsilon_{v\alpha} - \hbar\omega}. \quad (78)$$

Inserting the matrix element from Eq. (77), we thus find that the OV excites interband coherences with $m' - m = \ell$, $k'_z - k_z = q_z$ and in general arbitrary k'_r and k_r.

In second order Eqs. (73) give rise to intraband coherences and, as a special case, the populations in the conduction and the valence band. For the populations of the conduction band states one gets

$$\rho^{(2)}_{c,\alpha'\alpha'} = 4 \sum_{\alpha} \frac{|\langle c\alpha'|\, h^{(1)}_{OV}\, |v\alpha\rangle|^2}{(\varepsilon_{c\alpha'} - \varepsilon_{v\alpha} - \hbar\omega)^2} \times \sin^2\left(\frac{(\varepsilon_{c\alpha'} - \varepsilon_{v\alpha} - \hbar\omega)t}{2\hbar}\right). \quad (79)$$

While the populations start to grow quadratically in t, for longer time the growth is linear with a growth rate given by Fermi's golden rule, as is expected for transitions in a continuous spectrum.

Important observables that one can calculate from the coherence are the OAM and the electric current in the electronic system. Gauge invariance imposes the need to express appropriately the quantities for which expectation values are to be calculated. In the Coulomb gauge, as is the case here, the OAM and electric current depend on the mechanical momentum of electrons $\mathbf{p} - q\mathbf{A}$; the first (second) term gives rise to the so-called paramagnetic (diamagnetic) contributions. A detailed calculation of the OAM and electric current has been done in Quinteiro and Tamborenea (2010). The results, in agreement with those from the simple model for Bloch states, show that the interband coherence produces a fast oscillation of the OAM and a current with zero average, while the occupations and intraband coherences induce a permanent transfer of OAM from the light to the electrons that generate a slow electric current with a non-zero mean value. The latter can be seen as the consequence of tilted transitions when plotting the energies of the valence and conduction band states versus their angular momentum quantum number m, a feature that will be discussed in more detail in the context of the excitation of quantum rings (Sect. IV.A.3.a); note that the OAM associated with the beam is also proportional to the square of the field amplitude, as seen in Eq. (1).

Yet another extension to the simple single-particle bulk model is the inclusion of the Coulomb interaction, which allows for the description of excitons. Excitonic effects are important for a correct description of light-matter interaction close to the band edge, in particular at low excitation densities, because they qualitatively modify the absorption spectrum leading to discrete lines below the band-to-band continuum. In fact, excitonic effects appear already at the lowest order in the field amplitude, i.e., by considering the EoM for the interband coherence alone (Haug and Koch, 2009). Quinteiro (2010) considered the excitation of a bulk semiconductor with two energy bands by a monochromatic and transverse OV in a Bloch state representation. The non-vertical nature of optical transitions induced by OVs makes it convenient to work in a mixed representation of momentum and space coordinates, in analogy to the general approach based on Wigner functions discussed by Rossi and Kuhn (2002).

The derivation of the contributions to the EoM of the single-particle density matrix elements due to the electron-electron interaction Hamiltonian [Eq. (62)] has been discussed in Sect. III.C.3 and the results on the level of the time-dependent Hartree-Fock theory has been given for the case of a homogeneous two-band semiconductor in Eqs. (64)-(67). The excitation by an inhomoegenous light field, in particular by an OV, leads to inhomogeneous excitations, which are described by non-diagonal density matrices $\rho_{vc,\mathbf{kk'}}$, $\rho_{v,\mathbf{kk'}}$, and $\rho_{c,\mathbf{kk'}}$. The derivation of the EoM proceeds in the same way as for a homogeneous system, only in the factorization of the four-operator terms like in Eq. (63) also off-diagonal terms have to be kept. This has two consequences: (*i*) The renormalizations of the field and the energies [see Eqs. (65)-(67)] become non-diagonal in $\mathbf{k}$ and $\mathbf{k'}$; (*ii*) the renormalizations of the energies get additional contributions from Hartree terms, which vanish in the homogeneous case due to charge neutrality. The full, off-diagonal terms (in an electron-hole representation) can be found in Rossi and Kuhn (2002). Here we will restrict ourselves to the lowest order, i.e., to the linear response of the semiconductor to the excitation with an OV.

From the discussion above we recall that interband density matrices appear in odd orders of the field and intraband density matrices in even orders. Restricting ourselves to the linear order therefore implies setting $\rho_{v,\mathbf{kk'}} = \delta_{\mathbf{kk'}}$ and $\rho_{c,\mathbf{kk'}} = 0$. Since the renormalizations of the energies are caused by deviations of the intraband density matrices from their equilibrium value, they do not contribute to the first order response. The equation of motion for the interband density matrix then reads

$$i\hbar \frac{d}{dt}\rho_{vc,\mathbf{kk'}} = \Delta_{c\mathbf{k'},v\mathbf{k}}\rho_{vc,\mathbf{kk'}} + \langle c\mathbf{k'}|\, h_{OV}\, |v\mathbf{k}\rangle - \sum_{\mathbf{g}\neq 0} V_{\mathbf{g}}\rho_{vc,\mathbf{k}-\mathbf{g}\,\mathbf{k'}-\mathbf{g}}\,, \quad (80)$$

with $\Delta_{c\mathbf{k'},v\mathbf{k}} = \varepsilon_{c\mathbf{k'}} - \varepsilon_{v,\mathbf{k}}$.

The evolution of the coherence is driven by the OV-matter matrix element Eq. (75) which, for the case of excitation by a Bessel beam can be translated into a non-

vanishing matrix element $\langle c\mathbf{k}+\bar{\boldsymbol{\kappa}}|\, h_{OV}\,|v\mathbf{k}\rangle$, with $\bar{\boldsymbol{\kappa}} = q_r\cos\varphi_\kappa\hat{\mathbf{x}} + q_r\sin\varphi_\kappa\hat{\mathbf{y}} + q_z\hat{\mathbf{z}}$, in which q_r and q_z are fixed by the corresponding parameters of the beam and φ_κ is variable. Once again we find the connection to the modal decomposition and the solution of the bulk problem in Bloch states: the matrix element gives rise to a non-vanishing contribution for each plane wave on a cone.

Instead of using a non-diagonal $\mathbf{k}$-representation of the density matrix elements also various types of mixed $(\mathbf{k},\mathbf{r})$-representations can be useful. Starting point is typically a transformation from the wave vectors $\mathbf{k}$, $\mathbf{k}'$ to some relative and center-of-mass wave vectors according to $\mathbf{k} = \mathbf{K}-\eta\boldsymbol{\kappa}$, $\mathbf{k}' = \mathbf{K}+\eta'\boldsymbol{\kappa}$ with $\eta+\eta' = 1$. A spatial variable is then obtained by Fourier transformation with respect to one of the wave vectors. Choosing $\eta = \eta' = \frac{1}{2}$ and Fourier transforming with respect to $\boldsymbol{\kappa}$ leads to an interband Wigner function [and correspondingly to intraband Wigner functions when transforming the intraband density matrices (Rossi and Kuhn, 2002)]. Especially for the interband variable in the case of parabolic bands with $\varepsilon_{c\mathbf{k}} = E_g + \hbar^2k^2/(2m_c)$ and $\varepsilon_{v\mathbf{k}} = -\hbar^2k^2/(2m_v)$ with conduction band and valence band masses m_c and m_v, respectively, and band gap E_g, the choice $\eta' = m_c/M$, $\eta = m_v/M$ with $M = m_c + m_v$ can be more convenient, because it leads to $\Delta_{c\mathbf{k}',v\mathbf{k}} = \hbar^2K^2/(2\mu) + \hbar^2\boldsymbol{\kappa}^2/(2M) + E_g$ with $\mu^{-1} = m_c^{-1}+m_v^{-1}$. In contrast to Fourier transforming with respect to $\boldsymbol{\kappa}$, as in the case of the Wigner function, here it is more useful to perform a Fourier transform with respect to $\mathbf{K}$. Performing additionally a temporal Fourier transform the function $\widetilde{\rho}_{\boldsymbol{\kappa}}(\omega,\mathbf{r})$ is defined as

$$\widetilde{\rho}_{\boldsymbol{\kappa}}(\omega,\mathbf{r}) = \frac{1}{2\pi}\sum_{\mathbf{K}}\int dt\rho_{vc,\mathbf{K}+\frac{m_v}{M}\boldsymbol{\kappa},\mathbf{K}-\frac{m_c}{M}\boldsymbol{\kappa}}(t)e^{i(\mathbf{K}\cdot\mathbf{r}+\omega t)}, \tag{81}$$

which satisfies the equation of motion

$$\begin{aligned}&\left[\hbar\omega - E_g - \frac{\hbar^2\boldsymbol{\kappa}^2}{2M} + \frac{\hbar^2}{2\mu}\nabla^2 + V(\mathbf{r})\right]\widetilde{\rho}_{\boldsymbol{\kappa}}(\omega,\mathbf{r})\\ &= V\delta(\mathbf{r})\langle c, \frac{m_c}{M}\boldsymbol{\kappa}|\, h_{OV}\,|v, -\frac{m_v}{M}\boldsymbol{\kappa}\rangle\\ &= -V\delta(\mathbf{r})\frac{2q}{\pi m_0 q_r R_0}(-i)^\ell\mathbf{p}_{cv}\cdot\mathbf{A}_0\delta_{q_r,\kappa_r}\delta_{q_z,\kappa_z}e^{i\ell\varphi_\kappa},\end{aligned} \tag{82}$$

where we have used the identity $\sum_{\mathbf{K}}\exp(i\mathbf{K}\cdot\mathbf{r}) = V\delta(\mathbf{r})$ and assumed an excitation by a transverse Bessel beam with topological charge ℓ and longitudinal (transverse) wave vector q_z (q_r).

The homogeneous part of Eq. (82) has the form of a Wannier equation for a quasiparticle with mass M and center-of-mass momentum $\hbar\boldsymbol{\kappa}$. The relative motion of electron and hole reflects the motion of a particle with the reduced mass μ in the Coulomb potential $V(\mathbf{r})$. The right hand side is the source term which describes the excitation by the OV. Equation (82) is solved by a composition $\widetilde{\rho}_{\bar{\boldsymbol{\kappa}}} = \sum_\nu b_\nu\psi_\nu$ of solutions ψ_ν to the homogeneous equation [see Chapter 10 of Haug and Koch (2009)], where ν summarizes the quantum numbers for both the relative and the center-of-mass motion.

Due to the function $\delta(\mathbf{r})$ in the source term we notice that also in the case of excitation by an OV only excitons with s-type wave function of the relative motion can be excited. As a consequence of the factors $\delta_{q_r,\kappa_r}\delta_{q_z,\kappa_z}$ a superposition of excitons with non-vanishing center-of-mass wave vector in longitudinal and radial direction, determined by the corresponding wave vector components of the beam, is excited with relative phases determined by the topological charge ℓ.

By an inverse Fourier transform, the coherence in momentum space is recovered, and can be used to derive the local polarization of the system, from it the susceptibility and optical response. The spectrum presents a small shift compared to the conventional exciton theory, due to the center-of-mass motion.

So far we have discussed dipole-allowed excitonic transitions, as they appear in many III-V or II-VI semiconductors. In some materials the microscopic dipole ($\mathbf{d}_{cv}$) or momentum ($\mathbf{p}_{cv}$ matrix element between the band edge states vanishes for symmetry reasons and one has to go to the next order in the expansion of the microscopic wave function with respect to $\mathbf{k}$ (Elliott, 1957). This is the case, e.g., in bulk Cu_2O, a material which has recently regained a lot of attention because of the observation of Rydberg excitons with quantum numbers up to ~ 26 (Kazimierczuk *et al.*, 2014). In this material selection rules different from the typical zincblende semiconductors hold. By using group theoretical methods, Konzelmann *et al.* (2019) analyzed the selection rules for the excitation of large (about 400nm radius) Rydberg excitons in bulk Cu_2O by OVs, and concluded that s-d envelope wave function excitons are addressable by light with topological charge $\ell = 1, 3$.

A number of experiments have been performed on bulk semiconductors that shed light on the excitation by OVs of bulk systems. Ueno *et al.* (2009) performed a four-wave mixing (FWM) experiment in bulk GaN using a pair of LG beams to study the coherent dynamics of excitons. The FWM signal was measured to carry predominantly the topological charge $2\ell_2 - \ell_1$, which is the expected value for excitons picking the OAM of pump and probe pulses with ℓ_1 and ℓ_2, respectively. Shigematsu *et al.* (2016) extended these studies by analyzing the transfer of OAM to other values than the expected one of $2\ell_2-\ell_1$. In fact, additional values of OAM are carried by the signal, as shown in Fig. 10. According to their theoretical analysis, this can be attributed to a space dependent dephasing, which generates a distribution of ℓ in the OAM spectrum even in the case of excitation with beams with well-defined OAM. The dephasing was analyzed by comparing experiments, theory and numerical simulations. From the experimental data they extracted a decay of the degree of OAM, with a decay time of 88±3 ps that happens to be much longer than the exciton de-

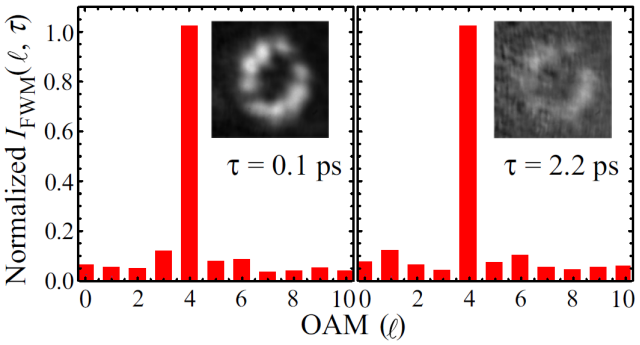

FIG. 10 (color online) Experimental evidence of OAM transfer to excitons in bulk GaN. The plot shows the OAM spectrum and intensity profile (inset) of the FWM signal produced by pump with $\ell_1 = -2$ and probe with $\ell_2 = 1$ after a delay τ giving rise to a signal with $\ell = 4$ in agreement with theory. Adapted from Shigematsu *et al.* (2016).

phasing time $T_2 = 1.9$ ps, suggesting that the OAM of the excitons is more robust than its phase coherence. Numerical simulations also show the detrimental effect of a defect on the OAM spectrum, supporting the hypothesis that space-dependent dephasing causes broadening of the OAM signal. Four-wave mixing experiments with OVs have also been performed on quantum wells (Persuy *et al.*, 2015), and they will be discussed in Sect. IV.A.3.d.

In a different type of experiment Noyan and Kikkawa (2015) studied the dynamics of OAM transfer to the electronic degrees of freedom in doped and un-doped bulk GaAs. By using time-resolved pump-probe spectroscopy and concentrating on the incoherent regime they extended the results on the exciton dynamics beyond the coherent regime addressed in four-wave mixing spectroscopy. The results show an unusually long decay time (pico- to nanoseconds) of the time-resolved OAM dichroism, that can neither be explained by the typical decay times associated with momentum scattering nor by the effect of transfer of OAM from the electronic spatial to the spin degree of freedom.

The experimental work by Noyan and Kikkawa (2015) and Shigematsu *et al.* (2016) agree on the fact that the decay time of the OAM signal is longer than expected from traditional arguments in similar systems excited by non-vortex light. One may try to explain from topology these long-lived OAM states. We have previously shown that the electric-field pattern is imprinted in the electronic state polarization. As its name suggests, every OV carries a different topological charge ℓ, and imprints a particular pattern on matter. A change to the topologically-distinct electronic polarization implies therefore a global change that is unlikely to occur with local interactions.

The impact of OAM on the spin polarization of photoelectrons in unstrained GaAs excited by LG beams was experimentally studied by Clayburn *et al.* (2013), who found no supporting evidence that the OAM of light is transferred to the spin of photoexcited electrons. Later, Solyanik-Gorgone and Afanasev (2019) studied the photoionization of electrons using a theoretical model with near and remote basis functions, allowing for a calculation of selection rules using the Wigner-Eckart theorem. The authors' results agree with those of Clayburn *et al.* (2013) after they are averaged over space; however, their model provides insight into the spatial dependence of the optical orientation, which is not available in the experiment and would be relevant in the photoexcitation of small semiconductor systems. Cygorek *et al.* (2015) showed that the spin-orbit interaction in extended systems fails to transfer orbital to spin angular momentum of the photoexcited electron, thus complementing the theoretical explanation of the null experimental result of Clayburn *et al.*

Another argument to understand the null experimental results is that the OV acts on the envelope part of the wave function [Eq. (69)], and thus does not affect the optical orientation that is only dictated by the polarization (spin AM) of light. On the other hand, a recent experiment has shown a measurable effect on the polarized photocurrent generated by LG beams on GaAs photocathodes (Sordillo *et al.*, 2019). Clearly, the seemingly different results from different experimental setups, and what theory explains, reflects a controversy that calls for more research in the subject.

3. Semiconductor elementary nanostructures

Material, geometry and dimensionality strongly influence the properties of elementary nanostructures. Those based on semiconductor materials are among the most studied ones, and they are building blocks for more complex structures, for instance, microcavities (Sect. IV.B). They are quantum dots (0D) (Biasiol and Heun, 2011; Jacak *et al.*, 2013; Reimann and Manninen, 2002), quantum rings (1D) (Biasiol and Heun, 2011; Fomin, 2014), quantum wires (1D) (Barrigoón *et al.*, 2019; Zhang *et al.*, 2017), and quantum wells (Kelly and Nicholas, 1985; Rosencher *et al.*, 2012; Weber *et al.*, 1999). Other systems with reduced dimensionality, which have become highly topical in the past decade, are atomically thin (2D) materials –or van der Waals materials– with the prototype graphene (Novoselov, 2011) and the class of transition metal dichalcogenides (TMDs) (Mak *et al.*, 2010; Splendiani *et al.*, 2010) which, when rolled up, e.g., into carbon nanotubes, can again form 1D systems (Fig. 6). Here, 0D, 1D, and 2D refers to effectively zero-, one-, and two-dimensional systems, respectively, where the dimensionality reflects the number of spatial dimensions with a continuous spectrum. Nanostructures can be fabricated by molecular beam epitaxy, chemical vapor deposition, self assembly, catalytic growth, exfoliation, etc. (Ihn,

2010; Moriarty, 2001).

The analytical description of their electronic properties often uses the envelope function approximation with resulting electron wave function $\psi_{b\alpha}(\mathbf{r}) = \mathcal{E}_{b\alpha}(\mathbf{r})u_b(\mathbf{r})$ [see Eq. (52)], where $u_b(\mathbf{r})$ is the microscopic Bloch wave function at the band edge and $\mathcal{E}_{b\alpha}(\mathbf{r})$ the envelope wave function with α denoting the necessary quantum numbers for the specific structure being considered. As an example, the envelope wave function for a one-dimensional quantum ring is $\mathcal{E}_{bm}(\mathbf{r}) = N\exp(im\varphi)R_b(r)Z_b(z)$, with normalization N and OAM (or magnetic) quantum number m. The restriction to one-dimensional motion implies fixed radial (R_b) and height (Z_b) wave functions which, however, may be different for different bands.

Two main distinctions in the OV-matter interaction arise when the size of the material system is reduced below the characteristic size of the beam. On the one hand, the studies on bulk semiconductors (Sect. IV.A.2) have been done exclusively in terms of vector and scalar potentials, because the approximations involved in the use of other gauges that set up the interaction in terms of fields often create difficulties when applied to extended systems. However, other gauges are often useful in treating the OV-nanostructure interaction; these are: the twisted-light gauge (Quinteiro *et al.*, 2015), the Poincaré gauge (Cohen-Tannoudji *et al.*, 1989; Quinteiro *et al.*, 2017b), the electric-field or dipole-like coupling gauge (Herbst *et al.*, 2003; Khitrova *et al.*, 1999; Reiter *et al.*, 2006, 2007; Rossi and Kuhn, 2002), and the Power-Zienau-Woolley gauge (Cohen-Tannoudji *et al.*, 1989) –we exclude the dipole-moment approximation or Göppert-Mayer transformation because by completely neglecting the space-dependence of the field it misses the characteristics of OVs. We will discuss different gauges, summarized in Table II at the appropriate point in the following. On the other hand, to observe new effects related to OVs the electron's wave function should span the phase singularity. The new effects are strongest when the nanostructure is fully centered with the singularity; this will be first discussed, and only later the dependence of the light-matter interaction and selection rules on the lateral displacement of nanostructure and OV singularity axes will be reviewed.

a. The paradigmatic case of the quantum ring: As the name suggests, quantum rings (QRs) are structures that confine electrons and holes to an annular region, which can be 1D if only a single transverse wave function in each band is involved, or 2D or 3D if several subbands contribute. Quantum rings of high quality have been fabricated by molecular beam epitaxy in GaAs (Tong *et al.*, 2012) and GaSb (Kobayashi *et al.*, 2004), and in Si by chemical vapor deposition (Yu *et al.*, 2007). They are among the basic semiconductor nanostructures extensively studied in the past few decades, for they help to understand basic principles –e.g., the Aharonov-Bohm effect and persistent currents (Bluhm *et al.*, 2009; Kleemans *et al.*, 2007; Schwiete and Oreg, 2009)–, and because they promise various uses in nanotechnology, for instance, the control of spin states near the ring (Räsänen *et al.*, 2007), or the possibility to build lasers out of a stack of rings (Suárez *et al.*, 2004). Quantum rings represent the archetypical system to theoretically study OV-semiconductor interaction. This is simply due to the fact that both, QRs and OVs are most naturally represented in cylindrical coordinates.

A model that captures the kinematics of electrons in a 1D-QR including two bands without Coulomb interaction already reveals interesting features. Quinteiro and Berakdar (2009) considered, in a second quantization formalism, interband transitions induced by the transverse component of the vector potential in the Coulomb gauge [$\gamma = 1$ in Eq. (72)] with centered OV and QR axes. The OV-QR interaction matrix element [Eq. (71)] between wave functions with envelope $\mathcal{E}_m(\mathbf{r}) = N\exp(im\varphi)R(r)Z(z)$ having fixed radial and longitudinal wave functions yields the simplest possible result in the RWA $\langle cm'|\, h^{(1)}_{OV}\,|vm\rangle \propto \delta_{m',m+\ell}$. The EoM

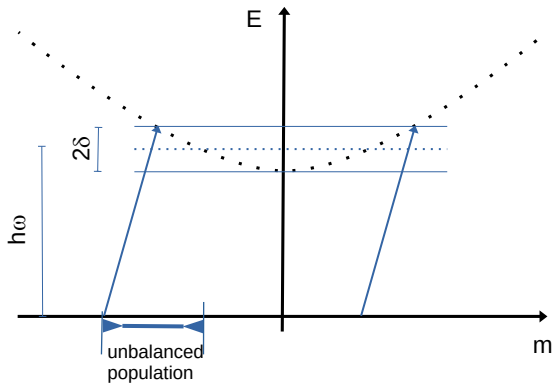

FIG. 11 (color online) Pictorial representation of tilted transitions in a QR by a finite-width (2δ) OV with center frequency ω. For an easier understanding of the revelant process, we have (realistically) approximated the valence band as flat; the inclusion of the finite mass of holes is straightforward. The optical excitation generates a population imbalance, in the valence band for this simplified example, that brings about electric currents.

(73) become

$$\begin{aligned}
\hbar\frac{d}{dt}\rho_{v,m\,m} &= 2\,\mathrm{Im}\left[\xi^*\,\widetilde{\rho}_{vc,m\,m+\ell}\right]\\
\hbar\frac{d}{dt}\rho_{c,m+\ell\,m+\ell} &= -2\,\mathrm{Im}\left[\xi^*\,\widetilde{\rho}_{vc,m\,m+\ell}\right]\\
i\hbar\frac{d}{dt}\,\widetilde{\rho}_{vc,m\,m+\ell} &= \widetilde{\Delta}_{cm+\ell,vm}\,\widetilde{\rho}_{vcm\,m+\ell}\\
&\quad +\xi\,\left(\rho_{v,m\,m}-\rho_{c,m+\ell\,m+\ell}\right)\,, \qquad (83)
\end{aligned}$$

with $\widetilde{\Delta}_{cm+\ell,vm} = \varepsilon_{cm+\ell} - \varepsilon_{vm} - \hbar\omega$ and $\xi = -(q/m_0)\mathbf{p}_{vc}$.

TABLE II Light-matter interaction Hamiltonians and their uses with optical vortex.

LIGHT-MATTER INTERACTION HAMILTONIAN					
	Hamiltonian	**Applicable to Bulk**	**NanoStr.**	**Note**	**Reference**
Minimal coupling	$[\mathbf{p}-q\mathbf{A}(\mathbf{r},t)]^2/(2m)+q\Phi(\mathbf{r},t)$	✓	✓	Difficult to interpret and compare to experiments	(Cohen-Tannoudji *et al.*, 1989)
Dipole moment	$-\mathbf{d}\cdot\mathbf{E}(t)$	✗	✗	Ignores completely the phase singularity / only applicable for a component of the OV with no singularity	(Cohen-Tannoudji *et al.*, 1989; Göppert-Mayer, 1931)
Dipole-like electric	$-\mathbf{d}\cdot\mathbf{E}(\mathbf{r},t)$	✗	✗	Does not properly capture phase singularity / only applicable for a component of the OV with no singularity	(Herbst *et al.*, 2003; Khitrova *et al.*, 1999; Reiter *et al.*, 2006, 2007; Rossi and Kuhn, 2002)
Twisted light	$-[(1/(\ell+1)]\mathbf{d}_\perp\cdot\mathbf{E}(\mathbf{r},t)$	✗	✓	Applicable to flat structures $z\ll r_\perp$	(Quinteiro *et al.*, 2015)
Poincaré	$-\mathbf{d}\cdot\mathbf{E}^{\rm eff}(\mathbf{r},t)-\mathbf{m}_B\cdot\mathbf{B}^{\rm eff}(\mathbf{r},t)$	✗	✓	Applicable to all OVs	(Cohen-Tannoudji *et al.*, 1989; Quinteiro *et al.*, 2017b)

$\mathbf{A}_0\exp(iq_zz_0)$, where equal envelope functions in the conduction and valence bands have been assumed. The equations are written in the rotating frame $\rho_{vc,mn}=\widetilde{\rho}_{vc,mn}\exp(-i\omega t)$. As in the case of the semiconductor Bloch equations for non-interacting electrons in a homogeneous bulk system [Eq. (64)], the EoM are completely decoupled, and electrons undergo one-to-one transitions, but tilted in m-space, see Fig. 11. The clearest possible description of an optical excitation process with an OV is thus achieved with 1D-QRs, which in that sense are to OVs, what bulk is to plane waves.

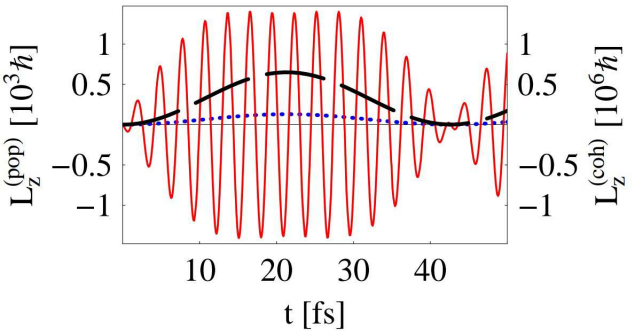

FIG. 12 (color online) The OAM of electrons in a QR. Interband (solid red) and intraband ($\ell=1$ in dotted blue and $\ell=5$ in dashed black) contributions. A similar plot holds for the electric current, calculated from simple argument based on an electric current loop. From Quinteiro and Berakdar (2009).

From the EoM (83), in complete analogy with what was done for bulk, one calculates the OAM transfer to electrons that contains "interband" coherence and "intraband" populations contributions, see Fig. 12. The latter can be increased by increasing $|\ell|$, has non-zero mean value and follows the Rabi oscillations between bands. In the low excitation regime and for short times the z-component of the angular momentum is given by $L_z^{(pop)}=(2n+1)\hbar\ell(\mathcal{R}_0t)^2$, with $\mathcal{R}_0$ the Rabi frequency, t the time, and $(2n+1)$ the number of transition channels coupled by the light field (assuming that the OV has a spectral width, as shown in Fig. 11). It can be put to use by shaping the pulse duration to set permanent electric currents and generate magnetic fields (Sect. V).

The intraband transitions in QRs deserve also attention. The theoretical simplicity exhibited by the 1D-QR calls for further studies, in particular to unveil the possible long-sought coupling of light's orbital and matter spin AM, with direct implications to technology –e.g., the generation of photoelectrons from bulk, see Sect. IV.A.2. To this end, a QR with Rashba spin-orbit interaction was theoretically considered (Quinteiro *et al.*, 2011) in a one-band model with intraband processes induced by the transverse component of a single-singularity centered OV. The problem requires the inclusion of the spin degree of freedom, transforming wave functions to spinors. The Rashba Hamiltonian reads $h_{SOI}=(\alpha_R/\hbar)(\boldsymbol{\sigma}\times\boldsymbol{\pi})_z$, in which α_R is the Rashba constant, $\boldsymbol{\sigma}$ is the vector of Pauli matrices, and $\boldsymbol{\pi}$ is the mechanical momentum containing the vector potential (Sect.III.C.1). The full Hamiltonian is

$$h=\frac{\mathbf{p}^2}{2m_c}+V(\mathbf{r})+\frac{\alpha_R}{\hbar}(\boldsymbol{\sigma}\times\mathbf{p})_z \\ -\frac{q}{m_c}\mathbf{A}(\mathbf{r},t)\cdot\mathbf{p}-\frac{q\alpha_R}{\hbar}[(\boldsymbol{\sigma}\times\mathbf{A}(\mathbf{r},t)]_z\,, \quad (84)$$

with m_c being the effective mass in the considered band and the Coulomb and radiation gauge have been assumed. An analytical solution is possible by separating h_0 from the perturbation [second line of Eq. (84)]. The

expectation is that the term containing the product of Pauli matrices and OV vector potential may lead to coupling between light's orbital and matter spin AM. From time-dependent perturbation theory without the RWA the authors concluded that the rate of spin conversion is not proportional to ℓ, in contrast to the original expectation. Besides, the authors found that anti-parallel momenta beams produce unusual situations, an interesting finding given that other later reports also point to the fact that the interaction of antiparallel OV beams with matter present uncommon features (Quinteiro and Kuhn, 2014; Quinteiro *et al.*, 2015, 2017c, 2019b), see e.g., Fig. 14.

Mike *et al.* (2018) studied a 2D-QR by numerical calculations, and described selection rules for the intraband transitions induced by OVs. The emission of light from OV-excited 2D-QRs was numerically studied by Kraus *et al.* (2018). A few-picosecond light pulse induces rapid intraband transitions, and the subsequent dynamics under the action of electron-phonon relaxation emits light at different frequencies, whose time dependence can also be analyzed. Specially interesting is the influence of the external OV topological charge on the spectrum of short-lived high-harmonics emitted light.

A different photovoltaic effect was studied in a 2D-QR by numerical simulations (Wätzel *et al.*, 2017; Wätzel and Berakdar, 2016). The authors investigated in detail a centrifugal-type generation of electric currents, in which the electrons separate in the radial direction due to their OAM, and are collected by a ring or wire electrode.

A preliminary micro-photoluminescence experiment using OVs with $\ell = 1$ on an ensemble of GaAs QRs yielded negative results (Johnson *et al.*, 2017). The authors speculate that the lack of observable effects is due to problems related to ensemble measurements (Sect. IV.A.3.b).

b. Excitation of QRs with tilted and/or displaced OV beams: On nanostructures smaller than the characteristic size of the beam the relative position of the electron wave function to the optical axis matters –in fact, this applies as well to atoms (Afanasev *et al.*, 2018; Quinteiro *et al.*, 2019a), trapped excitons to impurities/defects in bulk (Shigematsu *et al.*, 2016), etc. The effects of OVs are indeed strongest when the electron cloud is centered with respect to the beam axis and excited at normal incidence. The dependence of the light-matter interaction and selection rule on the lateral displacement and tilt of field axis and nanostructure clarifies the outcome and precautions of experiments on single and ensemble of nanostructures.

A reasonable strategy to cope with tilted and/or displaced beams is to use what we learned on head-on excitation. Thus, we must convert the incoming beam to a superposition of normal incident OVs referred to the reference frame centered on the nanostructure: To reorient the incoming field one simultaneously transforms coordinates and rotates polarization vectors. Once the beam is transformed to a superposition of OVs at normal incidence, we rewrite each one as a superposition of OVs centered at the nanostructure. The composition of rotation and parallel transport of a single-singularity beam leads to a superposition of multiple single-singularity beams seen as impinging the nanostructure head-on. Every one of these OVs –with various topological charges– produces an optical transition on its own. Alternatively, one may state that from the reference frame attached to the nanostructure, the displaced beam exhibits an extrinsic OAM (Bliokh and Nori, 2015), that can be converted –by translation– to a multitude of beams with intrinsic OAM.

A simpler scenario is that of a normal incident OV, whose optical axis is displaced by a distance D from the nanostructure (Quinteiro *et al.*, 2010), as schematically shown in Fig. 13. Consider the transverse component of its vector potential $\mathbf{A}(\mathbf{y},t)$ [Eqs. (4) and (21)] with topological charge ℓ and profile $\tilde{A}(\mathbf{y}_\perp) = A_0 F_\ell(\mathbf{y}_\perp) = A_0 J_\ell(q_r y)\exp(i\ell\varphi_y)$, for which the coordinate $\mathbf{y}$ is measured from the optical axis located at $\mathbf{D}$ from the nanostructure reference frame (see Fig. 13). Using the identity (Korenev, 2002)

$$J_\ell(q_r y)e^{i\ell\psi} = \sum_{s=-\infty}^{\infty} J_{\ell+s}(q_r D)J_s(q_r r)e^{is\phi}\,, \quad (85)$$

one obtains

$$\begin{aligned} F_\ell(\mathbf{y}_\perp) &= \sum_{s=-\infty}^{\infty} J_{\ell+s}(q_r D)J_s(q_r r)e^{is\phi}e^{i\ell(\varphi_y-\psi)} \\ &= \sum_{s=-\infty}^{\infty} (-1)^s J_{\ell-s}(q_r D)J_s(q_r r)e^{-is\phi}e^{i\ell(\pi+\phi+\varphi)} \\ &= \sum_{s=-\infty}^{\infty} (-1)^{\ell-s} F_{\ell-s}(\mathbf{D})F_s(\mathbf{r}_\perp)\,, \end{aligned} \quad (86)$$

and the azimuthal angles with respect to a fixed axis are related by $\varphi_y = \pi + \psi + \phi + \varphi$ and $\varphi_D = \phi + \varphi$ (see Fig. 13). Thus, $\mathbf{A}(\mathbf{y},t)$ can be written as a superposition of vector potentials $\mathbf{A}(\mathbf{r},t)$ with topological charge s. The weight $F_{\ell-s}(\mathbf{D})$ of each component in the superposition depends on $\ell - s$, $q_r D$ and the angle ϕ. Therefore, the interaction with a QR produces one-m-to-many-m transitions induced by

$$h^{(+)} = \sum_{s=-\infty}^{\infty} (-1)^{\ell-s} F_{\ell-s}(\mathbf{D}) \left[-\frac{q}{m_0}\mathbf{A}_s^{(+)}\cdot\mathbf{p}\right]\,, \quad (87)$$

as shown in Fig. 13.

Even non-vortex fields, such as Gaussian beams, exhibit the same behavior. When the optical axis is displaced and the beam width is of the same order or smaller than the size of the nanostructure, non-vertical transitions become allowed.

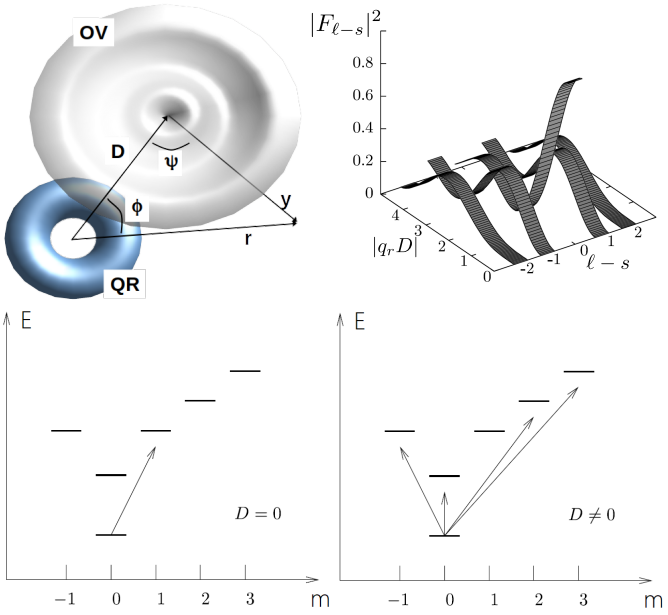

FIG. 13 (color online)Excitation of nanostructures by a displaced normal-incidence OV. Upper panel, left: Pictorial representation of the nanostructure (QR) and a displaced beam located at a distance D. Upper panel, right: Weights of the decomposition into vector potentials centered at the nanostructure, see Eq. (87). Lower panel: Allowed optical interband transitions in a QR with magnetic quantum number m, examples for an OV with $\ell = 1$. Left: head-on excitation ($D = 0$), a pure one-to-one transition is predicted [Sect. IV.A.3.a]; Right: once the field is displaced, transitions with other values of OAM transfer are possible. Adapted from Quinteiro *et al.* (2010).

Somewhat connected to this discussion is the study on the interband transitions in a QR induced by inclined plane waves (Vänskä *et al.*, 2011). The authors found that the tilt of the beam with respect to the QR axis results in new selection rules such that the OAM of the electrons envelope ($\hbar m$) is not conserved. Moreover, by expressing the plane wave in terms of Bessel functions they conclude that the original beam can be seen as a superposition of OVs with various topological charges.

Finally, the preceding discussion clarifies a possible strategy to cope with a multiple-singularity field interaction, e. g. superposition of displaced single-singularity beams, Mathieu beams, etc (Sect. II.D). If multiple singularities shine on a coherent electronic excitation (for example in a mesoscopic QR), each one of them can be converted to OVs centered on the excitation [Eq. (86)]. The total interaction is then given by the sum of interaction terms as in Eq. (87), which translates into a sum of the responses in the regime of linear optics.

c. Quantum dots: Within the class of man-made nanostructures, quantum dots (QDs) are certainly among the most prominent ones. From a theoretical point of view, they are specially interesting for they present a discrete set of energy levels, much like atoms. This makes them particularly interesting candidates for applications in the field of quantum information technology, e.g., as emitters of single photons (Dusanowski *et al.*, 2019; Michler *et al.*, 2000) or pairs of entangled photons (Schimpf *et al.*, 2021; Stevenson *et al.*, 2006). They are fabricated in a variety of different materials and shapes. Those fabricated from semiconductors inherit the band structure of the bulk material, and the discrete energy levels are grouped in shells, making them sensible to excitation by light.

Before engaging on the OV-QD interaction, we remind the reader that within the envelope function approximation the wave function of electrons in a cylindrically symmetric nanostructure is given by Eq. (52) with the envelope function $\mathcal{E}_{bmn} = N \exp(im\varphi) R_{bmn}(r) Z_b(z)$ with angular momentum (m) and radial (n) quantum numbers (Jacak *et al.*, 2013). Here, a factorization of in-plane and out-of-plane directions has been assumed and the thickness has been taken to be so small that only a single function Z_b contributes. The spin or –in the presence of spin-orbit coupling– the total angular momentum of the microscopic Bloch states can be included in the band index b. In addition to the envelope OAM $\hbar m$, the electron (or hole) has band and spin contributions to the AM. From the functional form of $\mathcal{E}_{bmn}(\mathbf{r})$ one immediately realizes that there will be a selection rule for the envelope AM, but as it happened in bulk for cylindrical wave functions, a multitude of radial states are excited by an OV with a single topological charge.

Geometry dictates to a large extent the complexity of the interaction with light; we have seen that the simplest structure for OV-nanostructure interaction is the QR. Therefore, our discussion will be mainly focused on lens-shaped, cylindrically symmetric self-assembled QDs; however, we will also comment on the effects due to reduced symmetry, like for example, in elongated QDs. Self-assembled QDs are routinely fabricated in laboratories around the world, and the theoretical and experimental knowledge is vast. In the early times of QD research experiments were commonly performed on ensembles of QDs exhibiting a distribution of sizes and, thus, of transition energies and dipole matrix elements; as a result of highly refined sample fabrication and detection efficiencies nowadays measurements on single QDs with impressive precision in the positioning of light beams with respect to the QD are routinely performed.

Let us reexamine the generic Bessel-type OVs of Eqs. (21)-(24). From a viewpoint of control, these fields are highly tunable by changing the topological charge ℓ, the circular polarization σ, the relative OAM to SAM direction, the degree of paraxiality expressed by the ratio q_r/q_z, and the type of beam as determined by γ. The freedom in shaping the beam allows one to envisage different sorts of excitation modes, see Fig. 14 for

TABLE III Dominant fields for the three modes of excitations of a self-assembled quantum dot. The parallel symbol ($\|$) refers to the relative orientation of SAM and OAM, "arb." denotes an arbitrary value of γ. For comparison, we also present the excitation mode of a plane wave.

EXCITATION MODES OF A QUANTUM DOT						
Mode	γ	σ	ℓ	$\mathbf{q_r/q_z}$	$\|$	**Dominant field**
(a)	-	±1	0	0	-	$\tilde{\mathbf{E}}(\mathbf{r}) = E_0\mathbf{e}_\pm$
(b)	arb.	±1	$\pm n$	$\ll 1$	P	$\tilde{\mathbf{E}}(\mathbf{r}) = E_{0n}(q_r r)^n e^{\pm in\varphi}\mathbf{e}_\pm$
(c)	arb.	∓1	±1	$\simeq 1$	AP	$\tilde{\mathbf{E}}(\mathbf{r}) = \mp E_0(q_r/q_z)\mathbf{e}_z$
(d)	arb.	∓1	±2	$\simeq 1$	AP	$\tilde{\mathbf{B}}(\mathbf{r}) = \mp B_0(q_r/q_z)^2\mathbf{e}_\pm$

just three examples. One foresees that OVs have a potential to applications that will be considered in Sect. V. Here we will concentrate on basic properties that are associated with the excitation of QDs by OVs with different values of their parameters. As shown schematically in Fig. 14, we will discuss three modes of excitation of a cylindrically symmetric QD treated in an effectively six-band model (conduction, heavy hole and light hole bands, each with two orientations of the intrinsic angular momentum) without taking into accout two-particle interactions. In the s-type conduction band the band and spin angular momentum consists only of a spin part with $J_z = \pm 1/2$, in the p-type valence bands the heavy hole band is characterized by $J_z = \pm 3/2$ and the light hole band by $J_z = \pm 1/2$.

The first mode [panel (b) in Fig. 14] makes use of OV parameters $\ell = \pm n$, $\sigma = \pm 1$ (parallel momenta beam), and $q_r/q_z \ll 1$; for any value of γ the transverse field component dominates the interaction (see Table III) connecting the usual heavy-hole $J_z = \mp 3/2$ to the conduction $J_z = \mp 1/2$ band states transferring the OAM and producing non-vertical transitions in the envelope quantum number m. Note that in this review we use the electron picture; the angular momenta of the valence band states therefore have the opposite sign compared to the corresponding valence band hole. A detailed study based on Fermi's Golden Rule (Quinteiro and Tamborenea, 2009b) concluded in addition that the strength of the excitation depends on the ratio ζ (typically small) of QD to beam sizes, and it compares to the strength of excitation by plane waves (a) as

$$\frac{|h_{OV}|^2}{|h_{PW}|^2} \simeq \zeta^\ell \,. \tag{88}$$

Moreover, the absorption spectrum for different types of OVs can be predicted (Kuhn *et al.*, 2015).

The second mode (c) of excitation relies on antiparallel spin and orbital momenta with $\ell = \pm 1$, $\sigma = \mp 1$, a high non-paraxiality degree $q_r/q_z \simeq 1$ and again arbitrary γ (Quinteiro and Kuhn, 2014). For these sets of values, the interaction is dominated by an essentially homogeneous electric field in the longitudinal direction –a curious feature of OVs anticipated in Sect. IV.A. The interaction matrix element can be conveniently calculated using the dipole-moment approximation expressing the Hamiltonian in terms of fields –the lack of spatial dependence of the longitudinal component over the region of the QD enables one to use this approximation despite the fact that other components exhibit a phase singularity. If the frequency of the beam is tuned to excite electrons from the light hole band with Bloch microscopic part $u_\pm(\mathbf{r}) = \langle \mathbf{r}|\, J, J_z\rangle$ (Bastard, 1988), $|J, J_z\rangle$ being

$$\begin{aligned} |3/2,+1/2\rangle &= -\frac{1}{\sqrt{6}}\left[(\,|p_x\rangle + i\,|p_y\rangle)\downarrow -2\,|p_z\rangle\uparrow\right] \\ |3/2,-1/2\rangle &= -\frac{1}{\sqrt{6}}\left[(\,|p_x\rangle - i\,|p_y\rangle)\uparrow +2\,|p_z\rangle\downarrow\right] \,, \end{aligned} \tag{89}$$

with atomic orbitals $|p_j\rangle$ and the spin orientation indicated by the arrows, the E_z-component couples to the p_z orbital producing electron-hole pairs with total (envelope+band+spin) angular momentum equal to zero. Moreover, the strength of the interaction is, in contrast to the previous mode of excitation, comparable to that of irradiation by plane waves; this is due to the fact that $E_z(t)$ is approximately homogeneous over the extension of the QD.

In the third example (d), the beam is tuned to $\ell = \pm 2$, $\sigma = \mp 1$, a high non-paraxiality degree $q_r/q_z \simeq 1$ and $\gamma = 1$ (Quinteiro and Kuhn, 2014; Quinteiro *et al.*, 2017a). The dominant contribution to the interaction comes from the in-plane components of the magnetic field that, close to the phase singularity, can be approximated by a constant –once again, as anticipated in Sect. IV.A, this is another unusual behavior of OVs, for it is a magnetic interaction at optical (ultra-high) frequencies. The interaction can be again expressed in terms of fields, though the use of the dipole-moment approximation is inappropriate. A correct and general theoretical description of the interaction with antiparallel momenta beams is provided by the Poincaré gauge (Quinteiro *et al.*, 2017a) that results in the Hamiltonian

$$h_{OV} = -\frac{q}{2m_0}\mathbf{B}_\perp(\mathbf{r},t)\cdot(\mathbf{r}\times\mathbf{p})\,,$$

resembling the well-known magnetic-dipole interaction but with a space-dependent field. When resonant with the transitions from light hole bands [Eq. (89)], the OV induces a non-vertical transition in m with zero band+spin angular momentum.

The studies above expose the unlocking of new selection rules in QDs, i. e., transitions with changes in the envelope as well as the microscopic parts of the wave function. Most notable is the excitation of electron-hole pairs with unusual AM, which results from the combination of a longitudinal electric field or a transverse magnetic field with LH states; the action of these OV components on bulk has not yet been reported (Sect. VI).

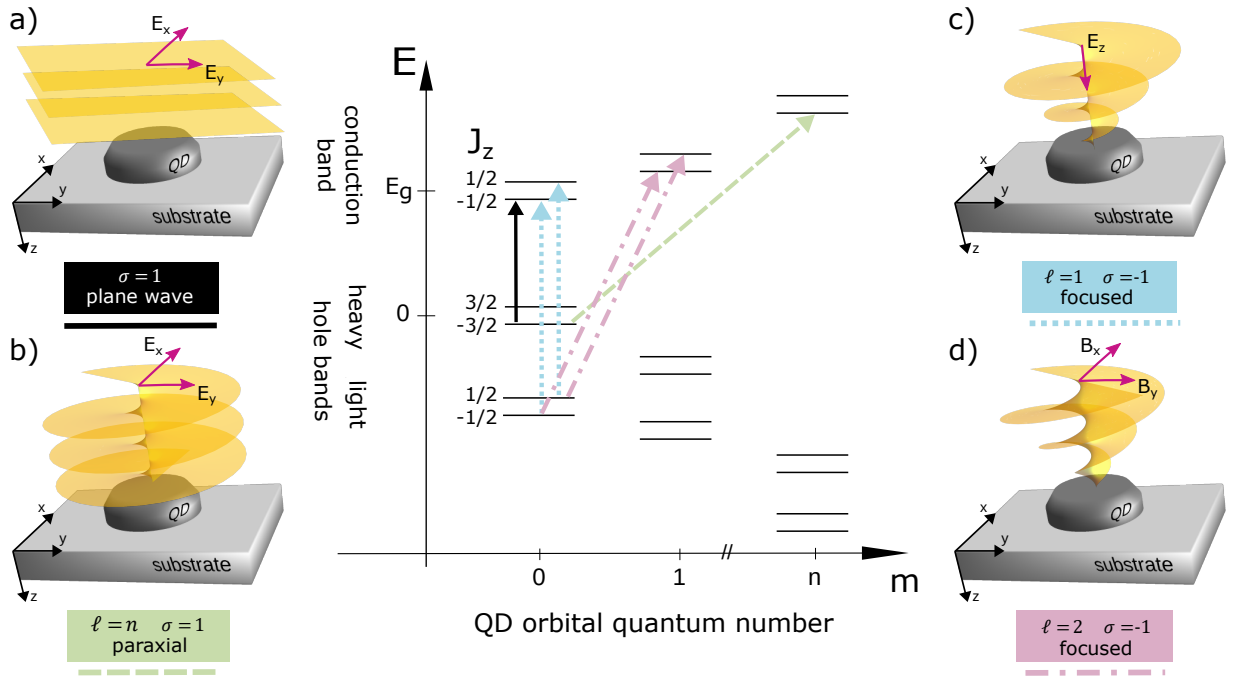

FIG. 14 (color online) Three possible modes of excitation of a lens-shaped semiconductor QD by varying the OV beam parameters ℓ, σ, γ, and q_r/q_z. For the sake of comparison, panel (a) presents the usual excitation by a plane wave. Panels (b),(c) and (d) are pictorial representations of the field, material system and modes of excitation, see Table III. Center: Single-particle QD energy levels and characteristic transitions induced by the corresponding beam in each panel.

Naturally, a more realistic model of a QD includes two-particle interactions and other effects. Such a model serves to verify/falsify the findings of the aforementioned simple model, can be used to predict new effects and – most importantly– is useful to compare predictions to experiments. Holtkemper *et al.* (2020, 2021) included the Coulomb interaction, valence-band mixing, and the effects of QD asymmetry using a Configuration-Interaction approach. Figure 15 compares the spectra of a single-particle (reduced) model with the spectra of the full model with interactions.

One observes that the full model reproduces important features of the simplified model, for instance, the important predicted zero total AM e-LH pair $S \to s\,LH \pm 0$ (for nomenclature see the caption of Fig. 15); but, in addition we learn that this e-h pair will strongly mix with the $d \to s\,HH \pm 2$ pair. Moreover, by using a longitudinal electric field one can excite high-energy dark excitons, such as $d \to s\,HH \pm 2 (+S \to s\,LH \pm 0)$. It is worth noting that the state with band+spin AM zero is not completely dark, for it can radiate into a field that propagates in the in-plane direction with electric field in z-direction. In contrast, the exciton with band+spin AM equal to two is truly dark. The full model awaits for experiments, specially on single QDs.

Quantum dot ensembles are a common, easy to prepare and measure experimental system. Though tempting for the study of OV-QD interaction, the analysis of signals obtained from such measurements presents a significant challenge. In Sect. IV.A.3.b we have seen that nanostructures illuminated by tilted and/or displaced single-singularity OVs exhibit complex excitation paths, that would result in complex spectra. And clearly, different QDs will react according to where the optical axis of the single-ℓ OV impinges the ensemble. An extinction experiment on an ensemble of QDs could record the intensity of the light passing through the sample as a function of the energy, in a range that spans a number of QD levels. Simulated spectra are shown in Fig. 16. A simple or reduced model (see Fig. 15 and Fig. 14), as shown in the upper panel, is used. We compare, for two values of the topological charge, the absorption spectra of an ensemble of QDs and a single centered QD. The ensemble spectra reveal no qualitative difference for $\ell = 0$ (Gaussian) and $\ell = 1$ (OV) beams, and would make hard the interpretation of measurements. On the contrary, the single-QD spectra show clear differences, most notable, the peak at $E_g + \hbar\omega_c$ is only seen for $\ell = 1$.

d. Other nanostructures The peculiarities of OVs result in interesting new effects also in other nanostructures besides QRs and QDs. This is the case with two-dimensional systems and nanoparticles.

In a combined theoretical/experimental work Persuy *et al.* (2015) analyzed the OAM contributions to different diffraction orders of wave-mixing experiments. By per-

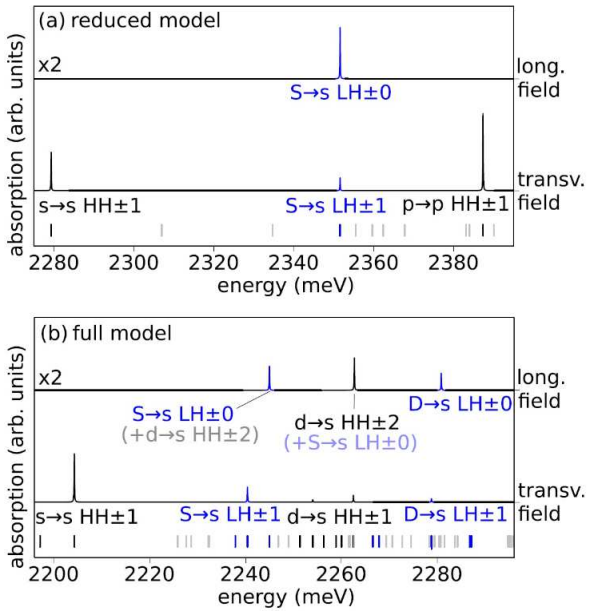

FIG. 15 (color online) Calculated spectra for a QD excited by the transverse and longitudinal components of an OV. Top panel: Single-particle picture; lines correspond to electron-hole pairs. Bottom panel: Model including Coulomb interaction and valence-band mixing; lines correspond to excitons. Each line is named according to its "envelope-hole → envelope-electron" pair, with the additional information of its light (LH) or heavy (HH) hole character and the microscopic (band+spin) angular momentum. The energy levels are grouped in shells $s, p, d, \ldots$ for electrons and heavy holes and $S, P, D, \ldots$ for light holes. In the full model, exciton states are superpositions of non-interacting pairs; when the superposition is dominated by more than one e-h pair, the second contribution appears in between parenthesis, for example, $d \rightarrow s\,HH \pm 2(+S \rightarrow s\,LH \pm 0)$ is a high-energy exciton with an admixture of HH-e and LH-e pairs in which the holes are in different shells (d and s). From Holtkemper *et al.* (2021).

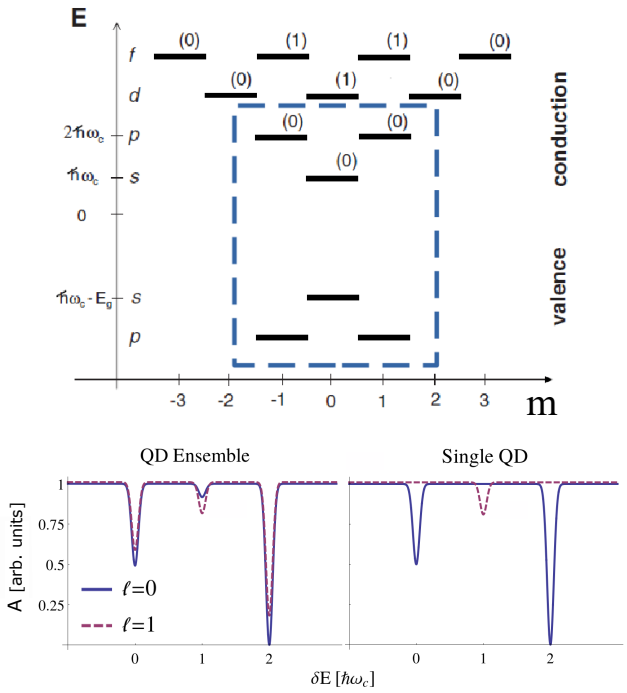

FIG. 16 (color online) Simulated extinction experiment on a single centered and an ensemble of QDs. Upper panel: Single-particle energy levels of a QD in a reduced model, with m the envelope OAM, and in between parenthesis the radial quantum number (Quinteiro and Tamborenea, 2009b). Lower panel: extinction spectra using beams with $\ell = 0$ (Gaussian) and $\ell = 1$ (LG). The light frequency $\omega = (E_g + \delta E)/\hbar$ scans the energy leveles within the blue dashed box (upper panel). The absorption appears as dips in the extinction spectra. No qualitative difference exists between the Gaussian and LG excitation for the ensemble measurement; in contrast, clear differences appear for an experiment on a single QD.

forming four-wave mixing spectroscopy with LG beams on a CdTe quantum well sample, they demonstrate that the selectivity of the OAM transfer can be used to extract the four-wave mixing signal even in the case of collinear pump and probe beams which suggests the possibility of enhanced spatial resolution by excitation through a microscope objective.

The action of a longitudinal electric field component in the excitation of a quantum well was investigated theoretically by Sbierski *et al.* (2013). The authors considered an excitation in the infrared range to induce intersubband transitions, using OVs with different topological charges that impinge the sample at normal incidence. As is the case for the interaction with QDs (Sects. IV.A.3.c and V), the claim is that the excitation by an E_z component is experimentally easiest if done at normal incidence, because it does not require cleaving of the sample.

Cygorek *et al.* (2015) studied theoretically QWs (and QDs) with Rashba interaction in order to explore the possibility of transferring angular momentum from an OV to the spin of electrons via the spin-orbit interaction. It was found that spin-orbit interactions at the level of the effective mass approximation are unable to produce the desired net transfer in large systems (thermodynamic limit), leaving quantum disks/dots and rings as the only possible scenarios for significant OAM to SAM transfer.

Tikhonova and Voronina (2021) analyzed the interband transitions in a semiconductor quantum well (disk) induced by a quantum non-classical OV field, revealing a transfer of correlations to the electronic system.

The selection rules, transfer of OAM and induced photocurrents in a two-dimensional electron gas were theoretically studied by Takahashi *et al.* (2018, 2019). They found that the current in bulk is canceled out but there remains a current that flows along the edge of the system inducing magnetization.

The electronic wave function kinematics in a macroscopic stripe of GaAs was numerically simulated using Schrödinger's equation (Wätzel *et al.*, 2012). The deflec-

tion of the wave package occurs in the region where the OV intensity is significant; moreover, the report shows that even the use of OVs with random additional phases, simulating natural light, produce deviations of the electron's trajectory.

In a report combining experiments and Mie theory Nechayev *et al.* (2019) considered the inverse problem of orbital-to-spin AM conversion. They showed that a ~~focused~~ linearly-polarized OV focused on a silicon nanoparticle results in circularly polarized scattered light.

Using a time-dependent Keldysh-Green's function method, Shintani *et al.* (2016) considered the effects of OV pulses on the disordered surface of a three-dimensional doped topological insulator. They determined the local charge and spin densities, showed that the inhomogeneous nature of the field plays an important role, and demonstrated that the OV imprints its polarization pattern on the charge densities, in agreement with what was found in Sect. IV.A.2 for bulk and will be seen later in Sect. IV.B in the case of microcavities. Most interesting is that, due to the locking between electron spin and momentum, the optical polarization pattern determines a spatially structured spin density. The momentum-spin locking might be an indirect way to control the spin using OVs. The imprinting of the spatial

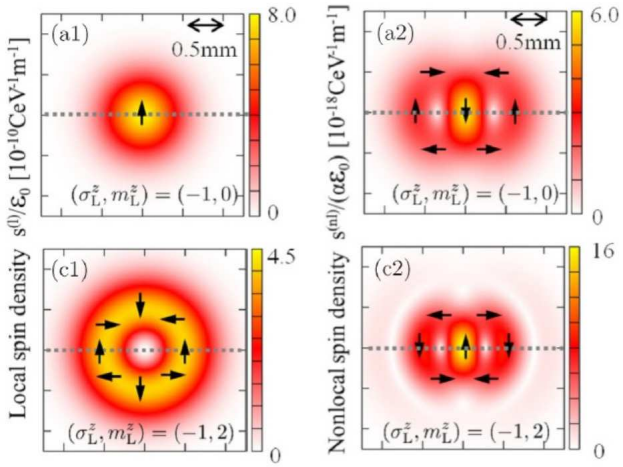

FIG. 17 (color online) Spin density induced by the electric field of an optical vortex. The left (right) panels show the local (nonlocal) spin density. The color map and the direction of the arrow show the magnitude and direction of the spin density, respectively. $\sigma_L^z = \pm 1$ and m_L^z are the spin and orbital AM of the beam, respectively. Adapted from Shintani *et al.* (2016).

pattern of the OV field was also predicted in the excitation of two-dimensional chiral ferromagnets, leading to the formation of skyrmions (Fujita and Sato, 2017).

B. Microcavity exciton polaritons

Atoms, molecules and nanostructures placed inside optical cavities display a variety of new phenomena (Yamamoto *et al.*, 2000). A prominent example is the inhibition or enhancement of the spontaneous emission due to the Purcell effect (Purcell, 1946), but there is much more. Inside a cavity, photons and matter excitations can be strongly or weakly coupled, depending on the experimental conditions. In the weak coupling regime, the coupling between photons and matter excitations is smaller than the individual decay rates. As a result the particles retain their individual character, and the phenomena observed resemble that of free (off cavity) light-matter interaction. However, the matter-light interaction can be strongly reduced or enhanced depending on, e. g., the position of the active structure in the cavity. Under strong coupling, photons and matter states hybridize, and extraordinary effects take place.

In a cavity containing a semiconductor structure, photons couple to excitons, and in the strong-coupling regime form exciton-polariton quasi-particles that for not too high densities follow Bose-Einstein statistics. A semiclassical model of exciton polaritons is deduced in a similar way to that of plasmon polaritons (Sect. IV.C): From quantum mechanics one calculates an exciton dielectric function that is used in the wave equation for electromagnetic fields. For a fully quantum mechanical treatment, one quantizes the electromagnetic field and writes a Hamiltonian for excitons, photons and the mutual coupling (Haug and Koch, 2009; Khitrova *et al.*, 1999).

An extensively investigated system is that of a quantum well microcavity. The system is fabricated using on each side of the quantum well a set of thin layers of alternating refractive index that act as mirrors, called Distributed Bragg Reflectors. By optically exciting the system from outside, exciton-photon pairs or polaritons are formed. Many interesting phenomena have been reported. For low polariton losses and low density of polaritons, thermalization produces a large population of zero-momentum polaritons which under suitable conditions form a Bose-Einstein condensate (Kasprzak *et al.*, 2006; Wertz *et al.*, 2010) that may lead to lasing (Deng *et al.*, 2010, 2003; Schneider *et al.*, 2013; Tsintzos *et al.*, 2008). Under strong excitation and in the strong coupling regime, polaritons are seen to interact forming a liquid and exhibit superfluidity (Lerario *et al.*, 2017).

Before examining the research in OV-microcavity physics, we recall that we have so far only considered the action of external and fixed OVs on matter. Nevertheless, due to the strong coupling of excitons and photons inside a microcavity, there is a mutual interaction between these constitutive particles. Thus, exciton-polariton vortices (called "quantized vortices") can be observed without the need of pumping the microcavity with an external OV, as indeed reported by Lagoudakis

et al. (2008). The spontaneous formation of vortical structures in a polariton fluid in a CdTe microcavity was inferred from fork-like patterns in the interference of the luminescence signal coming out of the cavity, see Fig. 18. The exciton-polariton vortices are speculated to form out of a combination of system inhomogeneities and continuous (non-singular) pumping. Theoretical modeling using the Gross-Pitaevskii equation supports the experimental findings (Abdalla *et al.*, 2018; Lagoudakis *et al.*, 2008; Sigurdsson *et al.*, 2014).

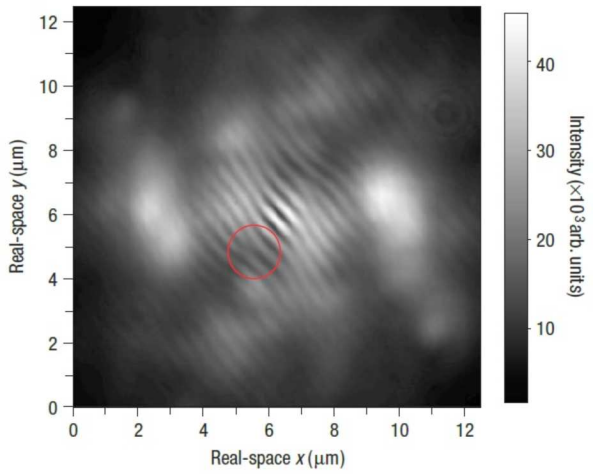

FIG. 18 (color online) Interferogram and extracted phase. The fork-like dislocation can be seen within the red circle. Adapted from Lagoudakis *et al.* (2008).

Further experimental investigations revealed also the existence of half-integer vortices in planar (Lagoudakis *et al.*, 2009) and ring (Liu *et al.*, 2015) cavities, first predicted in exciton-polariton systems by Rubo (2007). Half-integer vortices are known to occur in other systems, e.g., He^3 (Salomaa and Volovik, 1987), and result from the two-component nature of polariton condensates (Toledo-Solano *et al.*, 2014).

Of course microcavities can be pumped using OVs. An experiment conducted by Kwon *et al.* (2019) demonstrated, using again interferometric techniques on the condensate luminescence, that a non-resonant LG pulse can inject quantized exciton-polariton vortices in planar GaAs microcavities. Furthermore, the authors show that the chirality of the exciton-polariton vortex is highly controllable by the external field, which led them to the conclusion that the OAM of the pump beam is transferred to the exciton-polariton condensate.

An ingenious procedure to inject quantized vortices is that of Boulier *et al.* (2016), in which four tilted and non-overlapping Gaussian beams excite the microcavity in such a way to produce exciton polaritons with appropriate linear momentum, that convey OAM to the whole condensate. We note that the similarity with the modal decomposition of Sect. II.F is only apparent, since the four Gaussian beams neither overlap to interfere nor do they have the appropriate phase difference.

C. Plasmonics

When light propagates inside a metal or a structured material containing metal-dielectric interfaces, the electromagnetic fields interacts with conduction electrons producing quasi-particles called plasmon polaritons (Kawata *et al.*, 2001; Maier, 2007; Novotny, 2006). They exhibit notable effects, such as the confinement of the electromagnetic field to sizes of the order of the wavelength or less, and strong enhancement of fields. Plasmon polaritons exist in bulk and lower-dimensional systems. They are called surface plasmon polaritons (SPPs) when confined to a metal-dielectric interface, and localized plasmon polaritons (LPPs) if further confined, for example, to a tiny metallic sphere.

Surface plasmon polaritons are excitations that propagate along dielectric-metal interfaces, but are bound in the perpendicular direction, with a corresponding evanescent field decaying in both directions from the surface. The SPP dispersion relation deviates significantly from that of light in dielectric media. For a single-interface ideal-conductor system –the paradigmatic case– the dispersion relation exhibits a gap and a region where the in-plane wave vector can assume larger values than in dieletrics, without appreciable changes in the frequency.

Due to the spatial confinement in all directions, LPPs in plasmonic structures exhibit and are characterized by resonances in their response to external fields, e.g., resonance in polarizability. The resonance in polarizability results in a field enhancement, one of the main features exploited in applications. From the theory of the archetypical metallic sub-wavelength sphere in a dielectric medium, the understanding of other structures –such as ellipsoids and rods– can be built, in which other phenomena occur, like multiple resonances, response dependent on the polarization of the excitation field, and more.

The textbook SPP is an object represented in Cartesian coordinates propagating in a uniform 2D system. As plane waves in free space, it is a suitable building block for other more complex excitations. But, as previously discussed, other geometries are more adequate in problems related to OVs. Liu *et al.* (2005) experimentally demonstrated SPPs in a circular system that result in the focusing of light at the center. The edge can be viewed as a set of point-like sources (Ren *et al.*, 2011), each emitting waves that converge inwards.

Point-like sources are also building blocks that help understand, by the superposition principle, the SPP field of other plasmonic structures. A point-like source on a metal-dielectric interface produces cylindrical waves of SPPs describable in terms of Hankel functions (Chang *et al.*, 2005; Hecht *et al.*, 1996; Lee and Mok, 2016;

Nerkararyan *et al.*, 2010; Yin *et al.*, 2004).

The natural next step towards the study of singular SPPs is to consider a spiral or an array of spirals (also called an Archimedean structure) milled on the metal-dielectric system; excited from outside by a plane wave, the structure produces a vortex field around its center. The phenomenon is easy to understand: Regard the spiral as a set of point-like sources, each emitting a secondary cylindrical wave as a result of the excitation at normal incidence by a circularly polarized plane wave of handedness σ. Their superposition at the spiral center produce a vortex, as next explained.

The field of a point source at the origin of coordinates is dominated by the electric field z-component, which in the medium with evanescent constant χ reads, in analogy to Eq. (4), $E_z(\mathbf{r}) = \tilde{E}_z(\mathbf{r}_\perp)\exp(-\chi z - i\omega t) + \text{c.c.}$

$$\tilde{E}_z(\mathbf{r}_\perp) = E_0 e^{i\sigma\phi}\, H_1^{(1)}(k\rho)$$

with $H_1^{(1)}$ a Hankel function of the first kind (outward propagation) of order one, $\mathbf{r} = (\rho, \phi, z)$, and k the plasmon wavevector –we disregard in-plane attenuation. For observation points far from the source $k\rho \gg 1$, and $H_1^{(1)}(k\rho) \simeq \sqrt{2/(\pi k\rho)}\exp[i(k\rho - 3\pi/4)]$; then

$$\tilde{E}_z(\mathbf{r}_\perp) = E_0' e^{i\sigma\phi}\sqrt{\frac{1}{k\rho}}e^{ik\rho}$$

with $E_0' = E_0\exp(-i3\pi/4)\sqrt{2/\pi}$.

We imagine the spiral as a set of infinitesimal segment, each acting as a point-like source. To calculate the outgoing field of each, we displace E_z to the corresponding position $\mathbf{R} = (R(\Theta), \Theta, z)$ on the spiral with $|m|$ turns, parametrized by $R(\Theta) = R_0 + m\Theta/k$, see Fig. 19. The observation point is now indicated by $\mathbf{r} = (r, \varphi, z)$. We approximated the distance $\rho = |\mathbf{R} - \mathbf{r}| \simeq R(\Theta) - r\cos(\Theta - \varphi)$ for the exponential factor, $\rho = |\mathbf{R} - \mathbf{r}| \simeq R_0$ for the denominator factor (as customary), and $\phi \simeq \Theta + \pi$,

$$\tilde{E}_z(\mathbf{r}_\perp) = -E_0' e^{i\sigma\Theta}\sqrt{\frac{1}{kR_0}}e^{ik[R(\Theta) - r\cos(\Theta-\varphi)]}\,,$$

The contribution of all point sources on the spiral to the field in the region close to the center is

$$\tilde{E}_z(\mathbf{r}) = -E_0'\,\frac{e^{ikR_0}}{\sqrt{kR_0}}\left[R_0\int_0^{2\pi} d\Theta\, e^{-ikr\cos(\Theta-\varphi)}e^{i(m+\sigma)\Theta}\right],$$

Changing variables to $\eta = \Theta - \varphi$, the integral becomes of the form Eq. (36), and finally

$$E_z(\mathbf{r}, t) = E_0'' e^{i(m+\sigma)\varphi} J_{m+\sigma}(kr) e^{-\chi z - i\omega t} + \text{c.c.}\,, \quad (90)$$

with $E_0'' = -E_0'(-i)^{m+\sigma}2\pi\sqrt{R_0/k}\exp(ikR_0)$. Note the striking similarities with the modal decomposition of Bessel beams in free space Sect. II.F. Therefore, the superposed field close to the center presents a phase singularity. Figure 20 shows the numerical calculations of the field produced by twenty point-like sources located on a single-turn spiral. We also show fitting curves comparing Bessel functions and numerical data. One notes that, given a spiral with a particular sense of rotation, the field at the origin has a dramatic change for each polarization of the light exciting the structure (Yang *et al.*, 2009); this is why the system is also referred to as a plasmonic lens, and the effect as a spin-orbit interaction or spin-to-orbital AM conversion. The generation of plasmons by such structures is well documented in theoret-

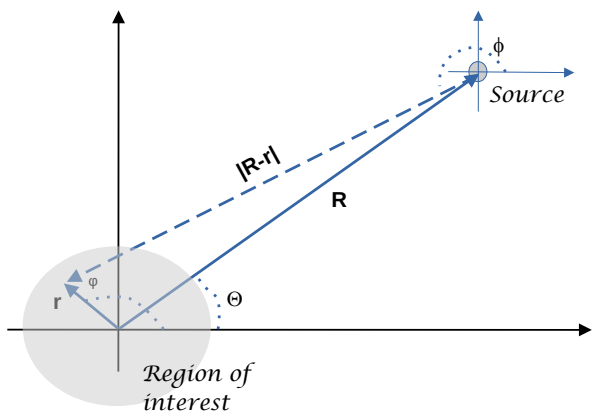

FIG. 19 (color online) Schematics of the coordinate transformation of a point-like source, which is used to generate the field of spirals.

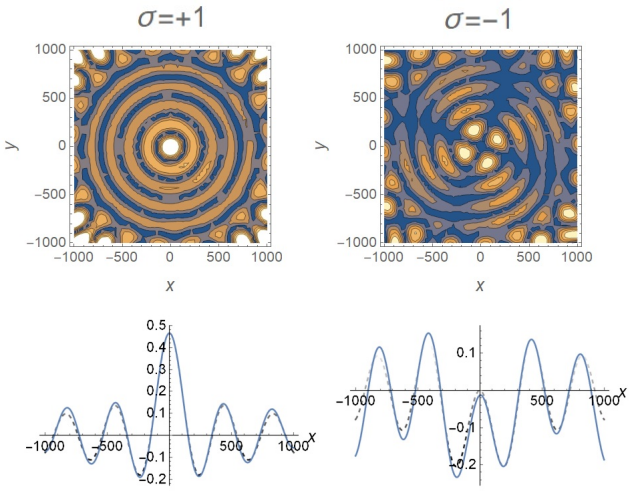

FIG. 20 (color online) Numerical calculations for a discrete single-turn spiral with $N = 20$ point sources and $m = -1$. First row: (arbitrary units) Intensity maps, at $r = 0$ with $\sigma = 1$ there is a bright spot, while for $\sigma = -1$ there is dark spot. Second row: (arbitrary units) For fixed $y = 0$ and as a function of x numerical field amplitudes (solid blue lines) fitted by a Bessel function J_0 ($\sigma = 1$) and J_{-2} ($\sigma = -1$) (dotted lines) showing very good match at short distances from the center and confirming the validity of the theoretical model Eq. (90).

ical and experimental reports (Boriskina and Zheludev, 2014; Gorodetski *et al.*, 2008; Guo *et al.*, 2017; Kim *et al.*, 2010; Ohno and Miyanishi, 2006; Spektor *et al.*, 2017; Yang *et al.*, 2009). Plasmonic vortices yield naturally sub-wavelenght fields, achieving for example, a lateral size of $\lambda/6$, with λ the wavelength of the incident external light (Spektor *et al.*, 2017). This is one of the most important features, for it allows one to explore a regime not accessible with far-field OVs that are limited by the diffraction limit.

Other plasmonic systems can generate singular fields, as demonstrated by Tsesses *et al.* (2019) using hexagonal structures. These act as sources of surface plane waves whose interference pattern produce a lattice of topological defects –we recall that the superposition of three or more plane waves results in singularities, see Fig. 2 and Dennis *et al.* (2010).

Interesting physics also occurs when exciting plasmonic structures with OVs. Sakai *et al.* (2015) numerically showed the creation of multipole LPPs in an air-suspended nanodisk (400 nm diameter/30 nm hight), by studying the plasmon resonance and field maps as a function of topological charge and polarization of an incident OV. Kerber *et al.* (2018) explored the generation of plasmonic vortices in Archimedean structures by OV excitation. Their numerical results reinforce the notion that the OAM of the plasmonic vortex arises from a combination of OV parameters (topological charge and polarization) and the chirality of the plasmonic structure (Forbes and Andrews, 2018a). Through theory and numerical simulations Cao *et al.* (2021b) showed that a metallic cylinder with a patterned surface reacts to incident OVs with positive and negative topological charge by either converting the incoming OAM or absorbing it.

D. Two-dimensional materials

A single layer of carbon atoms in a honeycomb lattice, known as graphene, displays striking features (Castro Neto *et al.*, 2009). It is best known for the Dirac-like behavior of electrons close to special points in k-space, where no band-gap exists, and the sublattice of graphene plays the role of (pseudo-)spin. The seminal work of Novoselov *et al.* (2004) in graphene boosted the research on a variety of 2D materials (Novoselov, 2011), together with their applications (Fiori *et al.*, 2014; Zeng *et al.*, 2020).

Two-dimensional Transition Metal Dichalcogenides (TMDs) –a combination of a transition metal, e.g., Mo or W, and a chalcogen like S, Se or Te– are complex systems of single or multiple layers of atomically thin covalently bound ions stacked and bound together by van der Waals forces (Berkelbach and Reichman, 2018; Das *et al.*, 2015; Miró *et al.*, 2014; Parvez, 2019; Shinde and Singh, 2019). In contrast to their bulk counterparts, they are direct band-gap semiconductors. A monolayer TMD shares with graphene the Dirac-like states, however, the electronic states in this case correspond to massive particles in a gapped two-band system. As in any semiconductor, exciton states are possible; in multiple layer structures excitons can be either spatially direct with electron and hole being in the same layer or spatially indirect, with an electron and a hole residing in different layers. Compared to other semiconductor materials, TMDs are characterized by very large exciton binding energies of the order of 500 meV, which is mainly due to the effectively strongly reduced screening in layers of these materials.

A first study of the interaction of graphene with OVs was conducted by Farias *et al.* (2013). They considered theoretically the interaction with the transverse component of an OV beam, described by the Hamiltonian

$$h = \hbar v_F(\alpha\sigma_x k_x - \sigma_y k_y) + ev_F[\alpha\sigma_x A_x(\mathbf{r},t) - \sigma_y A_y(\mathbf{r},t)]\,, \tag{91}$$

with $\alpha = \pm 1$ designating each Dirac point, and σ_i a Pauli matrix. Note the similarities with the Rashba Hamiltonian Eq. (84) for a QR: once again there is a term coupling (pseudo-)spin to vector potential suggesting the possible exchange of OAM and pseudo-SAM. Using the EoM, the evolution of the angular momentum and induced current were calculated, reflecting analog behavior to other systems excited by OVs in the intraband regime. New in the case of graphene is the fact that the light-matter interaction exchanges the pseudo-spin of electrons, moving them from one sublattice to the other, when the Rotating Wave Approximation is invoked; however, this effect is not exclusive to OVs. Inglot *et al.* (2018) included Rashba and a static magnetic field, and found also no effect of the topological charge of the light field on the electron spin dynamics.

In their theoretical investigation Cao *et al.* (2021a) considered the excitation by an OV of a graphene ring (*Corbino* disk) in the quantum Hall regime. The electric current between the inner and outer contacts was studied under disorder, and it was found that the current results from the transfer of OAM from light to electron states.

Simbulan *et al.* (2021) performed photoluminescence experiments in mono- and bi-layer MoS_2 excited with OVs, together with theoretical modeling and numerical simulations. They found a clear dependence of the energy shift on the OV topological charge, that can be interpreted as resulting from the transfer of OAM to valley A-excitons, see Fig. 21.

Transition metal dichalcogenides can easily be combined with other materials (Krasnok *et al.*, 2018). Guo *et al.* (2020) implemented a hybrid system consisting of a TMD WS_2 on top of a plasmonic spiral structures on aluminum. The plasmonic vortex conveys its chirality to the achiral C-excitons in WS_2, with a resulting second-harmonic generation emission that depends on the sense

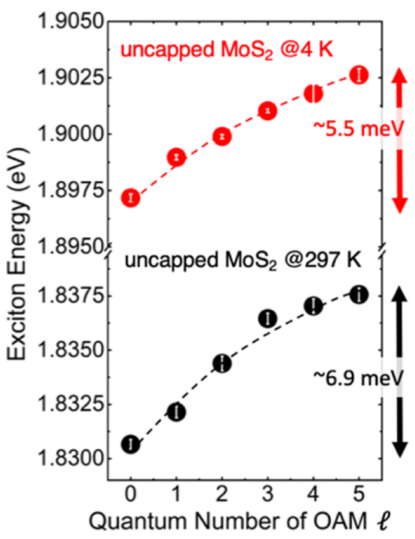

FIG. 21 (color online) Exciton energy shift for an uncapped MoS_2 sample at two different temperatures. The MoS_2 sample consists of one layer of MoS_2, one layer on h-BN and SiO_2/Si. Adapted from Simbulan *et al.* (2021).

of circular polarization of the light exciting the plasmonic structure. Li *et al.* (2017) explored the coupling between MoS_2 excitons and plasmons from spirals using spectroscopy and numerical simulations, and showed the enhancement of the photoluminescence signal for a particular state of polarization of the external light, see Fig. 22. These spin dependent effects are directly related to the spin-to-orbital AM conversion discussed in Sect. IV.C.

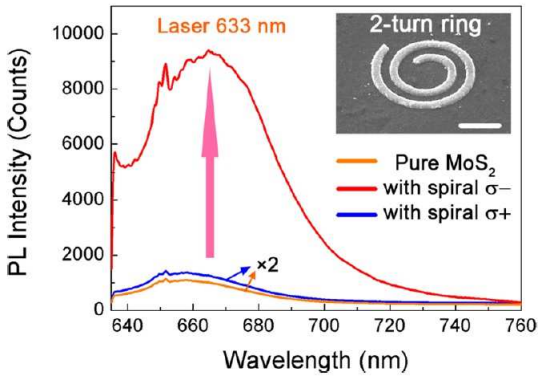

FIG. 22 (color online) Photoluminescence spectra of MoS_2 monolayer with and without spiral structures, under the excitation by light with different circular polarization at 633 nm and laser power at 2.1 mW. Inset: Cross section view of 2-turn spiral structure (scale bar is 400 nm). From Li *et al.* (2017).

V. APPLICATIONS

Condensed matter physics deals with basic physical phenomena as well as their applications. After having reviewed, in the previous section, basic properties of the OV-condensed matter interaction, it is time to turn our attention to actual and prospective technologies.

Electronics, a vital technology based on semiconductors, relies exclusively on the charge of electrons. In order to keep up with technological progress, spintronics seeks to control the spin of electrons in nanostructured systems. A set of discoveries in the 1980 boosted the interest in applications based on spin, mainly the giant magnetoresistance (Baibich *et al.*, 1988; Binasch *et al.*, 1989) but also the injection of spin-polarized electrons (Wolf *et al.*, 2001). Spintronics promises faster data processing, lower energy consumption and higher miniaturization (Ahn, 2020; Hirohata *et al.*, 2020).

Around the same time Feynman (1982) proposed the concept of quantum computing for the simulation of the hard-to-solve many-body quantum systems. The new computer, based entirely on the prinicples of quantum mechanics, may outperform any conceivable classical computer (Galindo and Martin-Delgado, 2002; Steane, 1998). Basic elements of a quantum computer are according to the famous five criteria formulated by DiVincenzo (2000): (*i*) A scalable system with logical units for storing and performing operations, the qubits, (*ii*) a procedure to prepare the set of qubits to a given initial state, (*iii*) long relevant decoherence times, much longer than the gate operation times, (*iv*) a "universal" set of quantum gates, which control the system dynamics via unitary transformations on qubits and thus implement the algorithms, and (*v*) a procedure to measure the final state of specific qubits, reading the output of the computation.

The field of quantum technology is a wide endeavor to outperform classical counterparts. Another example is the use of quantum light in quantum communication (Al-Amri *et al.*, 2021) for secure data transmission beyond classical protocols (Gisin and Thew, 2007; Liao *et al.*, 2018). Quantum computing, quantum communication and spintronics have only recently become a reality, boosting the further exploration of diverse platforms and tools to implement their components and operations in more effective ways. A key feature for quantum technologies is entanglement. In fact, entanglement of photons in OAM states have been observed in various experiments (Arnaut and Barbosa, 2000; Franke-Arnold *et al.*, 2002; Krenn *et al.*, 2017; Mair *et al.*, 2001) making OVs a valuable resource for applications in this field.

Solid-state physics has been an essential part of materials science, which aims to develop new fabrication and processing techniques of materials, including metals and semiconductors in various forms, for all sorts of applications. And material processing is starting to benefit from

the use of OVs.

In the following, we choose to classify applications by the area in which they were proposed or reported. Clearly, this scheme is arbitrary, since a proposed idea may well serve nowadays or in the future several fields; an example is the use of OVs in materials science, specifically in metal ablation as reported by Hamazaki *et al.* (2010), which may become in the future applicable in medicine to surgery (Jeffries *et al.*, 2007).

A. Semiconductor elementary nanostructures

Quantum dots are a platform for quantum technologies. Impurities or additional electrons charging the dot implement qubits via their spin. In quantum computing, one requires the control of single and pairs of qubits as building blocks of more complex operations and ultimately algorithms. The operations on qubits can be done by optical means, improving speed, and avoiding noise from electrical contacts for example. The single qubit operation requires the ability to control the spin direction at will. Many protocols have been devised to manipulate the in-plane (perpendicular to the nanostructure's z growth direction) spin component (Kroutvar *et al.*, 2004; Quinteiro *et al.*, 2012; Wolf *et al.*, 2001). However, it is challenging to control the longitudinal component, necessary to complete all possible one-qubit operations. Quinteiro and Kuhn (2014, 2015) proposed the use of a sequence of three light pulses ($P_{\ell,\sigma}$) in the sub-picosecond time scale to achieve full inversion of the spin z-component of an extra electron charging a self-assembled semiconductor QD. The pulse sequence is independent of the initial spin state of the extra electron, and works by inducing an e-LH pair with zero total AM (second excitation method of Fig. 14) in the QD. Figure 23 shows the results from numerical simulations of the density matrix ρ_{ij} using the master-equation formalism within a 4-level system $i = \{1 : |\uparrow 00\rangle, 2 : |\downarrow 00\rangle, 3 : |\uparrow\downarrow\Uparrow\rangle, 4 : |\uparrow\downarrow\Downarrow\rangle\}$, with single (double) arrow for electron (hole). It is worth noting that the addition of electron-electron interactions does not affect the proposal significantly; as seen in Sect. IV.A.3.c the full model still presents the most important ingredient of the proposal: the state $s \to s\,\mathrm{LH} \pm 0$ essential to the spin inversion.

In fact, the $s \to s\,\mathrm{LH} \pm 0$ transitions in QDs may prove useful in quantum storage, as shown by Holtkemper *et al.* (2021). The Coulomb interaction produces the admixture of high energy dark with optically active e-h pairs. In particular, as seen in Fig. 15, the e-HH pair $d \to s\,\mathrm{HH} \pm 2$ mixes with the e-LH $s \to s\,\mathrm{LH} \pm 0$ forming an exciton that can be excited by the longitudinal component of the antiparallel $\ell = \pm 1$, $\sigma = \mp 1$ OV (second excitation method of Fig. 14). After the light pulse is turned off, the system decays to its ground state; thus, the excited exciton relaxes, mainly by electron-phonon scattering without spin flip to the almost unmixed $s \to s\,\mathrm{HH} \pm 2$ state. This is optically forbidden, and so robust against radiative recombination. States $s \to s\,\mathrm{HH} + 2$ and $s \to s\,\mathrm{HH} - 2$ can be generated at will, and represent qubits of information.

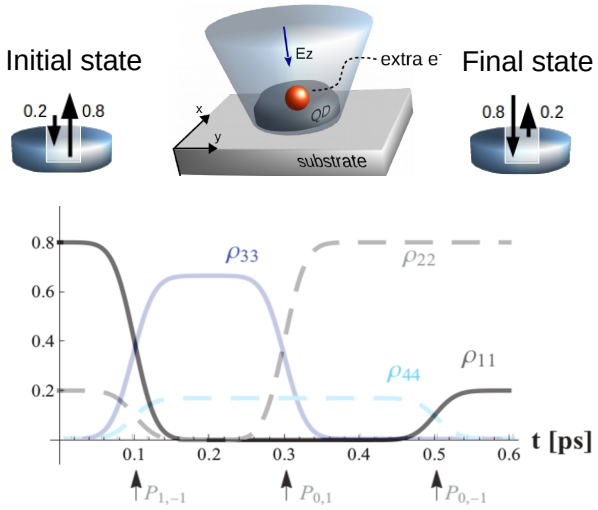

FIG. 23 (color online) Numerical simulations of the master equation for the extra electron plus e-LH system in a negatively charged QD, for the case when the initial spin states of the extra electron is a superposition of up and down s_z. After the application of three normal-incident pulses (one an OV), full inversion is achieved on a sub-picosecond time scale. Adapted from Quinteiro and Kuhn (2014).

Yet another application of QDs is their use for the conversion of light's orbital AM to electronic spin AM and vice versa. The device consists of a photonic crystal coupled to a QD, and it can work as an emitter/receiver for quantum communications (Fong *et al.*, 2018). For instance, in the emitter mode the spin state of the excited electron in the QD emits –upon recombination– light with a particular circular polarization. This drives a combination of quadrupole modes in the photonics crystal, which in turn are capable to emit light with OAM (see Fig. 24).

Structured light, including OVs, can extract the spatial phase information of the excitonic wave functions in QDs. Holtkemper *et al.* (2020) propose repeated absorption measurements of the state under investigation using complex fields formed out of a superposition of structured beams. A particular set of superposition coefficients will maximize the absorption. These coefficients can be directly related to the expansion coefficients of the exciton wave function in a given basis; in this way one deduces the complete exciton wave function including relative phases.

The transfer of OAM to nanostructures sets up an electric current that can be used in electronics, spintronics and communications. One such application is the generation of magnetic fields in nanostructures, e.g., a QR

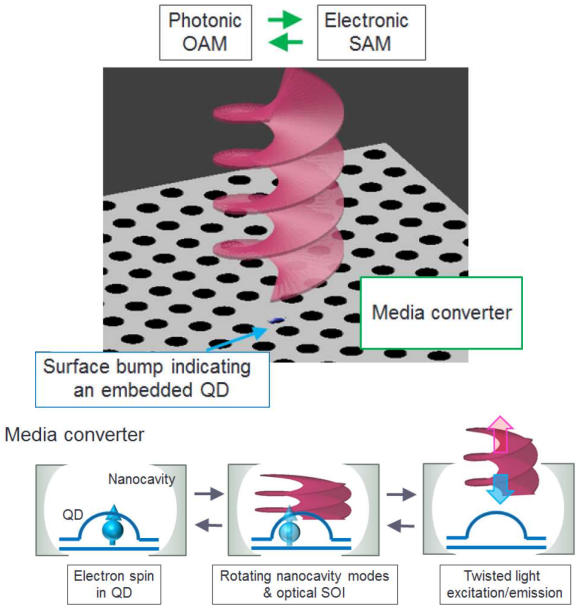

FIG. 24 (color online) Light's OAM to and from electron spin AM conversion. Top panel: The device consists of a photonic nanocavity with an embedded QD. Lower panel: Schematics of conversion process, from left to right: the light emission of a spin polarized electron drives the rotation of nanocavity modes, resulting in the nanocavity emitting an OV. From right to left: an OV drives the rotating modes, which in turn generates an electron spin in the QD. Adapted from Fong *et al.* (2018).

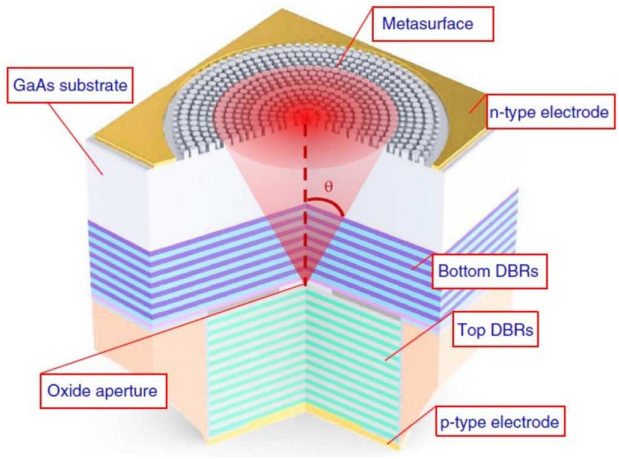

FIG. 25 (color online) Schematic of the Metasurface-VCSEL system: standard VCSEL structure and the beam-shaping metasurface integrated at the back side of the substrate. From Xie *et al.* (2020).

(Kraus *et al.*, 2018) or bulk (Quinteiro and Tamborenea, 2009c) to control the spin state of a nearby impurity, QD, etc. Ji *et al.* (2020) demonstrated that the circular photon-drag can serve to detect the OAM of light impinging a U-shape device on WTe_2, for the use of OAM-based communications.

The invention of new devices to generate OVs is an active field of research for possible uses in comunications, sensing and other applications (Kerridge-Johns, 2018). Semiconductor technology plays an important role in innovations to the field, specially in lasers that can create vortex fields from within the cavity, see also Sect. II.G. A good example is the vertical (external) cavity surface emitting laser (VCSEL/VECSEL) formed out of one or several semiconductor quantum wells coupled to additional intracavity devices, see Fig. 25. Examples of intracavity devices are metasurfaces (Seghilani *et al.*, 2016; Xie *et al.*, 2020) and spiral phase plates (Li *et al.*, 2015) that shape the beam to an OVs. Micrometer-size whispering gallery modes on solid-state systems can generate OVs with controllable topological charge and polarization state (Chen *et al.*, 2021; Miao *et al.*, 2016; Zhang *et al.*, 2020b) and microlasers producing fractional OAM that can be controlled at GHz frequencies were reported by Zhang *et al.* (2020c).

Stimulated emission depletion microscopy (STED), a technique that makes use of donut-shape beams including OVs (Keller *et al.*, 2007), can be used to read and control quantum states in nanostructures. Arroyo-Camejo *et al.* (2013) showed that individual nitrogen-vacancy (NV) color centers can be resolved with STED microscopy up to 15 nm. A similar technique, the so-called charge-state depletion (CSD) microscopy was used by Chen *et al.* (2015) to detect and manipulate the state of NV-centers in diamond, with applications to sensing and quantum computation. The manipulation procedure combines Gaussian and donut-shape beams to produce space-dependent changes in the populations of NV^0 and NV^- states, and the authors demonstrated subdiffraction manipulation on the order of few nanometers.

B. Exciton polaritons

Exciton-polariton vortices (or quantum vortices) driven by external optical perturbation have been shown to be robust entities against changes in power, shape and size of the pump (Borgh *et al.*, 2012; Kwon *et al.*, 2019; Ma *et al.*, 2020; Sigurdsson *et al.*, 2014). Ma *et al.* (2020) demonstrated control and switching of the vortex topological charge in a few hundreds of pico-seconds at non-resonant excitation. In their experiment a GaAs microcavity is excited by a ring-shape cw field that creates a vortex exciton-polariton condensate rotating in a random sense. The topological charge is controlled and switched by an additional Gaussian laser beam that breaks cylindrical symmetry. In addition, the authors show robustness against system's disorder and imperfection. Quantum vortices can also be trapped, moved, and mutually scattered, as shown by several authors (Dominici *et al.*, 2018, 2015; Pigeon *et al.*, 2011; Sanvitto *et al.*, 2011).

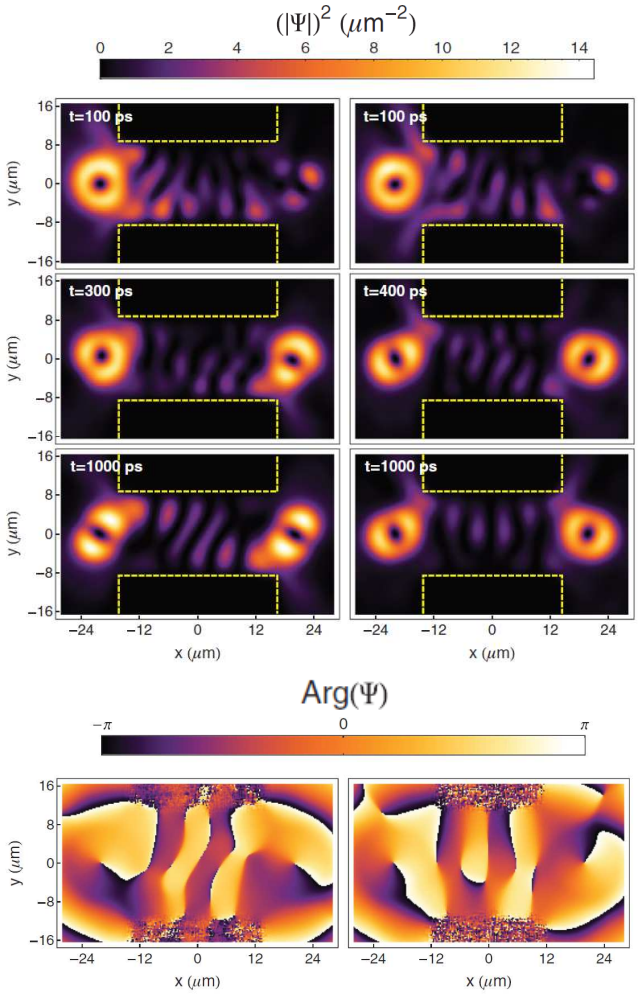

FIG. 26 (color online) Copying exciton-polariton vortices. Left column: Density plots of the copier process (same topological charge). Yellow dashed lines show the edges of the guide. At $t = 300$ps the transfer is complete and at $t = 1000$ps the state is nearly stationary. Right column: The inverter (opposite topological charge) process. At $t = 400$ps the transfer is complete and at $t = 1000$ps the state is nearly stationary. Bottom panels show the phase profiles at $t = 1000$ps. Adapted from Sigurdsson *et al.* (2014).

Motivated by possible applications to quantum technology in information transfer and storage Sigurdsson *et al.* (2014) consider in detail the switching and copying of quantum vortices of topological charge $\ell = \pm 1$ from one vortex to a second one created at a distance of tens of micrometers, see Fig. 26.

C. Plasmonics

Light in general, and OVs in particular, are used to trap and manipulate particles (Grier, 2003; Jones *et al.*, 2015), and recent studies suggest that the localization and enhancement of fields provided by plasmonics may improve optical tweezers. Liu *et al.* (2020) studied by numerical means plasmonic structures containing a spiral and a tip to trap or push away particles, depending on the topological charge of the plasmonic vortex. Hoshina *et al.* (2020) compared two scenarios to rotate a particle using light: The first makes direct use of a LG beam, which can only rotate the particle on a macroscopic scale, due to its large donut shape. The second employs the spin-to-orbital AM conversion by plasmon polaritons (Sect. IV.C): a circularly polarized light excites a nanostructure, consisting of four rectangular-shape metallic pieces, that creates localized plasmonic vortices that rotate the particle on the nanometer scale.

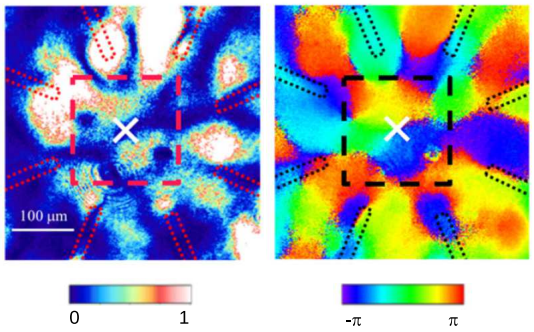

FIG. 27 (color online) Near-field distribution around the circular array antenna illuminated by a vortex beam with ring diameter 310μm: Intensity (left) and phase (right) image showing an intensity null at the center (white cross) and the 2π phase rotation. Adapted from Arikawa *et al.* (2017).

The squeezing of fields by plasmonic structures was also exploited by Heeres and Zwiller (2014), who showed by numerical simulations that a set of nanoantennas can focus an incident OV to a subwavelength lateral size, eluding the diffraction limit, and so enhancing the light intensity close to the phase singularity. Large field intensities reduce the excitation time, improving the quantum operation speed and diminishing the importance of the decay/decoherence of states. Later Arikawa *et al.* (2017) demonstrated very similar concepts in an experiment using THz OVs. They illuminate an array of eight antennas with an OV beam of ring diameter 310μm, and find within the array system that the OV is reduced to a ring diameter of 90μm, a factor of 3.4 smaller, see Fig. 27.

Much work is devoted to the exploitation of the additional degree of freedom of OAM (ℓ) for communication purposes, and high transfer rates have been achieved through fiber (Bozinovic *et al.*, 2013) and wireless (Wang *et al.*, 2012) channels by multiplexing with OAM states of light. Clearly, communication requires channels (Chen *et al.*, 2018), emitters (Jiang *et al.*, 2020) and receivers. Garoli *et al.* (2016) demonstrated an OV emitter. The authors designed a plasmonic device, consisting of a plasmonic lens (spiral structure) plus a hole in its center, and illuminated it by circularly polarized light. The plas-

monic lens converts the non-singular field, via the spin-to-orbital AM conversion effect, to a plasmonic vortex that upon interaction with the milled hole propagates an OV to the far-field, see Fig. 28.

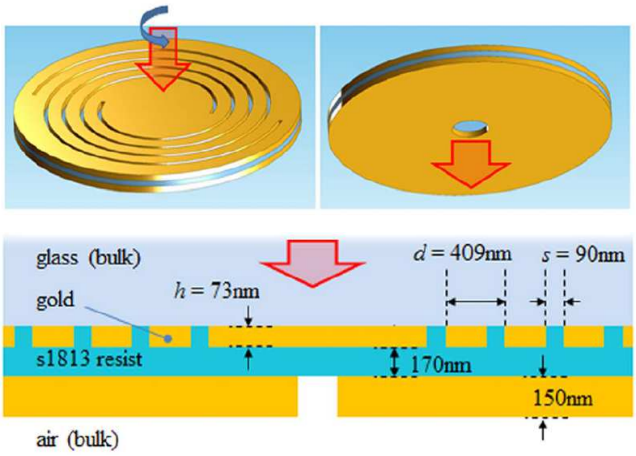

FIG. 28 (color online) Schematic illustration of the plasmonic structure emitter used to convert circularly polarized light into far-field OVs. Adapted from Garoli *et al.* (2016).

D. Materials science

A first use of OVs is to employ the donut shape of the beam, which can generate a different pattern to that of conventional Gaussian beams (Nolte *et al.*, 1997). Ablation in copper by OVs was demonstrated by Anoop *et al.* (2014), who showed the formation of annular structures of different character depending on the values of light fluence and number of pulses employed. Further investigation on the ablation dynamics of copper was conducted by Tsakiris *et al.* (2014) through experiments and numerical simulations. Optical vortices were reported to improve ablation on Ta plates, by creating with a lower ablation fluence clearer and smoother ablated zones and less debris (Hamazaki *et al.*, 2010). Oosterbeek *et al.* (2018) extended the D-Scan method (Samad *et al.*, 2008), used to determine the ablation threshold fluence, to weakly focused OVs, and put the method to test measuring ablation on silicon and quartz. In their inverse work, Nivas *et al.* (2015) sought to understand how an OV can be investigated via the ablation spots it produces. They found that spots features such as surface texture and size of the annulus depend on local fluence, number of pulses, and polarization (radial, azimuthal or circular).

Optical vortices can do more than ablate structures in annular shapes, and the formation of chiral structures has been demonstrated by several groups. Such chiral nanostructures may help to further probe the interaction of light with chiral matter, study the optical activity and chirality of molecules, and create new devices for quantum information purposes (Omatsu *et al.*, 2019). Chiral microstructures, such as needles and fibers, result from the direct illumination of intense OVs on metals (Omatsu *et al.*, 2010; Syubaev *et al.*, 2017, 2019; Toyoda *et al.*, 2012), silicon (Ablez *et al.*, 2020), azo-polymers (Ambrosio *et al.*, 2012; Juman *et al.*, 2014), isotropic polymer (Ni *et al.*, 2017), and photopolymerized resins (Lee *et al.*, 2018). Laser parameters control the formation of the structures, and most notably, the helicity of the structure results from a combination of light's OAM and SAM, see Fig. 29.

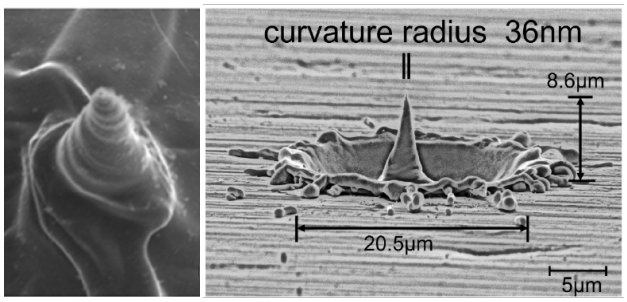

FIG. 29 (color online) Microneedles in tantalum fabricated by an optical vortex with a total AM $J = 2$. Left: 25° view, and right: side view. Adapted from Toyoda *et al.* (2012).

VI. CONCLUSIONS AND OUTLOOK

The early 1990s witnessed a breakthrough in optics with the development of techniques to generate coherent beams of highly inhomogeneous light, known as optical vortices (OVs) or twisted light. These objects exhibit unique features (most notably phase singularities and OAM) that challenge our intuition based on plane waves and Gaussian beams. These properties are more than a curiosity, and bring about new physics in their interaction with matter, with important implications to technology.

The present article reviewed the physics of the interaction of OVs and condensed-matter systems, providing the theoretical basis and a detailed account of the current progress in the theoretical and experimental research as well as in applications to the field. In the following Section we will summarize the main aspects discussed so far. We will then finish this review with an account of our own perspective on future directions that research in OV-condensed matter may take to unfold new physics and applications and on challenges associated with these developments. These are by no means exhaustive, they are meant to spark the readers' curiosity, and help discover their own research lines.

A. Concluding remarks

A historical account of discoveries leading to the understanding of light and its interaction with matter introduced the theoretical description of OVs. We briefly surveyed their most curious and relevant properties. A key concept in the classification of optical beams is the paraxial approximation, which has been the basis for the majority of theoretical and experimental studies on optical beams either with or without singularities. Beams in this regime are characterized by purely transverse electric and magnetic fields and OVs may exhibit a well-defined topological charge and circular polarization. The paraxial regime is limited to beams with characteristic lateral dimensions much larger than the wavelength. Going beyond this limit, the beams may exhibit intriguing new phenomena such as a strong component in the propagation direction or a dominant magnetic field close to the singularity and in general there are components with different topological charges. These features open new possibilities, e.g., for the optical control of nanostructures. We provided a detailed discussion and comparison of paraxial and full solutions of the Helmholtz equation, exemplified by the well-known Laguerre-Gauss and Bessel beams, respectively. Other solutions were mentioned, emphasizing the existence of OVs with multiple-singularities. We discussed the derivation of OVs from potentials and the role of the gauge, in particular in the non-paraxial regime, as well as the representation of OVs in terms of plane waves, aspects on generation and measurement of the OAM content, and the impact that subject has on physics, chemistry and biology.

The field of OV-condensed matter interaction builds on a long history of condensed-matter physics, in particular solid-state physics and condensed-matter optics. To provide the necessary background, we offered a focused overview of the basic concepts of solid-state physics relevant for the field. A recount of the crystalline state reminded the reader of the electronic state of semiconductors and metals that form the basis of simple and complex systems. Bulk materials and the relevant nanostructures, like quantum wells, dots, and rings, together with the modern two-dimensional materials were introduced. Motivated by the subject of the review, a focus was on condensed-matter optics. The issues of gauge choice and invariance were carefully examined, and then the usual approximation of vertical optical transitions for plane-wave like or weakly inhomogeneous light fields was revisited. The theoretical toolbox to treat the dynamics of condensed matter systems under light excitation was presented in considerable detail. The formalism most often applied in the field of OV-condensed matter interaction is based on the equations of motion for the single-particle density matrices and accommodates aptly both the light-matter and the electron-electron interactions, however also other approaches like non-equilibrium Green's functions have been used and are therefore briefly reviewed.

The preceding sections paved the way to the main part of the article: a cohesive analysis of the fundamental theory of the interaction of OVs with condensed-matter systems, alongside the review of the current literature in the field. Standard semiconductor optics is a rich discipline despite the fact that it is based on strong simplifying assumptions regarding the light-matter interaction. We pointed out that these customary and almost silent assumptions are the first conceptual sacrifices needed to describe the effects of structured light on matter. The main misleading assumptions that must be abandoned are the vertical-transition and the dipole-moment approximations. And other notions that hinder a sound understanding of this new field are the beliefs that light beams interact with matter mostly (or only) via their transverse electric field, that bulk semiconductors are the simplest model to understand the OV-matter interaction, and that light is always well represented by plane waves. Striped away from notions that lead us off track, we comprehensively studied the theory of crystal-OV interaction that constitutes the building block to tackle phenomena taking place in many systems.

In bulk semiconductors, the light-matter Hamiltonian matrix elements for the case of strongly inhomogeneous light fields has to be recalculated and novel selection rules are obtained, based on the conservation of total angular momentum. The OAM is transferred from the light beam to the photo-excited electrons, generating macroscopic currents and ultrafast local magnetic fields. Various experiments indeed confirmed this transfer of AM. When the electron-electron interaction is taken into account the rich physics of excitons comes into play, modified by the finite OAM of the structured light, which results in the creation of excitons in a superposition of states with non-zero center-of-mass momentum.

Semiconductor nanostructures add the complexity of their own spatial inhomogeneity, which is typically handled adequately by the envelope-function approximation. Here again novel matrix elements for the light-matter interaction dictate the allowed and forbidden optical transitions, distinct from the ones obtained in traditional optical excitation with plane waves. Quantum rings play a central role due to their especially adapted geometry to the cylindrical nature of the twisted light beams.

In semiconductor microcavities the strong coupling between excitons and light gives rise to the formation of exciton-polaritons. Here, vortical structures in the polariton fluid can also form spontaneously without the need of pumping by an OV. Analogously, in metallic nanostructures the light-matter coupling leads to plasmon-polaritons which again provide new features when studying their interplay with OVs. Of particular interest are spiral geometries which provide a singularity already in their structure and thus may create OVs

from excitation by plane waves. Angular momentum transfer has also been observed for OV excitation of two-dimensional materials. For all these systems theory and recent experiments have been reviewed.

The peculiarities of the interaction of OVs with condensed matter resulted in a bunch of –theoretically proposed or already experimentally realized– applications relevant for fields such as quantum technologies, communications, sensing, and materials science. They rely on the precise control and transfer of AM, conversion of spin and orbital AM, switching and copying of quantum vortices, squeezing of OVs to subwavelenght lateral size, creation of annular structures by ablation, to name just a few. Other applications can be envisaged. In the next section we will finish this review by our personal view on possible future directions in the field.

B. Current limitations and future perspectives

In a little more than a decade, the research in OV-condensed matter interaction has covered a large number of topics; nevertheless, it is safe to say that the topic is far from been exhausted. A better understanding of basic principles on explored topics (e.g., bulk semiconductors) is still hindered by several factors, while other topics have been only superficially studied. These include two-dimensional and other van der Waals materials, superconductors, skyrmions, localized plasmon polaritons, color centers, and non-linear effects in solids. In the following we discuss limitations in our present knowledge together with possible future directions to overcome these limitations.

1. Inhomogeneity and excitation strength

Inhomogeneity has been a central point throughout this review; we argued that, when matter fields (wave functions) are subjected to spatial variations in light's amplitude and phase, curious effects take place. Optical vortices are special objects, for they have an unavoidable phase inhomogeneity at the singularity: Irrespective of the extent of the matter field, the vortex causes unexpected effects, as demonstrated by the excitation of a single Ca ion by far-field OVs (Afanasev *et al.*, 2018; Quinteiro *et al.*, 2017c; Schmiegelow *et al.*, 2016). However, this strong spatial phase variation comes at a cost: the amplitude in its vicinity is small. Then, optical transitions are orders of magnitude weaker than their counterparts induced by non-singular beams [see Eq. (88)], with detrimental consequences to applications that require ultra-fast transitions to improve speed operation and avoid data-destroying decay or dephasing processes.

Needless to say, one can speak of near-field vs. far-field optics, and far-field beams can be further split into collimated/paraxial and strongly focused/non-paraxial ones. Loosely speaking, the degree of field inhomogeneity can be pushed furthest in near field optics, for which the diffraction limit does not apply. In contrast, strongly focused/non-paraxial far fields are limited to the order of the wavelength.

Most of our knowledge regards the action of far-field OVs on typical semiconductors, e. g., GaAs, for which optical transitions are weak. With applications in mind, it is then a must to improve fluence around the vortex.

Far-field optics with OVs can benefit from the use of high focusing techniques and materials with large band gaps. Abbe's diffraction-limit law states that the minimum resolution d is given by $d = \lambda/(2\,\mathrm{NA})$, with $\mathrm{NA} \lesssim 1.4$ (Chen *et al.*, 2017; Wang *et al.*, 2017) being the numerical aperture of the optical system –the resolution is a measure of the beam's lateral size. High focusing is achieved by increasing the NA to decrease the lateral size of the beam. Alternatively, a change in the wavelength will compress the minimally achievable lateral size too. In interband optical transitions, the size of the band gap determines the photon's wavelength. Semiconductors with larger band gaps (Andreev and O'Reilly, 2000; Arakawa and Kako, 2006; Jarjour *et al.*, 2007; Kako *et al.*, 2004; Ranjan *et al.*, 2003) are excited at shorter wavelength; thus, the lower bound d decreases. The interaction of highly focused OVs with large band-gap semiconductors is worth exploring.

An alternative is near-field optics. Little work has been done so far, but the experimental report by Arikawa *et al.* (2017) shows that the radius of the ring exhibiting the maximum intensity of the OV can be decreased by a factor $n \simeq 4$ (Sect. V.C); considering Eq. (88) the relative interaction strength would increase by a factor n^ℓ in QDs. More enthusiastic theoretical estimates promise an enhancement of the interaction by orders of magnitude (Heeres and Zwiller, 2014).

Another route to overcome weak excitation is to consider more extended quantum systems. A notable case, central to this review, is that of electronic excitations in bulk semiconductors, 1D and 2D nanostructures; nevertheless, we remind the reader that real solids have defects and impurities, that effectively reduce the span of the wave function (Leosson *et al.*, 2000; Martelli *et al.*, 1996; Takagahara, 1989), making important the pursue of more pure systems. Yet other quantum states of matter exhibit macroscopic wave functions ~~too,~~: superconducting circuits, superfluids, condensates, etc. (Wan, 2006).

2. Experiments

Experimental work reveals unexpected effects, and confirms/disproves theoretical predictions. The experiments in bulk by Noyan and Kikkawa (2015) and Shigematsu *et al.* (2016) indeed confirmed the transfer of OAM

to free carriers and excitons, while at the same time showed unexpected long lifetimes of OAM excitations.

There is an imbalance between theoretical and experimental work. While many theoretical predictions have been reported, only scarce experimental research was conducted, especially with elementary nanostructures. An exception is the field of microcavity exciton polaritons, where experimental and theoretical work seems to be well balanced.

Experiments with OVs and 0D nanostructures are indeed challenging. Two main obstacles hinder their realization. First, many experiments rely on ensemble measurements, which are easy to carry out but troublesome to interpret. Often, the growth process (e.g., self-assembly) forms nanostructures of slightly different sizes and shapes, resulting in large inhomogeneous broadening on very nearly spaced (few meV) energy levels, which causes difficulties in the extraction of information already from experiments with homogeneous light. For excitations by OVs an additional difficulty arises from the fact that the majority of nanostructures will be located off the optical axis, which causes on them multiple optical transitions as explained in Sect. IV.A.3.b and spoils many of the clear signatures of OV excitation seen in the ideal, centered case. Second, single-nanostructure measurements require more sophisticated techniques that, though available with current technology, face additional challenges when it comes to the excitation by OVs; these include the tight focusing and precise positioning of the beam to irradiate a single nanostructure out of an ensemble and align the singularity of the beam with the structure, and the read-out of low signals obtained from nanostructures positioned close to the singularity.

3. Analytical models and numerical simulations

From a theoretician's point of view, common sense dictates that a new field should be explored from basic phenomena, which can be addressed by relatively simple analytical and numerical models. We have reached now a good understanding of particular systems, namely, bulk semiconductors, quantum rings, quantum dots, and microcavities; in others, our theoretical understanding is rudimentary. Many important ingredients that would render a more complete picture of the system under scrutiny are still to be incorporated. Sophisticated analytical and numerical models are necessary to guide experimental work and propose future applications.

Essential elements of material systems that only in few cases have been considered are: (*i*) the electron-electron interaction responsible, for example, for the formation of excitons and thus exciton-polaritons, but also higher excitonic complexes such as biexcitons and trions; (*ii*) the electron-phonon interactions that drives relaxation and dephasing of electron populations and coherences, but also opens new and efficient ways of excitation of nanostructures, e.g., by employing phonon-assisted transitions; (*iii*) phenomena related to impurities and crystal defects, which cause loss of spatial coherence and localization of electronic states, but also provide new functionalities like single-photon emission; and (*iv*) the influence of temperature which plays a key role for applications.

Specific to nanostructures, we are in need of a description beyond the envelope function approximation. An assumption that underlies all our treatment is that of constant light field within the crystal unit cell [Eqs. (69)], an assumption supported by the order of magnitude difference in length scales of unit cell and far-field optical wavelengths. However, in Sect. VI.B.1 we argue that the very phase singularity is an unavoidable inhomogeneity at all scales. Therefore, one wonders what would result from lifting the restriction imposed by Eqs. (69). This is indeed a search worth pursuing, though not devoid from difficulties. The main one is the fact that the envelope function approximation is an assumption of a similar sort: the so-called envelope part of the wave function is a constant within the unit cell. An additional complication is that the variation of fields on the sub-nanometer scales would render the basic assumption of macroscopic electromagnetic fields in media invalid (Jackson, 1999). Thus, a reexamination of the validity of Eqs. (69) requires a concomitant reexamination of the envelope function approximation and macroscopic fields in media.

Another possible improvement concerns a better description of the nanostructure geometry by including interfaces. The external OV driving field goes through layers of different geometries and compounds that perturb it to some extent before it reaches the active region, where the optical excitation of interest takes place. Besides possibly unimportant attenuation by other partially active layers, reflection and refraction of OVs result in distortion and displacement of the field by complex mechanisms such as the Goos–Hänchen and Imbert–Fedorov shifts (Bliokh *et al.*, 2009; Lusk *et al.*, 2018; Novitsky and Barkovsky, 2008; Okuda and Sasada, 2008).

One can also improve the description of the driving field. This includes replacing the ideal Bessel beams by Bessel-Gaussian beams (Gori *et al.*, 1987; Li *et al.*, 2004), accounting for the imperfections introduced by the experimental generation of beams –e. g., producing beams with unintended multiple-singularity components (Bekshaev and Karamoch, 2008; Heckenberg *et al.*, 1992; Karimi *et al.*, 2007)–, or the use of multiple pulses. The addition of the interaction with the bath modes in weak and strong coupling regime reflects not only relaxation processes in matter (radiative recombination) but also the leakage of relevant modes outside cavities, and others.

The physics of optical vortices in microcavities treats fully quantum mechanically matter and light on equal footing (Sect. IV.B). Somewhat similarly, but in a semiclassical fashion, excitations in metal-dielectric interfaces

solves the coupled dynamics of matter and electromagnetic fields (IV.C). For other systems, an extension to a description of the self-consistent problem of the mutual light-matter interaction is in order, for instance, in systems embedded in cavities under the strong coupling regime. In addition, a quantum mechanical description of light is also desirable, for example, in situation of very low fluence (few photons case).

4. Structured light beyond Laguerre-Gauss and Bessel beams

Little is known about the interaction of condensed-matter systems with multiple-singularity OVs, and more general structured beams. Holtkemper *et al.* (2020) demonstrated in their theoretical study that structured light can unveil details of the exciton wave function in QDs (Sect. IV.A.3.c). This work shows that new physics and applications can be expected out of the simplest case of single-singularity OV. In particular, we expect that interesting research could arise from the study of Mathieu beams (Sect. II.D). We recall that these are the solutions of the Helmholtz equation in elliptical coordinates –Bessel beams are in a sense a particular case when the ellipse collapses to a circle. Mathieu beams exhibit one or several singularities, whose location, number and topological charge can be manipulated by adjusting the beam's parameters, see Fig. 3.

All these examples show that the topic of OV-condensed matter interaction is open in many directions and a variety of interesting results can be expected from future experimental and theoretical work in the field.

ACKNOWLEDGMENTS

G.F.Q.R. would like to thank the US agency Office of Naval Research Global for financial support through grants N62909-18-1-2090, and the Argentine agency Agencia Nacional de Promoción Científica y Tecnológica for financial support through grant PICT2016-1056. P.I.T. gratefully acknowledges the financial support through UBACyT 2018-2022 from the Universidad de Buenos Aires.

REFERENCES

Abbe, E. (1874), *Neue Apparate zur Bestimmung des Brechungs-und Zerstreuungsvermögens fester und flüssiger Körper* (Mauke's Verlag).
Abdalla, A., B. Zou, Y. Ren, T. Liu, and Y. Zhang (2018), Optics express **26** (17), 22273.
Ablez, A., K. Toyoda, K. Miyamoto, and T. Omatsu (2020), Appl. Phys. Express **13** (6), 062006.
Abrikosov, A. A. (1957), JETP **5**, 1174.
Abrikosov, A. A., L. P. Gorkov, and I. E. Dzyaloshinski (2012), *Methods of quantum field theory in statistical physics* (Courier Corporation).
Afanasev, A., C. E. Carlson, C. T. Schmiegelow, J. Schulz, F. Schmidt-Kaler, and M. Solyanik (2018), New J. Phys **20**, 023032.
Ahn, E. C. (2020), npj 2D Materials and Applications **4** (1), 1.
Al-Amri, M. D., D. L. Andrews, and M. Babiker (2021), in *Structured Light for Optical Communication*, Nanophotonics (Elsevier) pp. v–x.
Albrecht, S., L. Reining, R. Del Sole, and G. Onida (1998), Phys. Rev. Lett. **80**, 4510.
Allen, L., M. Babiker, W. Lai, and V. Lembessis (1996), Phys. Rev. A **54**, 4259.
Allen, L., S. M. Barnett, and M. J. Padgett (2003), *Optical angular momentum* (CRC press).
Allen, L., M. W. Beijersbergen, R. J. C. Spreeuw, and J. P. Woerdman (1992), Phys. Rev. A **45**, 8185.
Allen, L., M. Padgett, and M. Babiker (1999), Progress in optics **39**, 291.
Alperin, S. N., R. D. Niederriter, J. T. Gopinath, and M. E. Siemens (2016), Opt. Lett. **41**, 5019.
Alpmann, C., M. Bowman, R. and.Woerdemann, M. Padgett, and C. Denz (2010), Optics Express **18**, 26084.
Ambrosio, A., L. Marrucci, F. Borbone, A. Roviello, and P. Maddalena (2012), Nat. Commun. **3** (1), 1.
Anderson, N., and A. Arthurs (1990), International Journal of Electronics Theoretical and Experimental **69** (4), 575.
Andreev, A. D., and E. P. O'Reilly (2000), Phys. Rev. B **62** (23), 15851.
Andrews, D., L. D. Romero, and M. Babiker (2004), Opt. Commun. **237**, 133.
Andrews, D. L. (2008), *Structured light and its applications: An introduction to phase-structured beams and nanoscale optical forces* (Academic Press).
Andrews, D. L., and M. Babiker (2012), *The angular momentum of light* (Cambridge University Press).
Anoop, K., R. Fittipaldi, A. Rubano, X. Wang, D. Paparo, A. Vecchione, L. Marrucci, R. Bruzzese, and S. Amoruso (2014), J. Appl. Phys. **116** (11), 113102.
Arakawa, Y., and S. Kako (2006), Phys. Status Solidi A **203** (14), 3512.
Araoka, F., T. Verbiest, K. Clays, and A. Persoons (2005), Phys. Rev. A **71**, 055401.
Arfken, G. B., and H. J. Weber (1999), "Mathematical methods for physicists,".
Arikawa, T., S. Morimoto, and K. Tanaka (2017), Optics Express **25** (12), 13728.
Arlt, J., and K. Dholakia (2000), Opt. Commun. **177**, 297.
Arnaut, H., and G. Barbosa (2000), Phys. Rev. Lett. **85**, 286.
Arroyo-Camejo, S., M.-P. Adam, M. Besbes, J.-P. Hugonin, V. Jacques, J.-J. Greffet, J.-F. Roch, S. W. Hell, and F. Treussart (2013), ACS Nano **7** (12), 10912.
Ashcroft, N. W., and N. D. Mermin (1976), Pacific Grove: Brooks/Cole , 29.
Axt, V. M., and T. Kuhn (2004), Rep. Prog. Phys. **67**, 433.
Babiker, M., D. L. Andrews, and V. E. Lembessis (2018), J. Opt. **21**, 013001.
Babiker, M., C. R. Bennett, D. L. Andrews, and L. C. Dávila Romero (2002), Phys. Rev. Lett. **89**, 143601.
Baibich, M. N., J. M. Broto, A. Fert, F. N. Van Dau, F. Petroff, P. Etienne, G. Creuzet, A. Friederich, and J. Chazelas (1988), Phys. Rev. Lett. **61**, 2472.

Ballentine, L. E. (2014), *Quantum mechanics: a modern development* (World Scientific Publishing Company).

Balzer, K., and M. Bonitz (2013), *Nonequilibrium Green's functions approach to inhomogeneous systems* (Springer, Berlin).

Baranova, N., B. Y. Zel'Dovich, A. Mamaev, N. Pilipetskii, and V. Shkukov (1981), JETP Lett. **33**, 206.

Barnett, S. M., and L. Allen (1994), Optics communications **110** (5-6), 670.

Barnett, S. M., M. Babiker, and M. J. Padgett (2017), Phil. Trans. Roy. Soc. London, Ser. A **375**, 20150444.

Barrigoón, E., M. Heurlin, Z. Bi, B. Monemar, and L. Samuelson (2019), Chem. Rev. **119**, 9170.

Basdevant, J.-L., and J. Rich (2005), *Fundamentals in nuclear physics: From nuclear structure to cosmology* (Springer Science & Business Media).

Bassani, F., J. Forney, and A. Quattropani (1977), Phys. Rev. Lett. **39**, 1070.

Bastard, G. (1988), *Wave mechanics applied to semiconductor heterostructures* (Les éditions de physique Les Ulis).

Bekshaev, A. Y., and A. Karamoch (2008), Opt. Commun. **281** (6), 1366.

Berkelbach, T. C., and D. R. Reichman (2018), Ann. Rev. of Cond. Mat. Phys. **9**, 379.

Berkhout, G. C., and M. W. Beijersbergen (2008), Phys. Rev. Lett. **101**, 100801.

Berkhout, G. C., M. P. Lavery, J. Courtial, M. W. Beijersbergen, and M. J. Padgett (2010), Phys. Rev. Lett. **105**, 153601.

Berry, M. (2004), J. Opt. A **6**, 289.

Berry, M., M. Jeffrey, and M. Mansuripur (2005), J. Opt. A **7**, 685.

Beth, R. A. (1936), Phys. Rev. **50**, 115.

Bhowmik, A., P. K. Mondal, S. Majumder, and B. Deb (2016), Physical Review A **93** (6), 063852.

Biasiol, G., and S. Heun (2011), Phys. Reports **500**, 117.

Binasch, G., P. Grünberg, F. Saurenbach, and W. Zinn (1989), Phys. Rev. B **39**, 4828.

Bliokh, K. Y., M. A. Alonso, E. A. Ostrovskaya, and A. Aiello (2010), Phys. Rev. A **82**, 063825.

Bliokh, K. Y., and F. Nori (2015), Physics Reports **592**, 1.

Bliokh, K. Y., I. V. Shadrivov, and Y. S. Kivshar (2009), Opt. Lett. **34** (3), 389.

Bloch, F. (1928), Z. Phys. **52**, 555.

Bluhm, H., N. C. Koshnick, J. A. Bert, M. E. Huber, and K. A. Moler (2009), Phys. Rev. Lett. **102**, 136802.

Bock, M., J. Jahns, and R. Grunwald (2012), Opt. Lett. **37**, 3804.

Bohm, D., and D. Pines (1953), Phys. Rev. **92**, 609.

Borgh, M. O., G. Franchetti, J. Keeling, and N. G. Berloff (2012), Phys. Rev. B **86** (3), 035307.

Boriskina, S., and N. I. Zheludev (2014), *Singular and Chiral Nanoplasmonics* (CRC Press).

Born, M., and E. Wolf (2013), *Principles of optics: electromagnetic theory of propagation, interference and diffraction of light* (Elsevier).

Boulier, T., E. Cancellieri, N. D. Sangouard, Q. Glorieux, A. Kavokin, D. M. Whittaker, E. Giacobino, and A. Bramati (2016), Physical review letters **116** (11), 116402.

Boyd, R. W. (2020), *Nonlinear optics* (Academic press).

Boyle, R. (1661), *The sceptical chymist* (J. Calwell, London).

Bozinovic, N., Y. Yue, Y. Ren, M. Tur, P. Kristensen, H. Huang, A. E. Willner, and S. Ramachandran (2013), Science **340** (6140), 1545.

Bragg, W. H., and W. L. Bragg (1913), Proc. Roy. Soc. London, Ser. A **88**, 428.

Breuer, H.-P., and F. Petruccione (2002), *The theory of open quantum systems* (Oxford University Press, New York).

Brullot, W., M. K. Vanbel, T. Swusten, and T. Verbiest (2016), Science Adv. **2**, e1501349.

Cai, X., J. Wang, M. J. Strain, B. Johnson-Morris, J. Zhu, M. Sorel, J. L. O'Brien, M. G. Thompson, and S. Yu (2012), Science **338** (6105), 363.

Cajori, F. (1899), *A history of physics in its elementary branches: including the evolution of physical laboratories* (Macmillan).

Cameron, K., A. Gibson, J. Giles, C. Hatch, M. Kimmitt, and S. Shafik (1975), J. Phys. C: Solid State Phys. **8**, 3137.

Cao, B., T. Grass, G. Solomon, and M. Hafezi (2021a), arXiv preprint arXiv:2104.06579.

Cao, Y., Y. Fu, J.-H. Jiang, L. Gao, and Y. Xu (2021b), ACS Photonics **0**, null.

Carpentier, A. V., H. Michinel, J. R. Salgueiro, and D. Olivieri (2008), Am. J. Phys. **76**, 916.

Castro Neto, A. H., F. Guinea, N. M. R. Peres, K. S. Novoselov, and A. K. Geim (2009), Rev. Mod. Phys. **81**, 109.

Chang, S.-H., S. K. Gray, and G. C. Schatz (2005), Optics express **13** (8), 3150.

Chatterjee, R., I. M. Pavlovetc, K. Aleshire, and M. Kuno (2018), J. Phys. Chem. C **122**, 16443.

Chen, B., Y. Wei, T. Zhao, S. Liu, R. Su, B. Yao, Y. Yu, J. Liu, and X. Wang (2021), Nature Nanotechnology **16** (3), 302.

Chen, R., H. Zhou, M. Moretti, X. Wang, and J. Li (2019), IEEE Communications Surveys & Tutorials.

Chen, W. T., A. Y. Zhu, M. Khorasaninejad, Z. Shi, V. Sanjeev, and F. Capasso (2017), Nano Lett. **17** (5), 3188.

Chen, X., C. Zou, Z. Gong, C. Dong, G. Guo, and F. Sun (2015), Light: Science & Applications **4** (1), e230.

Chen, Y., J. Gao, Z.-Q. Jiao, K. Sun, W.-G. Shen, L.-F. Qiao, H. Tang, X.-F. Lin, and X.-M. Jin (2018), Phys. Rev. Lett. **121** (23), 233602.

Chow, W. W., and S. W. Koch (1999), *Semiconductor-laser fundamentals: physics of the gain materials* (Springer Science & Business Media).

Citrin, D. S. (1994), IEEE J. Quantum Electron. **30**, 997.

Ciuti, C., P. Schwendimann, and A. Quattropani (2001), Phys. Rev. B **63**, 041303.

Clayburn, N. B., J. L. McCarter, J. M. Dreiling, M. Poelker, D. M. Ryan, and T. J. Gay (2013), Phys. Rev. B **87**, 035204.

Cohen, M. L., and J. R. Chelikowsky (2012), *Electronic structure and optical properties of semiconductors*, Vol. 75 (Springer Science & Business Media).

Cohen-Tannoudji, C., J. Dupont-Roc, and G. Grynberg (1989), *Photons and Atoms: Introduction to Quantum Electrodynamics* (Wiley, New York).

Cohen-Tannoudji, C., J. Dupont-Roc, and G. Grynberg (1998), *Atom-photon interactions: basic processes and applications* (Wiley, New York).

Coullet, P., L. Gil, and F. Rocca (1989), Opt. Commun. **73**, 403.

Courtial, J., K. Dholakia, L. Allen, and M. Padgett (1997), Phys. Rev. A **56**, 4193.

Cundiff, S. T. (2008), Optics Express **16**, 4639.

Cundiff, S. T., and S. Mukamel (2013), Physics Today **66**, 44.

Cygorek, M., P. I. Tamborenea, and V. M. Axt (2015), Phys-

ical Review B **92** (11), 115301.
Dalgarno, A., and J. T. Lewis (1956), Proc. Phys. Soc. A **69**, 285.
Dalton, J. (1808), *A new system of chemical philosophy*, Vol. 1 (Bickerstaff, London).
Das, S., A. Bhowmik, K. Mukherjee, and S. Majumder (2020), J. Phys. B **53**, 025302.
Das, S., J. A. Robinson, M. Dubey, H. Terrones, and M. Terrones (2015), Ann. Rev. of Mat. Res. **45**, 1.
Dávila Romero, L. C., D. L. Andrews, and M. Babiker (2002), J. Opt. B **4**, S66.
De Morveau, G., A. L. Lavoisier, C. Berthollet, A. D. Fourcroy, and J. H. Hassenfratz (1787), *Methode De Nomenclature Chimique* (Chez Cuchet libraire, Paris).
Deng, H., H. Haug, and Y. Yamamoto (2010), Rev. Mod. Phys. **82**, 1489.
Deng, H., G. Weihs, D. Snoke, J. Bloch, and Y. Yamamoto (2003), Proc. Nat. Acad. Sci. **100**, 15318.
Dennis, M. R., R. P. King, B. Jack, K. O'Holleran, and M. J. Padgett (2010), Nature Physics **6** (2), 118.
Dennis, M. R., K. O'Holleran, and M. J. Padgett (2009), Progr. in Optics **53**, 293.
Dexter, D. L., and R. S. Knox (1965), *Excitons* (Interscience Publishers, New York).
Dirac, P. A. M. (1927), Proc. Roy. Soc. London, Ser. A **114**, 243.
DiVincenzo, D. P. (2000), Fortschritte der Physik-Progress of Physics **48**, 771.
Dominici, L., R. Carretero-González, A. Gianfrate, J. Cuevas-Maraver, A. S. Rodrigues, D. J. Frantzeskakis, G. Lerario, D. Ballarini, M. D. Giorgi, G. Gigli, *et al.* (2018), Nat. Commun. **9**, 1467.
Dominici, L., G. Dagvadorj, J. M. Fellows, D. Ballarini, M. De Giorgi, F. M. Marchetti, B. Piccirillo, L. Marrucci, A. Bramati, G. Gigli, *et al.* (2015), Science Adv. **1** (11), e1500807.
Dresselhaus, M. (2001), *Solid state physics part ii optical properties of solids*, Lecture Notes, Vol. 17 (Massachusetts Institute of Technology, Cambridge, MA).
Drude, P. (1900), Annalen der Physik **306**, 566.
Drueppel, M., T. Deilmann, J. Noky, P. Marauhn, P. Krueger, and M. Rohlfing (2018), Phys. Rev. B **98**, 155433.
Duc, H. T., T. Meier, and S. W. Koch (2005), Phys. Rev. Lett. **95**, 086606.
Durnin, J., J. Miceli Jr, and J. Eberly (1987), Phys. Rev. Lett. **58**, 1499.
Dusanowski, L., S.-H. Kwon, C. Schneider, and S. Höfling (2019), Phys. Rev. Lett. **122**, 173602.
Einstein, A. (1905), Annalen der Physik **17**, 132.
Elliott, R. J. (1957), Phys. Rev. **108**, 1384.
Farias, M. B., G. F. Quinteiro, and P. I. Tamborenea (2013), The European Physical Journal B **86** (10), 1.
Fermi, E. (1950), *Nuclear physics: a course given by Enrico Fermi at the University of Chicago* (University of Chicago Press).
Fetter, A. L., and J. D. Walecka (2012), *Quantum theory of many-particle systems* (Courier Corporation).
Feynman, R. (1955) (Elsevier) pp. 17–53.
Feynman, R. P. (1982), International Journal of Theoretical Physics **21** (6), 467.
Fiori, F., G.and Bonaccorso, G. Iannaccone, T. Palacios, D. Neumaier, A. Seabaugh, B. S. K., and . C. L. (2013), Phys. Rev. B **87**, 165306.
Fiori, F., G.and Bonaccorso, G. Iannaccone, T. Palacios, D. Neumaier, A. Seabaugh, B. S. K., and . C. L. (2014), Nat. Nanotechnol. **9**, 768.
Fomin, V. (2014), "Physics of quantum rings 2014 berlin,".
Fong, C. F., Y. Ota, S. Iwamoto, and Y. Arakawa (2018), Optics express **26** (16), 21219.
Foo, G., D. M. Palacios, and G. A. Swartzlander (2005), Opt. Lett. **30**, 3308.
Forbes, A. (2017), Phil. Trans. Roy. Soc. London, Ser. A **375**, 20150436.
Forbes, K. A., and D. L. Andrews (2018a), in *Complex Light and Optical Forces XII*, Vol. 10549 (International Society for Optics and Photonics) p. 1054915.
Forbes, K. A., and D. L. Andrews (2018b), Opt. Lett. **43**, 435.
Franke-Arnold, S. (2017), Phil. Trans. Roy. Soc. London, Ser. A **375**, 20150435.
Franke-Arnold, S., S. M. Barnett, M. J. Padgett, and L. Allen (2002), Phys. Rev. A **65**, 033823.
Franz, W. (1958), Z. f. Naturforschung A **13**, 484.
Frenkel, J. (1931), Phys. Rev. **37**, 17.
Fried, Z. (1973), Phys. Rev. A **8**, 2835.
Fujita, H., and M. Sato (2017), Physical Review B **95** (5), 054421.
Galindo, A., and M. A. Martin-Delgado (2002), Rev. Mod. Phys. **74** (2), 347.
Garoli, D., P. Zilio, Y. Gorodetski, F. Tantussi, and F. De Angelis (2016), Scientific Reports **6** (1), 1.
Ge, L. (2020), Science **368**, 707.
Ghosh Dastidar, M., S. Das, K. Mukherjee, and S. Majumder (2022), Physics Letters A **421**, 127776.
Giammanco, F., A. Perona, P. Marsili, F. Conti, F. Fidecaro, S. Gozzini, and A. Lucchesini (2017), Optics letters **42** (2), 219.
Gibson, A., M. Kimmitt, and A. Walker (1970), Appl. Phys. Lett. **17**, 75.
Gibson, A., and A. Walker (1971), Journal of Physics C: Solid State Physics **J. Phys. C: Solid State Phys.**, 2209.
Gippius, N., I. Shelykh, D. Solnyshkov, S. Gavrilov, Y. G. Rubo, A. Kavokin, S. Tikhodeev, and G. Malpuech (2007), Phys. Rev. Lett. **98**, 236401.
Gisin, N., and R. Thew (2007), Nat. Photonics **1**, 165.
Glauber, R. J. (1963), Phys. Rev. **130**, 2529.
Golde, D., T. Meier, and S. W. Koch (2008), Phys. Rev. B **77**, 075330.
Goldstein, H. (1980), *Classical mechanics* (Addison-Wesley, second edition).
Göppert-Mayer, M. (1931), Annalen der Physik **401**, 273.
Gori, F., G. Guattari, and C. Padovani (1987), Opt. Commun. **64** (6), 491.
Gorodetski, Y., A. Niv, V. Kleiner, and E. Hasman (2008), Physical review letters **101** (4), 043903.
Grier, D. G. (2003), Nature **424**, 810.
Grinberg, A. A. (1970), JETP **31**, 531.
Guo, W.-P., W.-Y. Liang, C.-W. Cheng, W.-L. Wu, Y.-T. Wang, Q. Sun, S. Zu, H. Misawa, P.-J. Cheng, S.-W. Chang, *et al.* (2020), Nano letters **20** (4), 2857.
Guo, Z., Z. Li, J. Zhang, K. Guo, F. Shen, Q. Zhou, and H. Zhou (2017), Nanomaterials **7** (11), 405.
Gutiérrez-Vega, J. C., M. Iturbe-Castillo, and S. Chávez-Cerda (2000), Opt. Lett. **25**, 1493.
Gutierrez-Vega, J. C., R. M. Rodriguez-Dagnino, M. D. I. Castillo, and S. Chavez-Cerda (2001), in *Proc. SPIE: Optical Pulse and Beam Propagation III*, Vol. 4271 (International Society for Optics and Photonics) pp. 73–80.

Haken, H. (1976), *Quantum field theory of solids. An introduction* (North-Holland, Amsterdam).
Hamazaki, J., R. Morita, K. Chujo, Y. Kobayashi, S. Tanda, and T. Omatsu (2010), Optics Express **18** (3), 2144.
Hamilton, W. R. (1837), Transact. of the Royal Irish Acad. **17** (part 1), 1.
Haug, H., and A.-P. Jauho (2008), *Quantum kinetics in transport and optics of semiconductors*, Vol. 2 (Springer).
Haug, H., and S. W. Koch (2009), *Quantum theory of the optical and electronic properties of semiconductors: fivth edition* (World Scientific Publishing Company).
He, J., X. Wang, D. Hu, J. Ye, S. Feng, Q. Kan, and Y. Zhang (2013), Optics Express **21**, 20230.
Hecht, B., H. Bielefeldt, L. Novotny, Y. Inouye, and D. Pohl (1996), Physical review letters **77** (9), 1889.
Heckenberg, N., R. McDuff, C. Smith, H. Rubinsztein-Dunlop, and M. Wegener (1992), Optical and Quantum Electronics **24** (9), S951.
Heeres, R. W., and V. Zwiller (2014), Nano letters **14** (8), 4598.
Henzler, P., C. Traum, M. Holtkemper, D. Nabben, M. Erbe, D. E. Reiter, T. Kuhn, S. Mahapatra, K. Brunner, D. V. Seletskiy, and A. Leitenstorfer (2021), Phys. Rev. Lett. **126**, 067402.
Herbst, M., M. Glanemann, V. M. Axt, and T. Kuhn (2003), Phys. Rev. B **67**, 195305.
Hernández-García, C., J. Vieira, J. T. Mendonca, L. Rego, J. San Román, L. Plaja, P. R. Ribic, D. Gauthier, and A. Picón (2017), Photonics **4**, 28.
Hernández-Hernández, R., R. Terborg, I. Ricardez-Vargas, and K. Volke-Sepúlveda (2010), Appl. Optics **49**, 6903.
Hess, O., and T. Kuhn (1996), Phys. Rev. A **54**, 3347.
Hirohata, A., K. Yamada, Y. Nakatani, I.-L. Prejbeanu, B. Diény, P. Pirro, and B. Hillebrands (2020), Journal of Magnetism and Magnetic Materials **509**, 166711.
Hohenberg, P., and W. Kohn (1964), Phys. Rev. **136**, B864.
Holtkemper, M., G. Quinteiro, D. Reiter, and T. Kuhn (2020), Physical Review B **102** (16), 165315.
Holtkemper, M., G. Quinteiro, D. Reiter, and T. Kuhn (2021), Physical Review Research **3** (1), 013024.
Honold, A., L. Schultheis, J. Kuhl, and C. W. Tu (1988), Appl. Phys. Lett. **52**, 2105.
Hopfield, J. (1958), Phys. Rev. **112**, 1555.
Hoshina, M., N. Yokoshi, and H. Ishihara (2020), Optics Express **28** (10), 14980.
Huang, K. (1963), *Statistical Mechanics* (Wiley, New York).
Huygens, C. (1690), Oeuvres completes XIX **1737**.
Ibach, H., and H. Lüth (2013), *Solid-state physics: an introduction to principles of materials science* (Springer Science & Business Media).
Ihn, T. (2010), *Semiconductor Nanostructures: Quantum states and electronic transport* (Oxford University Press).
Inglot, M., V. Dugaev, J. Berakdar, E. Y. Sherman, and J. Barnaś (2018), Applied Physics Letters **112** (23), 231102.
Jacak, L., P. Hawrylak, and A. Wojs (2013), *Quantum dots* (Springer Science & Business Media).
Jackson, J. D. (1999), *Classical electrodynamics* (Wiley).
Jarjour, A. F., R. A. Oliver, and R. A. Taylor (2007), Phil. Mag. **87** (13), 2077.
Jaroszewicz, Z., A. Burvall, and A. T. Friberg (2005), Optics and Photonics News **16**, 34.
Jauho, A. P., and K. Johnsen (1996), Phys. Rev. Lett. **76**, 4576.
Jáuregui, R. (2004), Phys. Rev. A **70**, 033415.
Jeffries, G. D., J. S. Edgar, Y. Zhao, J. P. Shelby, C. Fong, and D. T. Chiu (2007), Nano Lett. **7**, 415.
Jentschura, U. D., and V. G. Serbo (2011), Phys. Rev. Lett. **106**, 013001.
Ji, Z., W. Liu, S. Krylyuk, X. Fan, Z. Zhang, A. Pan, L. Feng, A. Davydov, and R. Agarwal (2020), Science **368**, 763.
Jiang, Y., Y. Cao, and X. Feng (2020), J. Phys. D **53** (30), 303002.
Johnson, A., M. Siemens, G. Quinteiro, S. Sanguinetti, and S. Bietti (2017), Bulletin of the American Physical Society **62**.
Jones, P. H., O. M. Marago, and G. Volpe (2015), *Optical tweezers: principles and applications* (Cambridge University Press).
Joschko, M., M. Woerner, T. Elsaesser, B. E., T. Kuhn, R. Hey, H. Kostial, and K. Ploog (1997), Phys. Rev. Lett. **78**, 737.
Juman, G., M. Watabe, K. Miyamoto, and T. Omatsu (2014), in *2014 Conference on Lasers and Electro-Optics (CLEO)-Laser Science to Photonic Applications* (IEEE) pp. 1–2.
Kadanoff, L. P., and G. Baym (1962), *Quantum Statistical Mechanics: Green's Function Methods in Equilibrium and Nonequilibrium Problems* (Benjamin-Cummings Publishing Company).
Kaiser, T., D. Flamm, S. Schröter, and M. Duparré (2009), Optics Express **17**, 9347.
Kako, S., K. Hoshino, S. Iwamoto, S. Ishida, and Y. Arakawa (2004), Appl. Phys. Lett. **85** (1), 64.
Kalt, H., and C. F. Klingshirn (2019), *Semiconductor Optics 1: Linear Optical Properties of Semiconductors* (Springer, Berlin).
Karimi, E., G. Zito, B. Piccirillo, L. Marrucci, and E. Santamato (2007), Opt. Lett. **32** (21), 3053.
Kasprzak, J., M. Richard, S. Kundermann, A. Baas, P. Jeambrun, J. Keeling, F. Marchetti, M. Szymańska, R. André, J. Staehli, *et al.* (2006), Nature **443**, 409.
Kavokin, A., J. J. Baumberg, G. Malpuech, and F. P. Laussy (2017), *Microcavities* (Oxford university press).
Kawata, S., M. Ohtsu, and M. Irie (2001), *Near-field optics and surface plasmon polaritons*, Vol. 81 (Springer Science & Business Media).
Kazak, N. S., N. A. Khilo, and A. A. Ryzhevich (1999), Quantum Electronics **29**, 1020.
Kazimierczuk, T., D. Fröhlich, S. Scheel, H. Stolz, and M. Bayer (2014), Nature **76**, 343.
Keldysh, L. V. (1958), JETP **34**, 1138.
Keldysh, L. V. (1965), JETP **20**, 1018.
Keller, J., A. Schönle, and S. W. Hell (2007), Optics Express **15**, 3361.
Kelly, M., and R. Nicholas (1985), Rep. Prog. Phys. **48**, 1699.
Kerber, R., J. Fitzgerald, X. Xiao, S. S. Oh, S. Maier, V. Giannini, and D. Reiter (2018), New Journal of Physics **20** (9), 095005.
Kerridge-Johns, W. (2018), *Diode-pumped alexandrite laser development and vortex mode generation*, Ph.D. thesis (Imperial College London).
Khitrova, G., H. Gibbs, F. Jahnke, M. Kira, and S. W. Koch (1999), Rev. Mod. Phys. **71**, 1591.
Kikkawa, J., and D. Awschalom (1999), Nature **397**, 139.
Kim, H., J. Park, S.-W. Cho, S.-Y. Lee, M. Kang, and B. Lee (2010), Nano letters **10** (2), 529.
Kira, M., F. Jahnke, W. Hoyer, and S. W. Koch (1999), Progr. Quantum Electron. **23**, 189.
Kittel, C. (1987), *Quantum Theory of Solids, 2nd Edition*

(John Wiley and Sons, New York).
Kleemans, N., I. Bominaar-Silkens, V. Fomin, V. Gladilin, D. Granados, A. Taboada, J. García, P. Offermans, U. Zeitler, P. Christianen, *et al.* (2007), Phys. Rev. Lett. **99**, 146808.
Kobayashi, S., C. Jiang, T. Kawazu, and H. Sakaki (2004), Jpn. J. Appl. Phys. **43**, L662.
Kobe, D. H. (1978), Phys. Rev. Lett. **40**, 538.
Koch, M., D. Weber, J. Feldmann, E. O. Göbel, T. Meier, A. Schulze, P. Thomas, S. Schmitt-Rink, and K. Ploog (1993), Phys. Rev. B **47**, 1532.
Koch, S. W., N. Peyghambarian, and M. Lindberg (1988), J. Phys. C: Solid State Phys. **21**, 5229.
Kohn, W., and L. J. Sham (1965), Phys. Rev. **140**, A1133.
Köksal, K., and J. Berakdar (2012), Phys. Rev. A **86**, 063812.
Köksal, K., and F. Koç (2017a), Computational and Theoretical Chemistry **1099**, 203.
Köksal, K., and F. Koç (2017b), Computational and Theoretical Chemistry **1105**, 27.
Koksal, K., V. Lembessis, J. Yuan, and M. Babiker (2020), JOSA B **37** (9), 2570.
Koksal, K., V. E. Lembessis, J. Yuan, and M. Babiker (2019), Journal of Optics **21** (10), 104002.
Konzelmann, A. M., S. O. Krüger, and H. Giessen (2019), Physical Review B **100** (11), 115308.
Korenev, B. G. (2002), *Bessel functions and their applications* (CRC Press).
Kotlyar, V. V., A. A. Almazov, S. N. Khonina, V. A. Soifer, H. Elfstrom, and J. Turunen (2005), J. Opt. Soc. Am. A **22**, 849.
Krasnok, A., S. Lepeshov, and A. Alú (2018), Optics express **26** (12), 15972.
Kraus, M., J. Wätzel, and J. Berakdar (2018), Optics Communications **427**, 390.
Krenn, M., M. Malik, M. Erhard, and A. Zeilinger (2017), Phil. Trans. Roy. Soc. London, Ser. A **375**, 20150442.
Kroutvar, M., Y. Ducommun, D. Heiss, M. Bichler, D. Schuh, G. Abstreiter, and J. J. Finley (2004), Nature **432** (7013), 81.
Krügel, A., A. Vagov, V. M. Axt, and T. Kuhn (2007), Phys. Rev. B **76**, 195302.
Kugler, M., K. Korzekwa, P. Machnikowski, C. Gradl, S. Furthmeier, M. Griesbeck, M. Hirmer, D. Schuh, W. Wegscheider, T. Kuhn, T. Schüller, , and T. Korn (2011), Phys. Rev. B **84**, 085327.
Kuhn, T., D. Reiter, and G. Quinteiro (2015), J. Phys.: Conf. Series **647**, 012012.
Kwon, M.-S., B. Y. Oh, S.-H. Gong, J.-H. Kim, H. K. Kang, S. Kang, J. D. Song, H. Choi, and Y.-H. Cho (2019), Physical review letters **122** (4), 045302.
Lagoudakis, K., T. Ostatnickỳ, A. Kavokin, Y. G. Rubo, R. André, and B. Deveaud-Plédran (2009), science **326** (5955), 974.
Lagoudakis, K. G., M. Wouters, M. Richard, A. Baas, I. Carusotto, R. André, L. S. Dang, and B. Deveaud-Plédran (2008), Nature physics **4** (9), 706.
Lamb Jr, W. E., R. R. Schlicher, and M. O. Scully (1987), Phys. Rev. A **36**, 2763.
Lavery, M. P., F. C. Speirits, S. M. Barnett, and M. J. Padgett (2013), Science **341**, 537.
Lavoisier, A. (1793), *Traité élémentaire de Chimie, 1* (Chez Cuchet, Libraire).
Lax, M., W. H. Louisell, and W. B. McKnight (1975), Phys. Rev. A **11**, 1365.
Lee, H.-I., and J. Mok (2016), Pacific Journal of Mathematics for Industry **8** (1), 1.
Lee, J., Y. Arita, S. Toyoshima, K. Miyamoto, P. Panagiotopoulos, E. M. Wright, K. Dholakia, and T. Omatsu (2018), ACS Photonics **5** (10), 4156.
Leosson, K., J. R. Jensen, W. Langbein, and J. M. Hvam (2000), Phys. Rev. B **61** (15), 10322.
Lerario, G., A. Fieramosca, F. Barachati, D. Ballarini, K. S. Daskalakis, L. Dominici, M. De Giorgi, S. A. Maier, G. Gigli, S. Kéna-Cohen, *et al.* (2017), Nat. Phys. **13**, 837.
Li, C.-F. (2009), Phys. Rev. A **80**, 063841.
Li, H., D. B. Phillips, X. Wang, Y.-L. D. Ho, L. Chen, X. Zhou, J. Zhu, S. Yu, and X. Cai (2015), Optica **2** (6), 547.
Li, Y., H. Lee, and E. Wolf (2004), J. Opt. Soc. Am. A **21** (4), 640.
Li, Z., Y. Li, T. Han, X. Wang, Y. Yu, B. Tay, Z. Liu, and Z. Fang (2017), ACS nano **11** (2), 1165.
Liao, S.-K., W.-Q. Cai, J. Handsteiner, B. Liu, J. Yin, L. Zhang, D. Rauch, M. Fink, J.-G. Ren, W.-Y. Liu, *et al.* (2018), Phys. Rev. Lett. **120** (3), 030501.
Liew, T., and I. Shelykh (2009), Phys. Rev. B **80**, 161303.
Lindberg, M., R. Binder, and S. Koch (1992), Phys. Rev. A **45**, 1865.
Lindberg, M., and S. W. Koch (1988), Phys. Rev. B **38**, 3342.
Lindblad, G. (1976), Commun. Math. Phys. **48**, 119.
Liu, G., D. W. Snoke, A. Daley, L. N. Pfeiffer, and K. West (2015), Proceedings of the National Academy of Sciences **112** (9), 2676.
Liu, K., N. Maccaferri, Y. Shen, X. Li, R. P. Zaccaria, X. Zhang, Y. Gorodetski, and D. Garoli (2020), Opt. Lett. **45** (4), 823.
Liu, Z., J. M. Steele, W. Srituravanich, Y. Pikus, C. Sun, and X. Zhang (2005), Nano letters **5** (9), 1726.
Lloyd, H. (1833), The London, Edinburgh, and Dublin Philosophical Magazine and Journal of Science **2**, 112.
Löffler, W., D. Broer, and J. Woerdman (2011), Phys. Rev. A **83**, 065801.
Loudon, R. (2003), Phys. Rev. A **68**, 013806.
Lu, W., and Y. Fu (2018), *Spectroscopy of Semiconductors* (Springer, Berlin).
Lusk, M. T., M. Siemens, and G. F. Quinteiro (2018), J. Opt. **21**, 015601.
Ma, X., B. Berger, M. Aßmann, R. Driben, T. Meier, C. Schneider, S. Höfling, and S. Schumacher (2020), Nature communications **11** (1), 1.
Maier, S. A. (2007), *Plasmonics: fundamentals and applications* (Springer Science & Business Media).
Maiman, T. H. (1960), Nature **187**, 493.
Mair, A., A. Vaziri, G. Weihs, and A. Zeilinger (2001), Nature **412**, 313.
Mak, K. F., C. Lee, J. Hone, J. Shan, and T. F. Heinz (2010), Phys. Rev. Lett. **105**, 136805.
Mandel, L. (1958), Proc. Phys. Soc. **72**, 1037.
Maragò, O. M., P. H. Jones, P. G. Gucciardi, G. Volpe, and A. C. Ferrari (2013), Nature nanotechnology **8** (11), 807.
Martelli, F., A. Polimeni, A. Patane, M. Capizzi, P. Borri, M. Gurioli, M. Colocci, A. Bosacchi, and S. Franchi (1996), Phys. Rev. B **53** (11), 7421.
Martin, J. D. (2019), Physics Today **72**, 30.
Masajada, J., and B. Dubik (2001), Opt. Commun. **198**, 21.
Mathevet, R., B. V. de Lesegno, L. Pruvost, and G. L. Rikken (2013), Optics Express **21**, 3941.

Mathieu, É. (1868), Journal de mathématiques pures et appliquées **13**, 137.
Matthews, M. R., B. P. Anderson, P. C. Haljan, D. S. Hall, C. E. Wieman, and E. A. Cornell (1999), Phys. Rev. Lett. **83**, 2498.
Matula, O., A. G. Hayrapetyan, V. G. Serbo, A. Surzhykov, and S. Fritzsche (2013), J. Phys. B **46**, 205002.
Maxwell, J. C. (1865), Phil. Trans. Roy. Soc. London **155**, 459.
Meier, F., and B. P. Zakharchenya (2012), *Optical orientation* (Elsevier).
Mendeleev, D. (1869), Z. Chem. **12**, 405.
Miao, P., Z. Zhang, J. Sun, W. Walasik, S. Longhi, N. M. Litchinitser, and L. Feng (2016), Science **353** (6298), 464.
Michler, P., A. Kiraz, C. Becher, W. V. Schoenfeld, P. M. Petroff, L. Zhang, E. Hu, and A. Imamoglu (2000), Science **290** (5500), 2282.
Mie, G. (1908), Annalen der Physik **330**, 377.
Mignaco, J. A. (2001), Brazilian Journal of Physics **31**, 235.
Mike, P., L. Z. Szabó, and P. Földi (2018), Journal of Russian Laser Research **39** (5), 465.
Mills, M. (2011), IEEE Annals of the History of Computing **33**, 24.
Miró, P., M. Audiffred, and T. Heine (2014), Chem. Soc. Rev. **43**, 6537.
Mohammadi, S. M., L. K. Daldorff, K. Forozesh, B. Thidé, J. E. Bergman, B. Isham, R. Karlsson, and T. Carozzi (2010), Radio Science **45** (4).
Mondal, P. K., B. Deb, and S. Majumder (2014), Phys. Rev. A **89**, 063418.
Monteiro, P. B., P. A. M. Neto, and H. M. Nussenzveig (2009), Phys. Rev. A **79**, 033830.
Moriarty, P. (2001), Rep. Prog. Phys. **64**, 297.
Mukherjee, K., S. Majumder, P. K. Mondal, and B. Deb (2017), J. Phys. B **51**, 015004.
Nechayev, S., J. S. Eismann, G. Leuchs, and P. Banzer (2019), Physical Review B **99** (7), 075155.
Nerkararyan, S., K. Nerkararyan, N. Janunts, and T. Pertsch (2010), Physical Review B **82** (24), 245405.
Newton, I. (1672), Philosophical Transactions **6**, 3075.
Ni, J., C. Wang, C. Zhang, Y. Hu, L. Yang, Z. Lao, B. Xu, J. Li, D. Wu, and J. Chu (2017), Light: Science & Applications **6** (7), e17011.
Nikitine, S. (1969), in *Optical Properties of Solids*, edited by S. Nudelman and S. S. Mitra (Springer, Boston, MA) p. 197.
Nivas, J. J., H. Shutong, K. Anoop, A. Rubano, R. Fittipaldi, A. Vecchione, D. Paparo, L. Marrucci, R. Bruzzese, and S. Amoruso (2015), Opt. Lett. **40** (20), 4611.
Nobahar, D., K. Hajisharifi, and H. Mehdian (2019), Optics & Laser Technol.. **117**, 165.
Nolte, S., C. Momma, H. Jacobs, A. Tünnermann, B. N. Chichkov, B. Wellegehausen, and H. Welling (1997), J. Opt. Soc. Am. B **14** (10), 2716.
Novitsky, A. V., and L. Barkovsky (2008), J. Opt. A **10** (7), 075006.
Novoselov, K. (2011), Rev. Mod. Phys. **83**, 837.
Novoselov, K. S., A. K. Geim, S. V. Morozov, D. Jiang, Y. Zhang, S. V. Dubonos, I. V. Grigorieva, and A. A. Firsov (2004), Science **306**, 666.
Novotny, B., L. Hetch (2006), *Principle of Nano-optics* (Cambridge University Press, New York).
Noyan, M. A., and J. M. Kikkawa (2015), Appl. Phys. Lett. **107**, 032406.
Nye, J. F., and M. V. Berry (1974), Proc. Roy. Soc. London, Ser. A **336**, 165.
Ohno, T., and S. Miyanishi (2006), Optics express **14** (13), 6285.
O'Holleran, K., M. J. Padgett, and M. R. Dennis (2006), Optics Express **14**, 3039.
Okuda, H., and H. Sasada (2008), J. Opt. Soc. Am. A **25** (4), 881.
Omatsu, T., K. Chujo, K. Miyamoto, M. Okida, K. Nakamura, N. Aoki, and R. Morita (2010), Optics express **18** (17), 17967.
Omatsu, T., K. Miyamoto, K. Toyoda, R. Morita, Y. Arita, and K. Dholakia (2019), Advanced Optical Materials **7** (14), 1801672.
Onida, G., L. Reining, and A. Rubio (2002), Rev. Mod. Phys. **74**, 601.
Oosterbeek, R. N., S. Ashforth, O. Bodley, and M. C. Simpson (2018), Optics Express **26** (26), 34558.
Otte, E., and C. Denz (2020), Appl. Phys. Rev. **7**, 041308.
Pabon, D., S. Ledesma, G. Quinteiro, and M. Capeluto (2017), Appl. Optics **56**, 8048.
Padgett, M., and L. Allen (2002), J. Opt. B **4**, S17.
Padgett, M., J. Courtial, and L. Allen (2004), Physics Today **57**, 35.
Pan, J., Y. Shen, Z. Wan, X. Fu, H. Zhang, and Q. Liu (2020), Phys. Rev. Applied **14**, 044048.
Parvez, K. (2019), in *Biomedical Applications of Graphene and 2D Nanomaterials* (Elsevier) pp. 1–25.
Patton, B., W. Langbein, U. Woggon, L. Maingault, and H. Mariette (2006), Phys. Rev. B **73**, 235354.
Persuy, D., M. Ziegler, O. Crégut, K. Kheng, M. Gallart, B. Hönerlage, and P. Gilliot (2015), Phys. Rev. B **92**, 115312.
Peshkov, A., S. Fritzsche, and A. Surzhykov (2015), Phys. Rev. A **92**, 043415.
Peshkov, A., D. Seipt, A. Surzhykov, and S. Fritzsche (2017), Phys. Rev. A **96**, 023407.
Peshkov, A., A. Volotka, A. Surzhykov, and S. Fritzsche (2018), Phys. Rev. A **97**, 023802.
Phelan, C., D. O'dwyer, Y. Rakovich, J. Donegan, and J. Lunney (2009), Optics Express **17**, 12891.
Pigeon, S., I. Carusotto, and C. Ciuti (2011), Phys. Rev. B **83** (14), 144513.
Planck, M. (1900), Verhandl. Dtsch. Phys. Ges. **2**, 202.
Portolan, S., O. Di Stefano, S. Savasta, F. Rossi, and R. Girlanda (2008), Phys. Rev. B **77**, 195305.
Power, E. A., and S. Zienau (1959), Phil. Trans. Roy. Soc. London, Ser. A **251**, 427.
Purcell, E. M. (1946), Proceedings of the American Physical Society **69** (11), 681.
Quinteiro, G. F. (2008), Phys. Rev. B **77**, 075301.
Quinteiro, G. F. (2010), Europhys. Lett. **91**, 27002.
Quinteiro, G. F., and J. Berakdar (2009), Optics Express **17**, 20465.
Quinteiro, G. F., P. Dmitruk, and A. Aligia (2012), Phys. Rev. B **86**, 035329.
Quinteiro, G. F., J. Fernández-Rossier, and C. Piermarocchi (2006), Phys. Rev. Lett. **97**, 097401.
Quinteiro, G. F., P. Grinberg, and C. T. Schmiegelow (2019a), in *CLEO: Applications and Technology* (Optical Society of America) pp. JTu2A–19.
Quinteiro, G. F., and T. Kuhn (2014), Phys. Rev. B **90**, 115401.
Quinteiro, G. F., and T. Kuhn (2015), in *CLEO: QELS Fun-*

damental Science (Optical Society of America) pp. FW1E–8.
Quinteiro, G. F., A. O. Lucero, and P. I. Tamborenea (2010), J. Phys. Condens. Matter **22**, 505802.
Quinteiro, G. F., and C. Piermarocchi (2005), Phys. Rev. B **72**, 045334.
Quinteiro, G. F., D. Reiter, and T. Kuhn (2017a), J. Phys.: Conf. Series **906**, 012014.
Quinteiro, G. F., D. E. Reiter, and T. Kuhn (2015), Phys. Rev. A **91**, 033808.
Quinteiro, G. F., D. E. Reiter, and T. Kuhn (2017b), Phys. Rev. A **95**, 012106.
Quinteiro, G. F., F. Schmidt-Kaler, and C. T. Schmiegelow (2017c), Phys. Rev. Lett. **119**, 253203.
Quinteiro, G. F., C. T. Schmiegelow, D. E. Reiter, and T. Kuhn (2019b), Phys. Rev. A **99**, 023845.
Quinteiro, G. F., and P. I. Tamborenea (2009a), in *European Quantum Electronics Conference* (Optical Society of America) p. JSIII2_5.
Quinteiro, G. F., and P. I. Tamborenea (2009b), Phys. Rev. B **79**, 155450.
Quinteiro, G. F., and P. I. Tamborenea (2009c), Europhys. Lett. **85**, 47001.
Quinteiro, G. F., and P. I. Tamborenea (2010), Phys. Rev. B **82**, 125207.
Quinteiro, G. F., P. I. Tamborenea, and J. Berakdar (2011), Optics Express **19**, 26733.
Ranjan, V., G. Allan, C. Priester, and C. Delerue (2003), Phys. Rev. B **68** (11), 115305.
Räsänen, E., A. Castro, J. Werschnik, A. Rubio, and E. K. U. Gross (2007), Phys. Rev. Lett. **98**, 157404.
Reimann, S. M., and M. Manninen (2002), Rev. Mod. Phys. **74**, 1283.
Reiter, D., M. Glanemann, V. M. Axt, and T. Kuhn (2006), Phys. Rev. B **73**, 125334.
Reiter, D., M. Glanemann, V. M. Axt, and T. Kuhn (2007), Phys. Rev. B **75**, 205327.
Ren, X., A. Liu, C. Zou, L. Wang, Y. Cai, F. Sun, G. Guo, and G. Guo (2011), Applied Physics Letters **98** (20), 201113.
Ritsch-Marte, M. (2017), Phil. Trans. Roy. Soc. London, Ser. A **375**, 20150437.
Rohlfing, M., and S. G. Louie (1998), Phys. Rev. Lett. **81**, 2312.
Rosales Guzmán, C. G. (2015), *Photonic applications based on the use of structured light*, Ph.D. thesis (Universitat Politècnica de Catalunya).
Rosati, R., R. C. Iotti, F. Dolcini, and F. Rossi (2014), Phys. Rev. B **90**, 125140.
Rosencher, E., B. Vinter, and B. F. Levine (2012), *Intersubband transitions in quantum wells*, Vol. 288 (Springer Science & Business Media).
Rossi, F. (2011), *Theory of semiconductor quantum devices: microscopic modeling and simulation strategies* (Springer Science & Business Media).
Rossi, F., and T. Kuhn (2002), Rev. Mod. Phys. **74**, 895.
Rubano, A., F. Cardano, B. Piccirillo, and L. Marrucci (2019), J. Opt. Soc. Am. B **36**, D70.
Rubo, Y. G. (2007), Physical review letters **99** (10), 106401.
Sakai, K., K. Nomura, T. Yamamoto, and K. Sasaki (2015), Scientific reports **5** (1), 1.
Salomaa, M., and G. Volovik (1987), Reviews of modern physics **59** (3), 533.
Samad, R. E., S. L. Baldochi, and N. D. Vieira Jr (2008), Appl. Optics **47** (7), 920.
Sanvitto, D., S. Pigeon, A. Amo, D. Ballarini, M. De Giorgi, I. Carusotto, R. Hivet, F. Pisanello, V. Sala, P. Guimaraes, *et al.* (2011), Nat. Photonics **5** (10), 610.
Savona, V., C. Piermarocchi, A. Quattropani, P. Schwendimann, and F. Tassone (1999), Phase transitions **68**, 169.
Savona, V., C. Piermarocchi, A. Quattropani, F. Tassone, and P. Schwendimann (1997), Phys. Rev. Lett. **78**, 4470.
Sbierski, B., G. Quinteiro, and P. Tamborenea (2013), J. Phys. Condens. Matter **25**, 385301.
Scheuer, J., and M. Orenstein (1999), Science **285** (5425), 230.
Schiff, L. I. (1955), "Quantum mechanics, mcgrawhill book co new york (1955),".
Schilp, J., T. Kuhn, and G. Mahler (1994), Phys. Rev. B **50**, 5435.
Schimpf, C., M. Reindl, D. Huber, B. Lehner, S. F. Covre Da Silva, S. Manna, M. Vyvlecka, P. Walther, and A. Rastelli (2021), Science Adv. **7**, 10.1126/sciadv.abe8905.
Schmidt, O. A., C. Schulze, D. Flamm, R. Brüning, T. Kaiser, S. Schröter, and M. Duparré (2011), Optics Express **19**, 6741.
Schmiegelow, C. T., J. Schulz, H. Kaufmann, T. Ruster, U. G. Poschinger, and F. Schmidt-Kaler (2016), Nat. Commun. **7**, 12998.
Schneider, C., A. Rahimi-Iman, N. Y. Kim, J. Fischer, I. G. Savenko, M. Amthor, M. Lermer, A. Wolf, L. Worschech, V. D. Kulakovskii, *et al.* (2013), Nature **497**, 348.
Scholz-Marggraf, H., S. Fritzsche, V. Serbo, A. Afanasev, and A. Surzhykov (2014), Physical Review A **90** (1), 013425.
Schulze, D., A. Thakur, A. S. Moskalenko, and J. Berakdar (2017), Annalen der Physik (Leipzig) **529**, 1600379.
Schwiete, G., and Y. Oreg (2009), Phys. Rev. Lett. **103**, 037001.
Scully, M. O., and M. S. Zubairy (1997), *Quantum Optics* (Cambridge University Press, Cambridge).
Seghilani, M. S., M. Myara, M. Sellahi, L. Legratiet, I. Sagnes, G. Beaudoin, P. Lalanne, and A. Garnache (2016), Scientific Reports **6**, 38156.
Serabyn, E., D. Mawet, and R. Burruss (2010), Nature **464**, 1018.
Serbo, V. G., A. Surzhykov, and A. Volotka (2021), Annalen der Physik , 2100199.
Shah, J. (1999), *Ultrafast Spectroscopy of Semiconductors and Semiconductor Nanostructures* (Springer, Berlin).
Shalygin, V., H. Diehl, C. Hoffmann, S. Danilov, T. Herrle, S. Tarasenko, D. Schuh, C. Gerl, W. Wegscheider, W. Prettl, *et al.* (2007), JETP Lett. **84**, 570.
Shelykh, I., Y. G. Rubo, G. Malpuech, D. Solnyshkov, and A. Kavokin (2006), Phys. Rev. Lett. **97**, 066402.
Shelykh, I. A., A. V. Kavokin, and G. Malpuech (2005), Phys. Status Solidi B **242**, 2271.
Shelykh, I. A., A. V. Kavokin, Y. G. Rubo, T. Liew, and G. Malpuech (2009), Semicond. Sci. Technol. **25**, 013001.
Shen, Y., X. Wang, Z. Xie, C. Min, X. Fu, Q. Liu, M. Gong, and X. Yuan (2019), Light: Science & Applications **8**, 1.
Shi, L., L. Lindwasser, W. Wang, R. Alfano, and A. Rodríguez-Contreras (2017), Journal of biophotonics **10**, 1756.
Shigematsu, K., K. Yamane, R. Morita, and Y. Toda (2016), Physical Review B **93** (4), 045205.
Shinde, P. V., and M. K. Singh (2019), in *Fundamentals and Sensing Applications of 2D Materials* (Elsevier) pp. 91–143.
Shintani, K., K. Taguchi, Y. Tanaka, and Y. Kawaguchi (2016), Phys. Rev. B **93**, 195415.

Shree, S., I. Paradisanos, X. Marie, C. Robert, and B. Urbaszek (2021), *Guide to optical spectroscopy of layered semiconductors*, Vol. 3 (Springer Nature).

Siegman, A. E. (1990), *Lasers* (University Science Books, Melville, NY).

Sigurdsson, H., O. Egorov, X. Ma, I. A. Shelykh, and T. C. H. Liew (2014), Physical Review B **90** (1), 014504.

Simbulan, K. B., T.-D. Huang, G.-H. Peng, F. Li, O. J. Gomez Sanchez, J.-D. Lin, C.-I. Lu, C.-S. Yang, J. Qi, S.-J. Cheng, *et al.* (2021), ACS nano **15** (2), 3481.

Solyanik-Gorgone, M., and A. Afanasev (2019), Physical Review B **99** (3), 035204.

Solyanik-Gorgone, M., A. Afanasev, C. E. Carlson, C. T. Schmiegelow, and F. Schmidt-Kaler (2019), J. Opt. Soc. Am. B **36** (3), 565.

Sommerfeld, A. (1928), Z. Phys. **47**, 1.

Sordillo, L. A., S. Mamani, M. Sharonov, and R. R. Alfano (2019), Applied Physics Letters **114** (4), 041104.

Sotier, F., T. Thomay, T. Hanke, J. Korger, S. Mahapatra, A. Frey, K. Brunner, R. Bratschitsch, and L. A. (2009), Nat. Phys. **5**, 352.

Spektor, G., D. Kilbane, A. Mahro, B. Frank, S. Ristok, L. Gal, P. Kahl, D. Podbiel, S. Mathias, H. Giessen, *et al.* (2017), Science **355** (6330), 1187.

Splendiani, A., L. Sun, Y. Zhang, T. Li, J. Kim, C.-Y. Chim, G. Galli, and F. Wang (2010), Nano Lett. **10**, 1271.

Steane, A. (1998), Rev. Mod. Phys. **61** (2), 117.

Stevenson, R. M., R. J. Young, P. Atkinson, K. Cooper, D. A. Ritchie, and A. J. Shields (2006), Nature **439**, 179.

Strinati, G. (1988), Riv. del Nuovo Cimento **11**, 1.

Suárez, F., D. Granados, M. L. Dotor, and J. M. Garcia (2004), Nanotechnology **15**, S126.

Sudarshan, E. C. G. (1963), Phys. Rev. Lett. **10**, 277.

Surzhykov, A., D. Seipt, V. Serbo, and S. Fritzsche (2015), Phys. Rev. A **91**, 013403.

Syubaev, S., A. Zhizhchenko, A. Kuchmizhak, A. Porfirev, E. Pustovalov, O. Vitrik, Y. Kulchin, S. Khonina, and S. Kudryashov (2017), Optics Express **25** (9), 10214.

Syubaev, S., A. Zhizhchenko, O. Vitrik, A. Porfirev, S. Fomchenkov, S. Khonina, S. Kudryashov, and A. Kuchmizhak (2019), Appl. Surf. Sci. **470**, 526.

Tabosa, J. W. R., and D. V. Petrov (1999), Phys. Rev. Lett. **83**, 4967.

Takagahara, T. (1989), J. Lumin. **44** (4-6), 347.

Takahashi, H. T., I. Proskurin, and J.-i. Kishine (2018), Journal of the Physical Society of Japan **87** (11), 113703.

Takahashi, H. T., I. Proskurin, and J.-i. Kishine (2019), arXiv preprint arXiv:1904.03083.

Tamburini, F., B. Thidé, G. Molina-Terriza, and G. Anzolin (2011), Nat. Phys. **7**, 195.

Thidé, B., F. Tamburini, H. Then, C. Someda, and R. Ravanelli (2014), arXiv preprint arXiv:1410.4268.

Thidé, B., H. Then, J. Sjöholm, K. Palmer, J. Bergman, T. Carozzi, Y. N. Istomin, N. Ibragimov, and R. Khamitova (2007), Phys. Rev. Lett. **99**, 087701.

Tikhonova, O., and E. N. Voronina (2021), Journal of Physics: Condensed Matter.

Toledo-Solano, M., M. Mora-Ramos, A. Figueroa, and Y. Rubo (2014), Physical Review B **89** (3), 035308.

Tong, C., S. F. Yoon, and L. Wang (2012), Nanoscale Res. Lett. **7**, 1.

Torres, J. P., and L. Torner (2011), "Twisted photons: Application of light with orbital angular momentum, edited by juan p. torres and lluis torner,".

Toyoda, K., K. Miyamoto, N. Aoki, R. Morita, and T. Omatsu (2012), Nano Lett. **12** (7), 3645.

Tsakiris, N., K. Anoop, G. Ausanio, M. Gill-Comeau, R. Bruzzese, S. Amoruso, and L. Lewis (2014), J. Appl. Phys. **115** (24), 243301.

Tsesses, S., K. Cohen, E. Ostrovsky, B. Gjonaj, and G. Bartal (2019), Nano letters **19** (6), 4010.

Tsintzos, S., N. Pelekanos, G. Konstantinidis, Z. Hatzopoulos, and P. Savvidis (2008), Nature **453**, 372.

Turpin, A., Y. V. Loiko, T. K. Kalkandjiev, and J. Mompart (2016), Laser Photon. Rev. **10**, 750.

Ueno, Y., Y. Toda, S. Adachi, R. Morita, and T. Tawara (2009), Optics Express **17**, 20567.

Vagov, A., M. D. Croitoru, M. Glässl, V. M. Axt, and K. T. (2011), Phys. Rev. B **83**, 094303.

Van Enk, S. (1994), Quantum Optics: J. of the European Opt. Soc. Part B **6**, 445.

Vänskä, O., M. Kira, I. Tittonen, and S. W. Koch (2011), Physical Review B **84** (16), 165317.

Vasilieva, O., A. Zingan, and P. Khadzhi (2018), Optics and Spectroscopy **125**, 439.

Volke-Sepulveda, K., V. Garcés-Chávez, S. Chávez-Cerda, J. Arlt, and K. Dholakia (2002), J. Opt. B **4**, S82.

Volyar, A., M. Bretsko, Y. Akimova, and Y. Egorov (2019), Appl. Optics **58**, 5748.

Wan, K. K. (2006), *From micro to macro quantum systems: a unified formalism with superselection rules and its applications* (World Scientific).

Wang, J., J.-Y. Yang, I. M. Fazal, N. Ahmed, Y. Yan, H. Huang, Y. Ren, Y. Yue, S. Dolinar, M. Tur, *et al.* (2012), Nat. Photonics **6** (7), 488.

Wang, J. J., T. Wriedt, J. A. Lock, and L. Mädler (2016), J. of Quantitative Spectroscopy and Radiative Transfer. **184**, 218.

Wang, M., F. Tang, X. Pan, L. Yao, X. Wang, Y. Jing, J. Ma, G. Wang, and L. Mi (2017), BBA clinical **8**, 7.

Wannier, G. H. (1937), Phys. Rev. **52**, 191.

Wätzel, J., I. Barth, and J. Berakdar (2017), Journal of Modern Optics **64** (10-11), 1088.

Wätzel, J., and J. Berakdar (2016), Scientific reports **6** (1), 1.

Wätzel, J., A. Moskalenko, and J. Berakdar (2012), Optics express **20** (25), 27792.

Weber, E. R., R. K. Willardson, H. Liu, and F. Capasso (1999), *Intersubband transitions in quantum wells: physics and device applications* (Academic press).

Weiner, J., and F. Nunes (2017), *LIGHT-MATTER INTERACTION 2/E* (Oxford University Press).

Weisbuch, C., M. Nishioka, A. Ishikawa, and Y. Arakawa (1992), Phys. Rev. Lett. **69**, 3314.

Wertz, E., L. Ferrier, D. Solnyshkov, R. Johne, D. Sanvitto, A. Lemaître, I. Sagnes, R. Grousson, A. V. Kavokin, P. Senellart, *et al.* (2010), Nat. Phys. **6**, 860.

Whewell, W. (1836), Phil. Trans. Roy. Soc. London **126**, 289.

Wigger, D., V. Karakhanyan, C. Schneider, M. Kamp, S. Höfling, P. Machnikowski, T. Kuhn, and J. Kasprzak (2020), Opt. Lett. **45**, 919.

Wolf, S., D. Awschalom, R. Buhrman, J. Daughton, v. S. von Molnár, M. Roukes, A. Y. Chtchelkanova, and D. Treger (2001), Science **294** (5546), 1488.

Woolley, R. G. (1971), Proc. Roy. Soc. London, Ser. A **321**, 557.

Woźniak, P., I. De Leon, K. Höflich, G. Leuchs, and P. Banzer (2019), Optica **6**, 961.

Xie, Y.-Y., P.-N. Ni, Q.-H. Wang, Q. Kan, G. Briere, P.-P. Chen, Z.-Z. Zhao, A. Delga, H.-R. Ren, H.-D. Chen, *et al.* (2020), Nat. Nanotechnol. **15** (2), 125.

Yamamoto, Y., F. Tassone, and H. Cao (2000), *Semiconductor cavity quantum electrodynamics* (Springer Science & Business Media).

Yang, K.-H. (1976), Ann. Phys. (NY) **101**, 62.

Yang, S., W. Chen, R. L. Nelson, and Q. Zhan (2009), Optics letters **34** (20), 3047.

Ye, L., J. R. Rouxel, S. Asban, B. Roesner, and S. Mukamel (2019), Journal of chemical theory and computation **15**, 4180.

Yin, J., W. Gao, and Y. Zhu (2003), Progr. in Optics **45**, 119.

Yin, L., V. Vlasko-Vlasov, A. Rydh, J. Pearson, U. Welp, S.-H. Chang, S. Gray, G. C. Schatz, D. Brown, and C. W. Kimball (2004), Applied physics letters **85** (3), 467.

Yu, L., K. Chen, J. Song, J. Xu, W. Li, X. Li, J. Wang, and X. Huang (2007), Phys. Rev. Lett. **98**, 166102.

Zang, X., and M. T. Lusk (2017), Phys. Rev. A **96**, 013819.

Zeng, S., Z. Tang, C. Liu, and P. Zhou (2020), Nano Research , 1.

Zhang, H., Ö. Gül, S. Conesa-Boj, M. P. Nowak, M. Wimmer, K. Zuo, V. Mourik, F. K. De Vries, J. Van Veen, M. W. De Moor, *et al.* (2017), Nat. Commun. **8**, 1.

Zhang, K., Y. Wang, Y. Yuan, and S. N. Burokur (2020a), Applied Sciences **10**, 1015.

Zhang, K., Y. Yuan, D. Zhang, X. Ding, B. Ratni, S. N. Burokur, M. Lu, K. Tang, and Q. Wu (2018), Optics Express **26**, 1351.

Zhang, L., B. Shen, Z. Bu, X. Zhang, L. Ji, S. Huang, M. Xiriai, Z. Xu, C. Liu, and Z. Xu (2021), Physical Review Applied **16** (1), 014065.

Zhang, Z., X. Qiao, B. Midya, K. Liu, J. Sun, T. Wu, W. Liu, R. Agarwal, J. M. Jornet, S. Longhi, *et al.* (2020b), Science **368** (6492), 760.

Zhang, Z., H. Zhao, D. G. Pires, X. Qiao, Z. Gao, J. M. Jornet, S. Longhi, N. M. Litchinitser, and L. Feng (2020c), Light: Science & Applications **9** (1), 1.

Zhao, Y., J. S. Edgar, G. D. Jeffries, D. McGloin, and D. T. Chiu (2007), Physical Review Letters **99** (7), 073901.

Zhu, J., X. Cai, Y. Chen, and S. Yu (2013), Optics letters **38** (8), 1343.